1960

Branching of transitions in some mirror nuclei

Willard Lindley Talbert Jr.
Iowa State University

BRANCHING OF TRANSITIONS IN SOME MIRROR NUCLEI

by

Willard Lindley Talbert, Jr.

A Dissertation Submitted to the
Graduate Faculty in Partial Fulfillment of
The Requirements for the Degree of
DOCTOR OF PHILOSOPHY

Major Subject: Physics

Approved:

Signature was redacted for privacy.

In Charge of Major Work

Signature was redacted for privacy.

Head of Major Department

Signature was redacted for privacy.

Dean of Graduate College

Iowa State University
Of Science and Technology
Ames, Iowa

1960

TABLE OF CONTENTS

		Page
I.	INTRODUCTION	1
	A. Mirror Nuclei	1
	B. Nuclear Matrix Elements	6
	C. Statement of the Problem	11
II.	EXPERIMENTAL INVESTIGATION	16
	A. Development of the Method	16
	B. Sample Materials	23
	C. Description of the Experimental Apparatus	30
	1. Detection of gamma rays	30
	2. Physical arrangement	38
	3. Electronics	47
	4. Cycling equipment	58
	D. Tests and Calibration	62
	E. Experimental Procedure	66
III.	ANALYSIS OF DATA	71
	A. Calculation of the Branching Ratio	71
	B. Corrections and Errors	79
	C. Analysis for the Nuclides Investigated	86
	1. Na^{21}	86
	2. Mg^{23}	90
	3. Al^{25}	96
	4. Si^{27}	101
	5. S^{31}	104
	6. Ca^{39}	110
IV.	DISCUSSION	114
	A. Decay Schemes	114
	1. Level diagrams	114
	2. Selection rules and expected branching	136
	B. Comparative Lifetimes	145
V.	SUMMARY	148

		Page
VI.	BIBLIOGRAPHY	150
VII.	ACKNOWLEDGMENTS	155

I. INTRODUCTION

A. Mirror Nuclei

The class of nuclei having the property that the mass number, A, and the proton number, Z, are related by $A = 2Z \pm 1$ is called the class of "mirror nuclei". These nuclei are found among the light nuclei and are generally thought of as starting with the neutron and extending through Sc^{41}. As implied in their class definition, mirror nuclei occur in pairs of nuclei, each nuclide of a pair having the same atomic number as the other but a different charge, or proton number. A mirror nuclei pair can be formed from each other by interchange of all protons and neutrons. One member of a mirror nuclide pair is radioactive, undergoing beta-decay in a transition to the other member. In the case of the two lightest mirror pairs, the neutron-proton pair and the H^3-He^3 pair, the low-Z member decays to the high-Z member by negatron emission. Starting with A = 11, the decay between mirror pairs is one of positron emission with the high-Z member the parent and the low-Z member the daughter nucleus. The region between A = 3 and A = 11 is complicated by the presence of nucleon emission instabilities for A = 5 and A = 9, while A = 7 is characterized by Be^7 undergoing electron capture to Li^7, insufficient energy being available for the mechanism of positron emission.

The experimental study of mirror nuclei has long been considered desirable for purposes of comparison to theoretical predictions. Since the parent nuclear system is quite similar to the daughter, several properties of nuclei and nuclear forces can be investigated with a minimum of complication in the case of mirror nuclei. The concept of a nuclear radius can be investigated by noting that the total disintegration energy is partly due to the change of nuclear coulomb energy when, for the mirror nuclei heavier than $A = 11$, there is a decrease in proton number, Z, from $Z = \frac{A + 1}{2}$ to $Z = \frac{A - 1}{2}$ as a result of positron emission. It is possible to find the change in coulomb energy from a knowledge of the total disintegration energy found by measurements of the positron end-point energy and relate this change to an effective nuclear radius (1, pp. 31-37, 2, 3, 4).

The question of charge symmetry in nuclear forces has been answered by studying the energetics involved in the decay of mirror nuclei. In the decay of a mirror nuclide, it is found that the energy available for decay involves only the neutron-proton mass difference, the electron mass, the coulomb energy difference, and a nuclear binding energy difference resulting from the difference of n-n and p-p forces. By examination of mirror nuclei data giving the maximum positron energies, it has been shown that there is only a slight, if any, difference between the n-n and p-p forces

(1, pp. 31-37). The study of energy levels in mirror pairs has also shown evidence of charge symmetry of nuclear forces through the isobaric spin formalism (5, pp. 254-262). This result indicates that the nuclear forces between nucleons which give rise to the excited states are the same for parent and daughter nuclides, when effects due to coulomb and mass differences are taken into account.

One property of the decay of a mirror nuclide which is of interest is its half-life. The half-lives encountered in the region A = 11 to A = 41 range from twenty minutes for C^{11} to less than a second for Sc^{41}. Since the half-life is related inversely to the total decay probability of the parent nucleus, the experimental half-life is necessary in describing the decay interaction. In case the decay is composed of two or more competing interactions, or branches, the half-life must be modified accordingly to account for the decay probability of each transition. Since each branch decay forms a portion of the total decay, the half-life of each branch is longer than the experimental half-life by an amount which can be determined from knowing the branching ratio, or percentage of the total transitions made by each branch. A nuclear beta-decay characterized by branching is called a complex decay, and a branch occurs in the form of a transition to an excited state of the daughter nucleus, usually followed by emission of a nuclear gamma ray as the

daughter nucleus de-excites.

The problems associated with the experimental study of mirror nuclei are unique. The production of the radioactive member of a pair is not often easily accomplished. For example, using photonuclear reactions, only half of the radioactive mirror nuclides over the range A = 11 to A = 41 can be produced without the presence of contaminant activities. The half-lives of the heavier mirror nuclides are too short for common methods of investigation, so special methods must be used for their study. Also, the decays of the heavier mirror nuclei are quite energetic, which poses problems for energy analysis of the positrons emitted. Until recently, the direct observation of the decay of mirror nuclei had been done mainly with scintillation counters, which are more easily applied to spectrum analysis for short-lived decays than other methods because they can sample the entire energy range of the spectrum in a short period of time. The most recent investigations of mirror nuclei using scintillation spectrometer analysis of the positron spectra were those of various individuals at the synchrotron laboratory of Iowa State University (6, 7, 8, 9). Subsequent to the time of these investigations, considerable effort has been spent at the same laboratory to further refine the scintillation technique, the refinements exposing new difficulties impossible to correct up to the time of this report.

Since the investigations above, two groups of investigations have been published reporting the analysis of positron spectra of mirror nuclei using magnetic spectrometer methods. Welch (10, 11) reported studying the decay of mirror nuclei with a 180° magnetic spectrometer in the mass region of A = 19 to A = 39. Kistner and co-workers (12, 13, 14, 15) used a thin-lens magnetic spectrometer to study the decays of O^{15}, A^{35}, and Ca^{39}. Because of the significant difference in the energy resolution between magnetic and scintillation spectrometers and the fact that the magnetic spectrometers were applied to study mirror nuclei more recently than the latest scintillation efforts, the magnetic methods should be considered to have given more accurate results for the positron end-point energies.

Recent determinations of the half-lives of parent mirror nuclides have been made by Welch (10, 11), Kistner and co-workers (12, 13, 14, 15), Mihailović and Povh (16), Arnell and co-workers (17), and Cline and Chagnon (18). There is excellent agreement between these determinations, indicating that the total transition probabilities of the mirror nuclei are now well known. In addition to the half-life, a determination of the branching in each decay is necessary to complete the experimental picture. Hunt (8) reported seeing no evidence for branching in several mirror nuclei by means of a search for the gamma radiation following branching.

Kistner and co-workers (12, 14), using the same approach, found weak branching in the decay of A^{35}, but none in that of Ca^{39}. No gamma rays have been found in the decays of C^{11} (19), N^{13} (19, 10), F^{17} (21, 22), Ne^{19} (23, 24), Na^{21} (24), and Mg^{23} (23). Branching ratios of less than one per cent have been indicated by the presence of gamma rays in the decays of Al^{25} (25, 26), P^{29} (27), and Cl^{33} (28). Welch (11) approached the problem of branching by looking for secondary beta groups in the beta ray spectrum analysis. He found evidence of branching in all the mirror decays from A = 19 to A = 35 except for the decays of Na^{21} and Al^{25}. Scobie and Lewis (29) have reported an electron capture branch in the decay of C^{11}.

B. Nuclear Matrix Elements

Fermi (30) first formulated a theory describing the interaction involved in beta decay. By the use of first-order perturbation theory, the transition probability per unit time for a transition from a given initial state to a given final state is

$$N = \frac{2\pi}{\hbar} \left(| \langle f | H^{int} | i \rangle |^2 \right) d\rho/dE ,$$

where $d\rho/dE$ is the density of final states per unit of total energy, and H^{int} is the interaction Hamiltonian for the system. For the process of beta decay, $n + \nu \rightarrow p + e^-$, H^{int}

is considered to arise from a point interaction, where its matrix element is then proportional to the probability amplitudes of the interacting particles at a point and integrated over all points in the interaction volume, or nucleus. The interacting particles are described by 4-component spinor wave functions, and the requirement that the interaction be Lorentz invariant limits the possible number of bilinear covariants to five: the scalar, 4-vector, antisymmetric 4-tensor, axial 4-vector, and pseudoscalar. For allowed transitions, such as those in mirror nuclei, any velocity-dependent terms are neglected, effectively making the interaction a non-relativistic limit. Under this limit, the scalar and axial vector terms reduce to the unit interaction, 1, the tensor and axial vector terms reduce to the spin interaction, $\vec{\sigma}$, and the pseudoscalar interaction is neglected. In the non-relativistic limit also, the light particle, or lepton, wave functions are approximately constant over the nuclear volume so that the square of the allowed transition matrix element is as follows:

$$|\langle f|H^{int}|i\rangle|^2 = F(Z,p)\left| C_F \psi^* \varphi \int d^3x \Psi^* \Phi + C_{GT} \psi^* \vec{\sigma} \varphi \int d^3x \Psi^* \vec{\sigma} \Phi \right|^2,$$

where C_F is the Fermi coupling constant, giving the strength of the combined scalar and vector interactions, C_{GT} is the Gamow-Teller coupling constant, indicating the strength of the combined tensor and axial vector interactions, φ's are

the wave functions of neutral particles, F(Z,p) indicates the nuclear coulomb effect on the electron wave function in the nucleus, capitalized wave functions are those of the nucleons, and the superscript "*" indicates complex conjugation of the particle wave functions. The integrals $\int d^3x \Psi^* \Phi$ and $\int d^3x \Psi^* \vec{\sigma} \Phi$ are called the nuclear matrix elements and are commonly abbreviated to $\int 1$ and $\int \vec{\sigma}$, respectively. It is presently thought that the Fermi interaction consists only of the vector interaction, while the Gamow-Teller term is due to the axial vector interaction (31, 32).

The density of final states in the interaction volume is found to be

$$d\rho/dE = \frac{V^2 16\pi^2}{h^6} (mc)^6 p^2 q^2 dp \frac{1}{mc^2} ,$$

where p is the electron momentum and q is the neutrino momentum. Summing the transition matrix over the lepton spins, the transition probability per unit time of emitting an electron in the momentum range dp is, then,

$$N(p)dp = \frac{2\pi}{\hbar} F(Z,p)\left[C_F^2 |\int 1|^2 + C_{GT}^2 |\int \vec{\sigma}|^2\right] \frac{(mc)^6}{4^2 h^6} p^2 q^2 \frac{dp}{mc^2}$$

$$= (\text{constant})\left[C_F^2 |\int 1|^2 + C_{GT}^2 |\int \vec{\sigma}|^2\right] F(Z,p)\, p^2 q^2 dp .$$

But, $q = W_o - W$, $p^2 dp = pW dW$, where $W = \sqrt{(1 + p^2)}$ is the total electron energy expressed in units of mc^2, and W_o is the maximum total electron energy. Thus, integrating over

the final electron momentum states, the total transition probability is

$$N = \frac{\ln 2}{t_{\frac{1}{2}}} = (\text{constant}) \left[C_F^2 \left| \int 1 \right|^2 + C_{GT}^2 \left| \int \vec{\sigma} \right|^2 \right] \int_1^{W_o} F(Z,p)\, W_p (W_o - W)^2 dW.$$

The integral $\int_1^{W_o} F(Z,p)\, W_p (W_o - W)^2 dW$ is abbreviated $f(Z,W_o)$, and the product $f(Z, W_o)\, t_{\frac{1}{2}}$ is called the comparative lifetime of the transition. The equation

$$f\, t_{\frac{1}{2}} = (\text{constant})\, (C_F^2 \left| \int 1 \right|^2 + C_{GT}^2 \left| \int \vec{\sigma} \right|^2)^{-1}$$

shows that the comparative lifetime can be interpreted as a measure of the magnitude of the nuclear matrix elements.

In the case of mirror nuclei, both Fermi and Gamow-Teller interactions are allowed in the ground-state to ground-state transitions. It can be shown that these interactions have the following selection rules for a transition (5, pp. 677-679): nuclear spin change is 0 for Fermi; 0, $\pm$ 1 (no 0→0) for Gamow-Teller; and the parity must not change between initial and final states. It is seen, then, that the Fermi interaction involves the emission of leptons in a singlet spin-state with no orbital angular momentum carried away by the leptons, whereas the Gamow-Teller interaction describes emission in a triplet state, with no orbital angular momentum carried away by the leptons.

For a mirror pair the calculation of the nuclear matrix elements can be carried out, with that for the Gamow-Teller

matrix element dependent upon the nuclear model chosen. The calculation of the Fermi matrix element depends only on the assumption of charge symmetry of nuclear forces in the case of mirror doublets and it is equal to 1 for all mirror transitions (33, pp. 171-176). In the investigation of mirror nuclei, therefore, the determination of the maximum positron energy and the half-life for the transition lead to a value for the comparative lifetime of the transition which can then be used to calculate the Gamow-Teller matrix element for the transition. Experimentally determined Gamow-Teller matrix elements can then be compared to those calculated from different nuclear models to suggest which, if any, model represents the experimental situation. Any model favorably selected by such a comparison should also predict the energies, spin and parity assignments, and the wave functions corresponding to the excited states of the nuclei for which the comparisons are made. In the case of the wave functions, experimental evidence on the presence or absence of configuration mixing in the levels may be applicable in predictions of possible intensities of branching to the excited levels.

Prior to making any far-reaching comparisons, however, it is necessary to have assurance that the comparative lifetimes and the ratios of the squares of the coupling constants for Fermi and Gamow-Teller transitions are known accurately.

Kistner and Rustad (15) have determined the ratio of the squares of the coupling constants for at least the heavier mirror decays using data from pure Fermi decays and the "doubly closed shell ± 1 nucleon" transitions of O^{15} and F^{17}, for which shell model calculations of $|\int\vec{\sigma}|^2$ are thought to be reliable. The values of $|\int\vec{\sigma}|^2$ for Ca^{39} and H^3, when corrected for magnetic moment effects, agree with the experimental values, using the ratio which was determined to be $C_{GT}^2/C_F^2 = 1.16$ in the last of a series of various approaches to the problem by different investigators (15, 34, 35, 36). Also lacking for the purposes of comparing the empirical Gamow-Teller matrix elements with calculated elements is the availability of calculations of Gamow-Teller matrix elements covering a large number of mirror nuclei and using many different nuclear models. Only a few such evaluations are available (33, pp. 171-176, 34, 37, 38, 39, 40).

C. Statement of the Problem

Following the discussion of the previous sections, the question is raised, what further investigation is desirable in the study of mirror nuclei? Clearly it is desirable to determine the values of the comparative lifetimes as accurately as possible. Since the errors in the best available values are rarely below five per cent, and commonly near ten per cent, and since the value of $f(Z,W_o)$ is quite sensitive

to variation in W_o, more accurate experimental determinations for W_o are desirable. The recent use of magnetic spectrometers for this purpose has brought more confidence into the values for W_o, but improvements are needed in the direction of obtaining better counting statistics on the spectral data, and in checking more closely for systematic errors in the equipment. The extensive survey by Welch (11) shows a need for higher counting rates and his results appear to exhibit an instrumental sensitivity change at about 2.7 Mev. However, because the resolution of his instrument is a factor of six or more better than that obtainable using scintillation methods while studying the same spectra, acceptance of his measurements for W_o is imperative at the present time. It is conceivable that developments in scintillation and magnetic spectrometer techniques will allow forthcoming measurements for W_o of higher reliability.

More calculation of Gamow-Teller matrix elements for all mirror nuclei is needed using all the presently conceived nuclear models. The calculations are not trivial except in the simplest schemes, but certainly the future efforts in this endeavor will be very meaningful.

Not to be overlooked in the experimental status of mirror nuclei is the determination of the transition rate. The measurements of $t_{\frac{1}{2}}$ have errors mostly between one and five per cent. Furthermore, the evidence of the presence or

absence of branching in mirror nuclei transitions is qualitative in all but a few cases. To have an accurate picture of the transition rate for the ground-state to ground-state transitions, then, not only must the total decay rate be known accurately, but the effects of branching by electron capture and ground-state to excited-state transitions need to be known. For example, a precisely known half-life value will not be accurate for description of the main transition if a weak undetected branch is present. The experimental picture of the decay interaction is subject, therefore, to inaccuracies arising from incomplete investigation of the scheme of decay.

The purpose of this experiment is in accord with the statements of the last paragraph. It is recognized that very little earnest investigation has been carried out in the past expressly looking for branches of ground-state to excited-state transitions in mirror nuclei. The observation of branches can be made in two ways: identification of secondary positron spectral groups by the appearance of the positron spectrum, or by identification of nuclear gamma rays following the branch transitions. The first method is not a desirable approach when scintillation methods are utilized since weak branches would escape notice due to the poor resolution of the spectrometer. A magnetic spectrometer, with its much better resolution, offers a better chance of

observing even fairly weak branches. However, it is difficult to observe weak low-energy beta groups since experimental difficulties always tend to give a larger number of low energy counts. These might then be interpreted as a secondary beta group.

Observation of the nuclear gamma rays following branching transitions is handicapped by the presence of large amounts of positron annihilation radiation and of the continuous gamma ray spectra obtained as a result of positron annihilation-in-flight and bremsstrahlung production. Certainly the observation of gamma rays in the vicinity of 0.511 Mev, the energy of annihilation radiation, would be hampered, especially if the branch should happen to be quite weak. If the transition occurs to an excited state of energy greater than 0.511 Mev, the gamma radiation following branching could be seen as a "bump" on the continuous spectrum from bremsstrahlung and annihilation-in-flight. Still, if weak branching occurs, the methods of spectrum analysis only recently available would be necessary to see such "bumps" due to high-energy gamma rays.

In this experiment, the identification of branching was made by searching for gamma radiation. The region around 0.511 Mev was cleared of most of the disturbance from annihilation radiation by a method described later, and this method also made possible better detection at higher energies.

The mirror nuclei investigated were chosen to be Na^{21}, Mg^{23}, Al^{25}, Si^{27}, S^{31}, and Ca^{39}. These nuclei can all be made rather easily by irradiating their naturally occurring elements in the X-ray beam of the Iowa State University Synchrotron. Na^{21}, Mg^{23}, Si^{27}, and S^{31} were chosen because of their relative purity of production from natural Na, Mg, Si, and S, respectively. Al^{25} was included in the investigation despite the fact that more Al^{26m} was produced during bombardment because no gamma rays from the decay of Al^{26m} are known to occur. Even though Kistner and Rustad (14) have placed a small upper limit on branching in the decay of Ca^{39}, this nuclide was included in the experiment because of its prominent role in recent investigations. Some K^{38} was expected to be present in the Ca^{39} investigation, but would not affect the energy range of interest.

II. EXPERIMENTAL INVESTIGATION

A. Development of the Method

The experimental method used to observe the gamma radiation following branching transitions in the mirror nuclei investigated underwent considerable evolution before it was considered adequate for use. When the problem was first considered, an energy spectrum analysis of the singles gamma radiation in the decay of Mg^{23} was made, using a NaI(Tl) scintillation crystal coupled to a photomultiplier tube as the energy-sensitive detector and an electronic 256-channel pulse-height analyzer for analysis of the gamma-ray spectrum. A more complete description of the detector system and the analyzer will be given in Section C of this chapter.

In the case of the decay of Mg^{23}, there was reason to suspect a positron transition to the first excited state of Na^{23} would be present from consideration of the spins and parities involved, and it was felt that this transition would be of appreciable intensity. A preliminary investigation of the ordinary (singles) gamma-ray spectrum indicated that, indeed, this branching transition may be present. At the expected gamma-ray energy of 0.440 Mev, just below the prominent photopeak of the 0.511 Mev annihilation radiation, a noticeable "bump" was seen on the spectrum, which is evident in Figure 13(a). An attempt was then made to estimate

the intensity of this gamma ray with respect to the annihilation radiation peak by obtaining a Mg^{23} spectrum of high precision and subtracting from this spectrum an equally precise spectrum of C^{11}, normalizing the spectra at the peak value of annihilation radiation. With both sources, the spectra were obtained by viewing the source through an aluminum absorber with a scintillation counter, the absorber being present to keep positrons from entering the crystal.

This technique of subtraction of two spectra showed only that the subtraction of two large numbers was not statistically effective in showing up a small difference. There were indications that the gamma ray in the Mg^{23} decay was present, but problems involving the effects due to the difference in end-point energies of the decays of Mg^{23} and C^{11} were undetermined and could have masked the identification of the gamma ray. Certainly, this method was not one in which a clear-cut observation of the gamma ray could be made. Using this method, too, the production of I^{128} in the detection crystal from neutron activation while the synchrotron beam was turned on would have had to be taken into account, since its intensity could have been different for the two singles spectra determinations.

Because of the fact that the singles spectra showed an enhancement of annihilation radiation by a factor of two compared to any gamma radiation present (there are two an-

nihilation quanta emitted per positron emitted in the decay compared to, at most, one gamma ray at a particular energy), a coincidence method was devised to try to depress the annihilation-to-gamma ratio. In one method (which was unsuccessful), the gamma radiation entering a NaI(Tl) detection crystal was accepted for energy analysis only if it was coincident with positrons entering an anthracene detection crystal on the opposite side of the source. The coincidence circuit used had a resolving time of two microseconds and was contained in the circuitry of the 256-channel analyzer. This technique did little to improve the observation of the possible gamma ray from the Mg^{23} decay because the resolving time of the coincidence circuit was too long. This allowed too many accidental coincidences to be analyzed. Also, the geometry used permitted some of the annihilation radiation originating in the anthracene crystal to be detected by the NaI(Tl) crystal.

The problem of observing the 0.440 Mev gamma ray from the decay of Mg^{23} was reviewed, and the conclusion was reached that a drastic reduction in the ratio of annihilation radiation to gamma radiation was necessary before any estimates of intensity of the branch transition could be made. One possible answer to the problem was to view the source with a NaI(Tl) scintillation detector but to make the positrons annihilate at some region of space from which the detector

could be shielded. An intensive effort was initiated to see if the positrons could be magnetically deflected from the detector or removed from the region around the source and made to annihilate at a known position or region away from the source and detector. If this were possible, the detector could be shielded from the region of annihilation and allowed to view the source without interference originating from the annihilation of the positrons in the decay.

The first attempt along this line of approach was based upon the work of Morinaga and Bleuler (41), who used magnetic deflection of positrons from the decay of P^{30} in an effort to reduce the gamma-ray background due to annihilation in flight while looking for a weak gamma ray in Si^{30}. Using a thin Na^{22} source, which emits a gamma ray in its decay to Ne^{22} as well as positrons, an arrangement similar to that of Morinaga and Bleuler was tested. A magnetron magnet was positioned between the source and detector so that positrons initially directed toward the detection crystal were deviated from this path by the magnetic field and made to strike an annihilator or the magnet pole pieces, both of which were shielded from the detector. Although some depression of the annihilation radiation peak was observed with respect to the intensity of the gamma-ray peak, the improvement was not sufficient for use in detecting the Mg^{23} gamma ray.

It was felt that the magnetron magnet did not have a

strong enough or extensive enough magnetic field to deflect the positrons sufficiently for the desired effect. A large "C" electromagnet, capable of producing a field of ten kilogauss and with pole pieces twenty inches in diameter was used next, with the source placed in the magnetic field and the detection crystal a short distance away, shielded from the pole faces. It was thought that this arrangement would cause the positrons to describe helical paths of small radius toward the pole faces where they would then annihilate. Comparisons of the annihilation radiation detected with the field on and off showed that very little annihilation radiation suppression was achieved. Measures were taken to correct such intervening factors as annihilation of the positrons in air, scattering of the positrons by air, annihilation in the source, and the shape of the magnetic field giving rise to a trapping effect leading to a magnetic bottle, but these corrective procedures in turn did not yield any further improvement.

The magnetic methods attempted, then, did not bring the desired results, and the development of the method again turned to the use of coincidence techniques. Since the previous coincidence method failed to depress the annihilation radiation mainly because of the slow resolving time of the coincidence circuit which allowed accidental coincidences to be intolerably frequent, a fast coincidence circuit was

constructed which had a resolving time of about 10^{-8} seconds. The detectors for the fast coincidence circuit consisted of two NaI(Tl) detection crystals coupled to 14-stage photomultiplier tubes and arranged so that the detectors were placed with their axes at a right angle. The source under investigation was placed at the apex of the angle and beyond any line connecting any portions of the detection crystals so that both annihilation photons (which are emitted in opposite directions) could not enter the two detectors. The analysis of the gamma radiation incident upon one crystal which was in fast coincidence with annihilation or gamma radiation incident upon the other crystal showed a marked improvement, for the case of Na^{22}, of gamma-ray intensity compared to the annihilation radiation intensity. However, application of this method to the decay of Mg^{23} did not allow clear observation of the gamma ray, but did indicate more strongly than had been done before that the gamma ray was present.

It was decided that further modification of the equipment was necessary on the basis of the above results. As it was, the equipment would register a gamma ray from the detector leading into the 256-channel analyzer which was coincident with annihilation radiation incident upon the other detector. The arrangement was symmetric, however, in that a gamma ray incident upon the second detector could allow

analysis of coincident annihilation radiation incident upon the first detector. An asymmetry was introduced into the system so that one detection channel responded only to the energies of incident radiation which were in the photopeak of annihilation radiation, and this channel gated the 256-channel analyzer which then analyzed coincident radiation incident upon the other detection channel.

A slow coincidence circuit, an amplifier, and a single-channel analyzer were incorporated in the system to provide the asymmetry needed as mentioned above. With the modification, the system had a manner of operation operation described below: Channel 1, consisting of a detection crystal and photomultiplier tube, was fed into the fast coincidence circuit and the amplifier and single-channel analyzer system. The outputs from Channel 2 were directed to the fast coincidence circuit and the single-channel analyzer of Channel 1 were directed into the slow coincidence circuit, whose output gated the 256-channel analyzer for analysis. Thus, with the window of the single-channel analyzer set to accept energies in the photopeak region of annihilation radiation, a signal from Channel 2 was analyzed only if it was in fast coincidence with radiation incident upon Channel 1 which had the same energy as annihilation radiation.

The experimental system just described above was the one used in the search for gamma rays in mirror nuclei. Using

Na^{22}, the coincidence spectrum obtained exhibited a great reduction of annihilation radiation intensity compared to that for the gamma ray, which can be seen by comparing Figures 10(b) and 11. The first use of this method to study the decay of Mg^{23} enabled the observation of the 0.440 Mev gamma ray with unmistakable identity and easily estimated intensity.

B. Sample Materials

The radioactive mirror nuclides for which the branching investigations were made in this experiment were produced by bombardment of their stable elements in the 45 Mev X-ray beam of the Iowa State University Synchrotron. The production of these nuclides was accomplished by means of the (γ,n) or $(\gamma,2n)$ photonuclear reactions. The reactions actually used were $Na^{23}(\gamma,2n)Na^{21}$, $Mg^{24}(\gamma,n)Mg^{23}$, $Al^{27}(\gamma,2n)Al^{25}$, $Si^{28}(\gamma,n)Si^{27}$, $S^{32}(\gamma,n)S^{31}$, and $Ca^{40}(\gamma,n)Ca^{39}$. In the case of $Al^{27}(\gamma,2n)Al^{25}$, the competing and more intense activity from the reaction $Al^{27}(\gamma,n)Al^{26m}$ was also observed, but this was not the situation for $Na^{23}(\gamma,2n)Na^{21}$, due to the long half-life of Na^{22} and the subsequent difficulty of observing it for the short bombardment and counting times used.

Not to be overlooked as competing photonuclear reactions were those of (γ,p) and (γ,pn). In all cases the (γ,p) process on the above target nuclei resulted in stable nuclei,

while for the (γ,pn) reaction, only Na^{23} and Al^{27} resulted in stable nuclei, although $Mg^{24}(\gamma,pn)Na^{22}$ was not expected to be troublesome due to the long half-life of Na^{22}. In the cases of Si^{28}, S^{32}, and Ca^{40}, the (γ,pn) reaction yielded Al^{26m}, P^{30}, and K^{38}, respectively. Of these radioactive products, only K^{38} was observed in the gamma-ray spectra, since it was the only activity with a branching transition of more than one per cent. The (γ,pn) reaction was expected to yield less activity than the (γ,n) reaction by at least an order of magnitude, so branching transitions of about five per cent intensity or more would have been necessary to have been observed by the method employed in the investigation. The decay of K^{38} was observed, as the positron decay is entirely a ground-state to excited-state transition, with the resulting gamma ray from A^{38} of 2.16 Mev. However, since this contaminating activity was present only in the investigation of branching in Ca^{39}, where the gamma-ray energy region close to 2.53 Mev was important, it was tolerated, for it did not affect the energy range of interest.

The effect of (γ,2n) reactions on Mg^{24}, Si^{28}, S^{32}, and Ca^{40} was not considered to be of great concern. Mg^{22}, while existent (42), has a half-life of only 0.13 seconds and so was not of concern after the delay of over one second in the analysis cycle occurring between the end of bombardment and the start of analysis in the experiment. The decay scheme

of Si^{26} is unknown (42), so its effect on the experiment was undetermined although, as was true for the other (γ,2n) reaction products, the amount of Si^{26} produced was about an order of magnitude less than that of Si^{27}, and any weak branching in the decay of Si^{26} would not have been readily noticeable. S^{30} is not known to exist, so presented an unknown effect in the investigation of S^{31}. Ca^{38} was present (43), but its decay had a branch with a gamma ray of energy 3.5 Mev, so did not affect the Ca^{39} investigation.

Contamination due to isotopic variations in the sample materials was not present in the studies of Na^{21} and Al^{25}, since stable Na and Al are mono-isotopic. Although the sample materials of Mg, Si, S, and Ca had more than one isotope, in all cases the mirror nuclide investigated was produced by the (γ,n) reaction on the most abundant isotope of each element, the photonuclear reactions on the other isotopes yielding either stable nuclei or nuclei which decayed by emitting negative electrons, for which there was no annihilation radiation with which the gamma rays of some of these decays could be in coincidence. Thus, even though some of the contamination resulting from the isotopic non-purity of the target elements were observed in the singles gamma-ray spectra of the investigations, it was absent in the coincidence spectra.

The samples were irradiated in the 45 Mev X-ray beam of

the synchrotron for a period equal to about three half-lives of the activities desired and were then transported by means of a pneumatic shuttle system to the experimental equipment for analysis, a distance of twelve feet. After analysis for a period equal to about three half-lives of the activities, the samples were drawn back to the irradiation position and the cycle repeated. As many as 1000 cycles were made in a single "run" in the investigation of the activities. The pneumatic shuttle tube consisted of a length of aluminum tubing with rectangular cross-section. The samples were transported in sample holders consisting of a balsa wood block with a cavity in it to accommodate the sample. Sample holders like that illustrated in Figure 1(a) were used for the Mg and Al samples, which were formed of laminations of thin sheets of metal. The sample holder pictured in Figure 1(b) is typical of those used with samples of Na, Si, S, and Ca. Not illustrated is the covering of one mil mylar film on each side of the holder at the site of the sample which protected the sample and sealed it from the air. One sample holder of each style was made with no sample, but was identical otherwise, these holders being used during the investigations to provide a monitor for the background activity produced in the sample holder by the X-ray beam of the synchrotron.

The samples were made thick simply to obtain as much

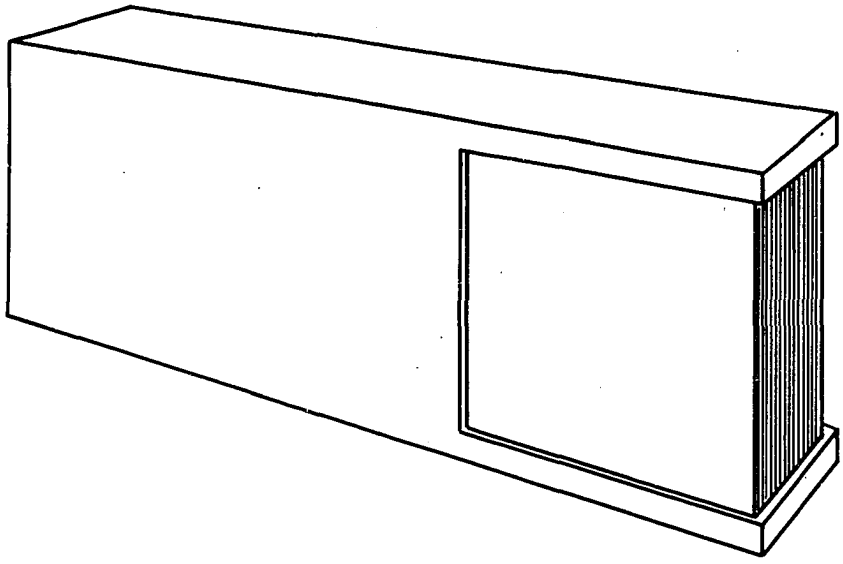

(a)

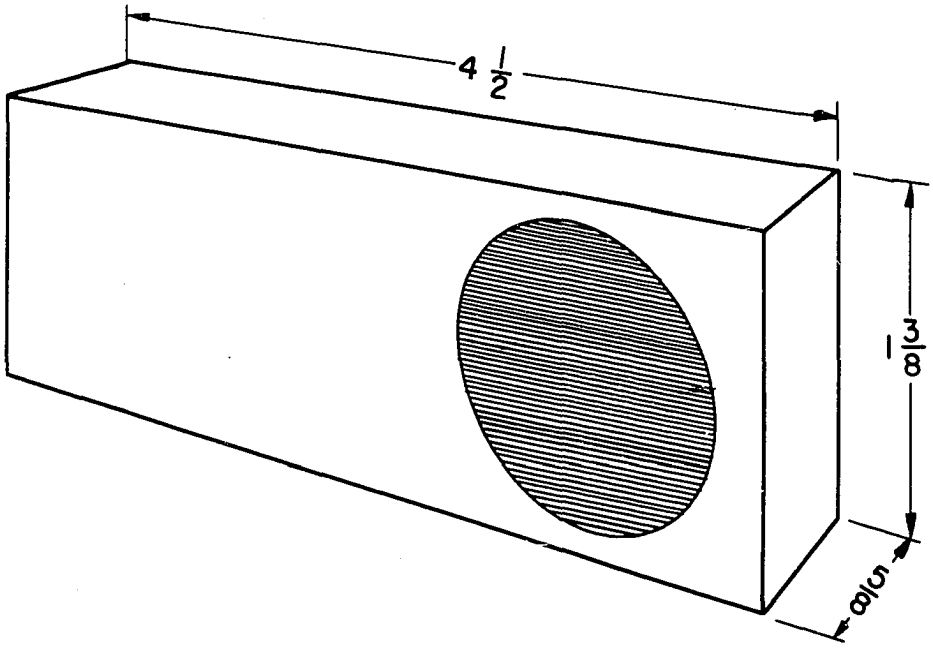

(b)

Figure 1. Drawings of the sample holders used in the experiment
(a) Sample holder for Mg and Al
(b) Sample holder for Na, Si, S, and Ca

activity as possible, and because the gamma radiation present was attenuated less by the samples than by the brass annihilator into which the samples were transported for analysis. The radiation thickness of the samples depended, of course, on the density of the sample materials. The linear thickness of the samples was one-half inch. The circular samples were 1-1/8 inches in diameter, and the laminated samples had dimensions of 1-1/2 inches by 1-1/8 inches.

The sample materials used in this experiment were all elemental. The Mg and Al samples consisted of thin sheets of metal, laminated to form a thick sample. The S sample was in the form of a large pellet made by pressing powdered sulfur in a hydraulic press to a pressure of 6000 pounds per square inch. The Si sample was shaped from an ingot of pure silicon, and the Ca sample was pieced together from slivers of multiply-distilled calcium metal stored in an argon atmosphere. The calcium sample developed a very thin outer layer of oxide upon exposure to the air, but covering the sample with mylar film arrested the oxide formation at an early stage. The Na sample was in the form of a molded pellet of sodium metal, which was molded and mounted in the sample holder while in a dry argon atmosphere.

Since sodium reacts so strongly with the water vapor in the air to form NaOH, a special sample holder was made to contain the sodium sample. This holder was identical in

dimension and shape to that pictured in Figure 1(b), but differed in that the half of the holder containing the sample was constructed of plexiglass, with a balsa wood skid running along the bottom so that it would move smoothly in the aluminum transport tube. This modification was made for the sodium sample in view of experience. An ordinary balsa wood sample holder had been used initially to contain the sodium sample, but the balsa wood proved porous enough to allow water in the air to come in contact with the sodium as well as the water bound in the balsa block. The resulting reaction corroded through the sample holder and exposed the sample to the aluminum of the shuttle tube. The corrosive action on the aluminum tube made the aluminum surface sufficiently coated to impede the transportation of the shuttle in the tube.

The elements used as samples in the investigations were all of good chemical purity, at least 99.5 per cent pure. The silicon and calcium samples were prepared at the Ames Laboratory of the Atomic Energy Commission, and the sulfur and sodium samples made from reagent grade materials. The magnesium sample was made of strips of spectroscopically pure magnesium metal, while the aluminum sample was made from strips of ten mil soft aluminum sheet metal, for which a spectrographic analysis showed very little impurity content.

C. Description of the Experimental Apparatus

1. Detection of gamma rays

The detection of gamma rays is dependent upon the interaction of the gamma rays with matter. There are three major modes for this interaction, the photoelectric effect, the Compton effect, and the pair production effect. In each of these modes, a photon is removed from an incident beam in a single event. The photoelectric effect is the dominant interaction at low photon energies, and its contribution to the total interaction probability increases as the Z of the absorbing material is increased. This effect describes the process by which the photon gives up all of its energy to a bound atomic electron which then breaks its binding to the atom with part of the energy and assumes the rest of the energy as kinetic energy. For the case of NaI, the photoelectric effect is dominant in the gamma-ray interaction at energies below 0.2 Mev.

The most important interaction to consider in terms of ordinary gamma-ray detection is that of the Compton effect. This effect is dominant in the interaction of gamma rays with materials for the energy in which gamma rays are most commonly found, which is around one Mev. The Compton effect consists of scattering of the incident photons by atomic electrons, where the energy of the incident photons is much

greater than the atomic binding energies of the electrons, and the electrons are treated as being unbound and at rest. For NaI, the Compton effect is dominant in the gamma-ray interaction for energies ranging from 0.2 Mev to 3 Mev.

Starting at 1.022 Mev and increasing in importance with energy until it dominates the interaction at high energies is the pair production effect, in which the photon disappears in a Coulomb field, creating an electron-positron pair which share a kinetic energy equal to the photon energy minus the mass energy of the pair. For NaI, pair production dominates in the gamma-ray interaction for energies higher than 3 Mev. A more detailed description of the interaction of gamma radiation with matter can be found in the literature (44).

For the purpose of detection, an important feature of the interaction of gamma radiation with matter is that ionizing particles are the results of the interaction. Thus, a detector which can detect electrons can also be used to detect gamma rays. Gas counters, such as Geiger counters and proportional counters, can be used to detect gamma radiation, but their efficiency of detection is very low at common gamma-ray energies due to the low probability of gamma radiation interacting with the detection volume or the inside surface of the container. However, Geiger counters can be used in many experimental applications for the detection of gamma rays. Proportional counters are quite similar to

Geiger counters but have the additional useful property that the height of the electrical output pulse is proportional to the energy lost in the counter by the ionizing particle. Thus, while Geiger counters can be used only to detect gamma rays, proportional counters can be used to analyze the energies of gamma rays, but with an efficiency of only about one per cent.

The three processes for the interaction of gamma rays with matter outlined above all produce ionizing particles but in conjunction with secondary, or modified, gamma radiation. The photoelectric effect produces a photo-electron which is accompanied by X-radiation in the atom from which the photo-electron was emitted. The Compton effect produces a so-called Compton electron, but in conjunction with a scattered photon, or modified photon. The production of pairs is always accompanied by annihilation radiation as the positron annihilates at rest or while in flight. Thus, the use of the proportional counter in analysis of the energies of gamma rays is limited not only by its inability to intercept a gamma ray, but also because the modified gamma radiation after an interaction is likely to escape the detection volume, leaving only a fraction of the energy of the original gamma ray detected by the counter.

Modern methods of gamma-ray detection utilize a device known as a scintillation counter. The scintillation counter

consists essentially of two parts: a scintillation medium, in which light is produced by moving charged particles, and a photomultiplier tube, which converts light into electrons by the photoelectric effect and multiplies the electrons to produce a detectable signal. The scintillating medium usually used for detecting gamma radiation is a solid single crystal of NaI(Tl). NaI(Tl) is especially suitable for this purpose in that it is a dense material which contains high-Z atoms (of iodine), and it produces a large number of light photons per Mev lost by ionizing particles, this number being independent of the energy of the particles. The density and high-Z content of a NaI(Tl) crystal are important when considering the probability with which gamma rays will interact with the crystal and which modes of interaction are used. The high-Z content favors complete absorption of gamma rays since the photoelectric and pair production effects are enhanced and the X-rays left by the photoelectric effect and the annihilation quanta resulting from pair production are rather easily absorbed. The Compton effect, however, gives rise to energetic modified photons which may more easily escape the crystal and prevent complete absorption of the gamma-ray energies. The fact that the light output of a NaI(Tl) crystal is linearly related to the energy lost in the crystal is a result from the property that the light produced in the crystal per Mev lost by the ionizing particles

is independent of the energy of the particles. This characteristic also allows any combination of the interaction processes in which the gamma ray is completely absorbed to produce the same light output.

The photomultiplier tube used in a scintillation detector provides two functions: conversion of the light output of a scintillating medium into an electrical impulse, and multiplication of this impulse to useful size. The light conversion is accomplished by means of a photo-sensitive surface, or photocathode, which produces photo-electrons when light is incident. At this point the multiplication process takes over, for the photo-electrons are accelerated to an energy of around 200 electron-volts and strike a secondary emission surface, or dynode, which emits secondary electrons. The number of secondary electrons is related to the number of incident electrons by a certain multiplication factor. After several stages of multiplication, the final secondary electrons are collected on an anode, and an electrical pulse of usable size is resultant. Since the conversion and multiplication processes provide outputs which are proportional to the inputs, the resultant pulse height at the anode is proportional to the amount of light emitted in the scintillating medium or, in the case of NaI(Tl), to the energy lost in the medium by the incident gamma ray. A scintillation counter is characterized by a resolution figure, defined in

terms of its nearly Gaussian response to incident mono-energetic radiation. This resolution arises mainly from the statistics encountered in the number of photo-electrons emitted from the photocathode, which commonly has a conversion efficiency of about ten per cent.

It is seen, then, that a scintillation detector utilizing NaI(Tl) as the detection crystal offers a more desirable detection system for gamma rays than a Geiger or proportional counter in that it has a high efficiency for detection and can be used for energy analysis of gamma rays at high energies. Two excellent detailed discussions of the properties of scintillation counters can be found in the literature (45, 46).

A scintillation counter exposed to mono-energetic gamma radiation produces a spectrum of output pulses rather than pulses of the same height. The appearance of the spectrum can be explained in terms of the interaction processes of the gamma radiation in the scintillation crystal. If NaI(Tl) is used as the scintillator, the spectrum for mono-energetic gamma-ray energies below 0.2 Mev will be nearly monochromatic, within the resolution of the detector. Since the photo-electric effect is the dominant type of gamma-ray interaction with the NaI(Tl) crystal at these energies, most of the interacting gamma rays will be absorbed completely, since only up to 25 per cent of the X-rays arising from the iodine atoms

can escape absorption by the crystal for gamma rays with energies as low as 0.03 Mev. Small peaks occurring at energies below the gamma-ray energies, the difference in energies being equal to the X-ray energy for iodine, represent events in which the X-rays did escape from the crystal and are called "escape peaks".

In the energy range of 0.2 Mev to about 3 Mev, the response of a scintillation counter to mono-energetic gamma rays will have a pulse height spectrum, which in its appearance consists of a prominent peak at the energy of the gamma rays, called a "photopeak", and a flat distribution of pulses at energies below that of the photopeak, connected with the photopeak through a spectral depression, or "valley". The dominant mode of gamma ray interaction in this energy range is that of the Compton effect for which only a fraction of the incident gamma rays lose all of their energy in the crystal, these events resulting in the photopeak. The photopeak also contains most of the results of the less probable photoelectric and pair production interactions in the crystal for this energy range. The flat distribution of the pulse heights at lower energies consists of Compton events in which the modified photons escape further absorption in the crystal, and corresponds, therefore, to a partial loss of energy by the gamma rays in the crystal.

At mono-energetic gamma-ray energies above 3 Mev, where

the interaction with the crystal most probably results in pair production, the spectrum has a small photopeak and is quite complex below the photopeak energy. There are secondary peaks 0.5 Mev and 1 Mev below the photopeak energy which correspond to single and double escape, respectively, of the annihilation quanta arising from the positron annihilation.

In actual experimental conditions, superimposed on the spectral appearances described above are effects of scattering by surrounding materials, which reduce the purity of monoenergetic radiation incident upon the crystal.

The gamma radiation found in most investigations is in the energy region in which detection is accomplished through the Compton effect interaction between the radiation and the crystal. If measurements of the source intensity are to be made for gamma rays, the gamma-ray spectrum provides a convenient method for intensity measurements. The approach used is to count the number of photopeak events present and relate this number to the total number of incident gamma rays of this energy by correcting for the detection efficiency of the crystal and its so-called "peak-to-total" ratio. The detection efficiency is expressed as the probability that an incident gamma ray will interact with the detection crystal, enabling its detection, and the peak-to-total ratio gives the probability that a gamma ray interacting with the crystal will lose all of its energy in the crystal and produce an

output pulse seen in the photopeak of the spectrum. Values of detection efficiency and peak-to-total ratios for NaI(Tl) are available as functions of gamma-ray energy, source distance from the crystal, and crystal size (45, 46, 47).

2. Physical arrangement

The experimental equipment which was used for the investigation was housed in the accelerator room of the synchrotron building, about twelve feet from the synchrotron. Except for the fast coincidence circuit, however, all the electronic circuitry which was used for analysis of the data was remotely located in the control room of the building, to which the appropriate signals were sent by means of coaxial cable. A top view of the experimental arrangement for the investigation is shown in Figure 2, where Figure 2(a) shows the equipment used for analysis of the samples and Figure 2(b) shows the arrangement for bombardment of the samples by exposure to the X-ray beam of the synchrotron.

The relative positions of the detectors and sample can be seen in Figure 2(a). The 1/16 inch brass cap on the end of the shuttle tube served as an annihilator, absorbing the positrons coming from the sample and causing their annihilation in a geometrical region where it was impossible for the annihilation quanta, which are emitted in opposite directions, to enter more than one of the detection crystals. The lead

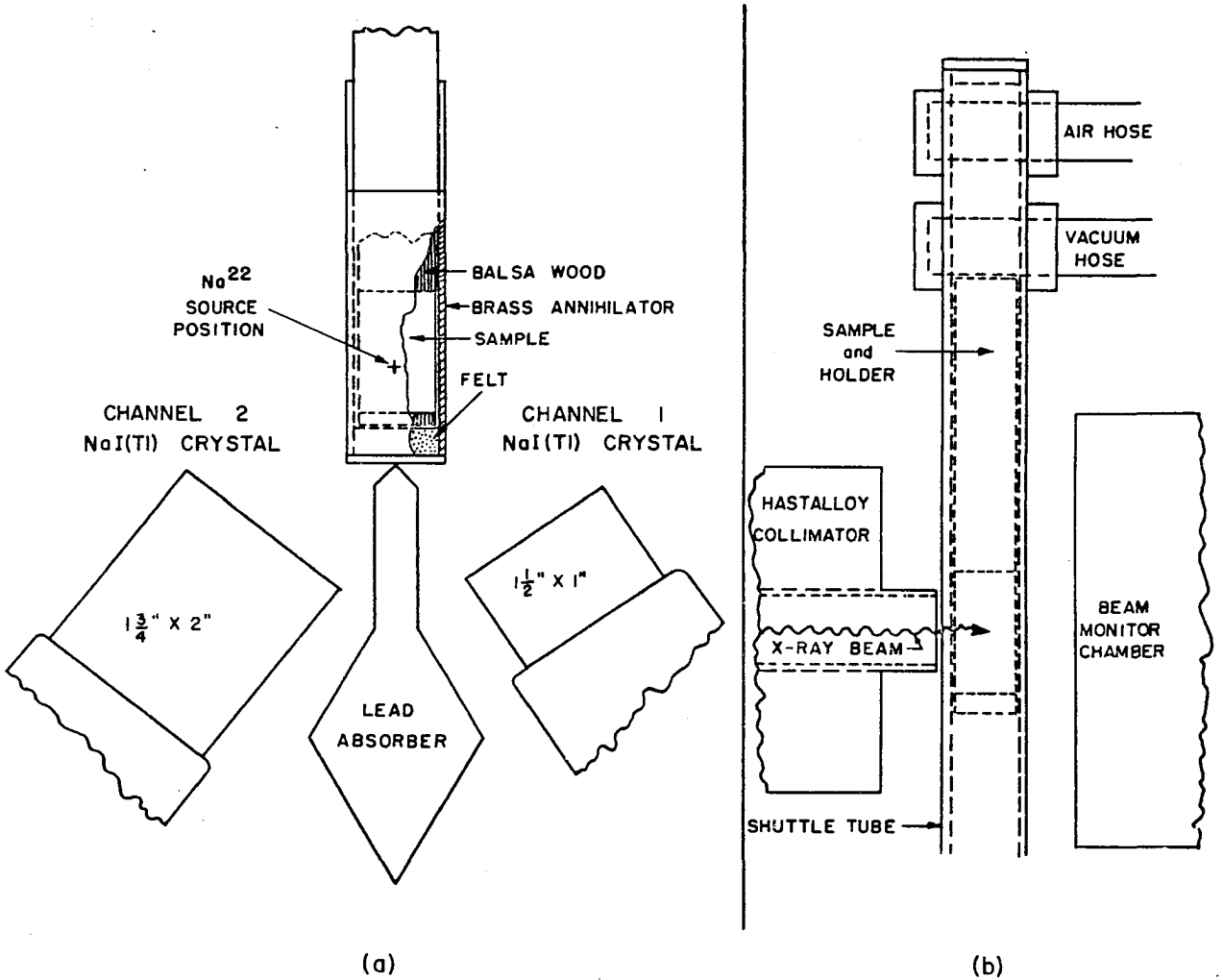

Figure 2. Experimental arrangement used in the analysis and bombardment of the samples
(a) Arrangement of equipment used in analysis
(b) Arrangement of equipment for bombardment

absorber between the two detectors served to prevent gamma rays scattering out of one detection crystal into the other, and producing an unwanted coincidence event. The scintillation counter with the smaller NaI(Tl) crystal was labelled "Channel 1" and served to detect annihilation radiation only. The other counter, with the larger NaI(Tl) crystal, was labelled "Channel 2" and detected the gamma radiation from the sample which was in fast coincidence with annihilation radiation incident upon Channel 1.

The solid angles subtended by the detectors near the center of the sample were about four per cent, with the larger crystal having a slightly larger solid angle than the smaller crystal. The detection apparatus was placed below the plane of the orbit of the circulating electrons in the synchrotron, and behind a wall of lead bricks for shielding against background radiation, and wax blocks and borax powder for shielding against synchrotron-induced neutrons. In this manner the room background and neutron-induced I^{128} activity in the NaI(Tl) crystals were reduced to tolerable levels. An oblique view of the equipment of analysis is shown in Figure 3. Visible are the two detectors, the fast coincidence circuit to the right rear of the picture, the lead absorber between the scintillation crystals of the two detectors, the shuttle tube with its brass annihilator cap, and the lead bricks used for shielding against room background.

Figure 3. Oblique view of the equipment used for analysis

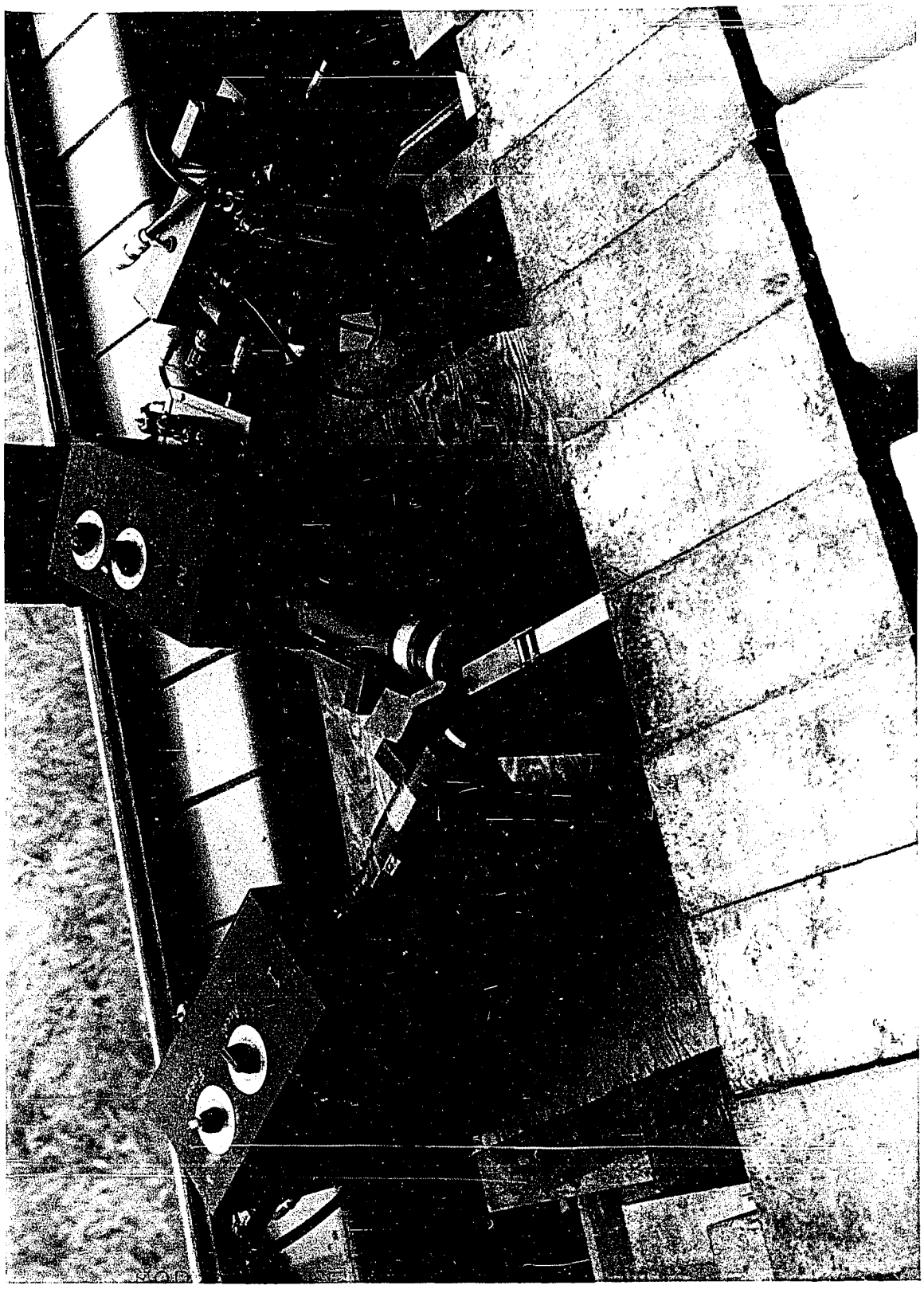

Because of the presence of the shielding and absorbing materials around the activated samples, the spectra obtained from the scintillation counters were expected to exhibit the effects of scattering from the surrounding shielding and absorbers of both annihilation radiation and the less intense gamma radiation, and also the effects from annihilation-in-flight radiation and bremsstrahlung resulting from the absorption of the positrons in the brass annihilator. The scattering of annihilation radiation from the shielding and absorbers was seen on all the spectra taken, including the coincidence spectra, since one annihilation radiation photon could be scattered and detected by Channel 2 in coincidence with the other photon directly incident upon Channel 1. Due to the proximity of the lead absorber to the detectors, in cases where the amplifier gain was turned high, as in Mg^{23}, the K X-ray from lead was seen as a result of the photoelectric interaction of gamma and annihilation radiation incident on the lead absorber and subsequent escape of the X-ray from the absorber.

The effects of annihilation in flight and bremsstrahlung were seen on both singles and coincidence spectra as continuous components which extended higher in energy than 0.511 Mev. These effects could be seen in the coincidence spectra because, in the case of bremsstrahlung, the motion of the positron in the brass annihilator could cause emission of

bremsstrahlung in the direction of Channel 2, while annihilation radiation was incident upon Channel 1 following the annihilation of the positron. The process of annihilation in flight emitted photons no longer opposite in direction and no longer restricted in energy to 0.511 Mev. Hence, it was possible either for the two quanta to be emitted in the directions of the two detectors and one lose 0.511 Mev in Channel 1, allowing coincident detection for Channel 2, or the photons could be detected simultaneously from scattering, provided 0.511 Mev was lost by one photon in Channel 1. There was one spectral disturbance which was peculiar to the singles spectra, and that was the additional continuous contribution due to the decay of neutron-induced I^{128} in the NaI(Tl) crystal. Since the crystals were shielded from each other, no coincidences due to the I^{128} decay were possible, but this decay was noticed on the singles spectra. It was more intense near the end of a day-long bombardment than at the beginning of the day, since the 25 minute half-life required appreciable time to reach its maximum activity.

The experimental arrangement seen in Figure 2(a) had the asymmetry desired in the experiment, for Channel 1 was set to respond only to annihilation radiation, so that any annihilation radiation seen in Channel 2 was not in coincidence with annihilation radiation incident upon Channel 1, due to the geometrical arrangement of the detectors. A small

amount of annihilation radiation was expected in Channel 2, however, and could arise in three ways. If the gamma ray was more energetic than annihilation radiation, it could enter the detection crystal of Channel 1 and lose only part of its energy. If this amounted to approximately 0.511 Mev, it could trigger an analysis of coincident annihilation radiation incident upon Channel 2. This process is illustrated in Figure 11, which shows the Na^{22} coincidence spectrum and exhibits the 0.511 Mev peak superposed upon the gamma-ray spectrum of the 1.28 Mev gamma ray in the decay of Na^{22}. Also, bremsstrahlung resulting from the absorption of the positrons in the brass annihilator could enter Channel 1, lose 0.511 Mev in the detection crystal, and permit analysis of annihilation radiation entering Channel 2. The third way that annihilation radiation could be analyzed in Channel 2 would be for it to be accidentally coincident with annihilation radiation detected in Channel 1, the radiations arising from two different positron decays occurring within the resolving time of the fast coincidence circuit. The annihilation radiation analyzed in Channel 2 as a result of these three processes was of low enough intensity so that it did not seriously interfere with the desired function of the arrangement, which was to permit analysis of gamma radiation detected in Channel 2 in coincidence with annihilation radiation detected in Channel 1.

The determination of the solid angle subtended by Channel 2 was necessary for each experimental determination. Since the expression for the branching ratio of a positron transition using the coincidence technique employed here involved the knowledge of this solid angle, the solid angle was determined experimentally by using a source of known branching ratio. Na^{22} was the source used here, since it decays almost entirely to the first excited state of Ne^{22}, and so has a branching ratio of nearly 100 per cent. In the determination of the solid angle, the Na^{22} source, which was a point source inside a cylindrical brass annihilator, was placed for analysis at the position shown in Figure 2(a), near the center of the sample when it was in the counting position. To do this, of course, the shuttle tube had to be removed. It was assumed throughout the investigation that the two geometries of analysis could be made equivalent. The geometries were made reproducible by means of templates which were used in arranging the equipment for each experimental run.

The experimental arrangement for bombardment of the sample can be seen in Figure 2(b). The connections for air and vacuum to the shuttle tube are shown, where the air valve was opened to blow the sample to the other end of the tube for analysis, the trip taking less than a second, and the vacuum valve was opened to draw the sample back into

bombardment position, the return trip taking about five seconds. The X-ray beam incident upon the sample was collimated to 3/4 inches in diameter, so that very little activity was induced in the sample holder. After passing through the sample, the beam was monitored by an ionization chamber, and the response of the monitor was recorded for each series of bombardments as indicative of the amount of activity produced in the sample.

3. Electronics

The block diagram of the electronic circuitry used in this investigation is shown in Figure 4. A coincidence event is illustrated with the gamma ray from a decaying nucleus entering the detection crystal of Channel 2 and the positron annihilating after coming to rest with one annihilation photon entering the detection crystal of Channel 1. The photomultiplier tubes which were used in the investigation were the 14-stage RCA 6810A tubes and gave a ten volt signal from the anodes into a 270 ohm load for annihilation radiation with a photocathode voltage of about -2300 volts. The anode signals from both detectors were fed directly into the fast coincidence circuit through coaxial cables of equal length. The output of the fast coincidence circuit was amplified and pulses arising from coincidences discriminated from singles pulses. The linear amplifier used for this

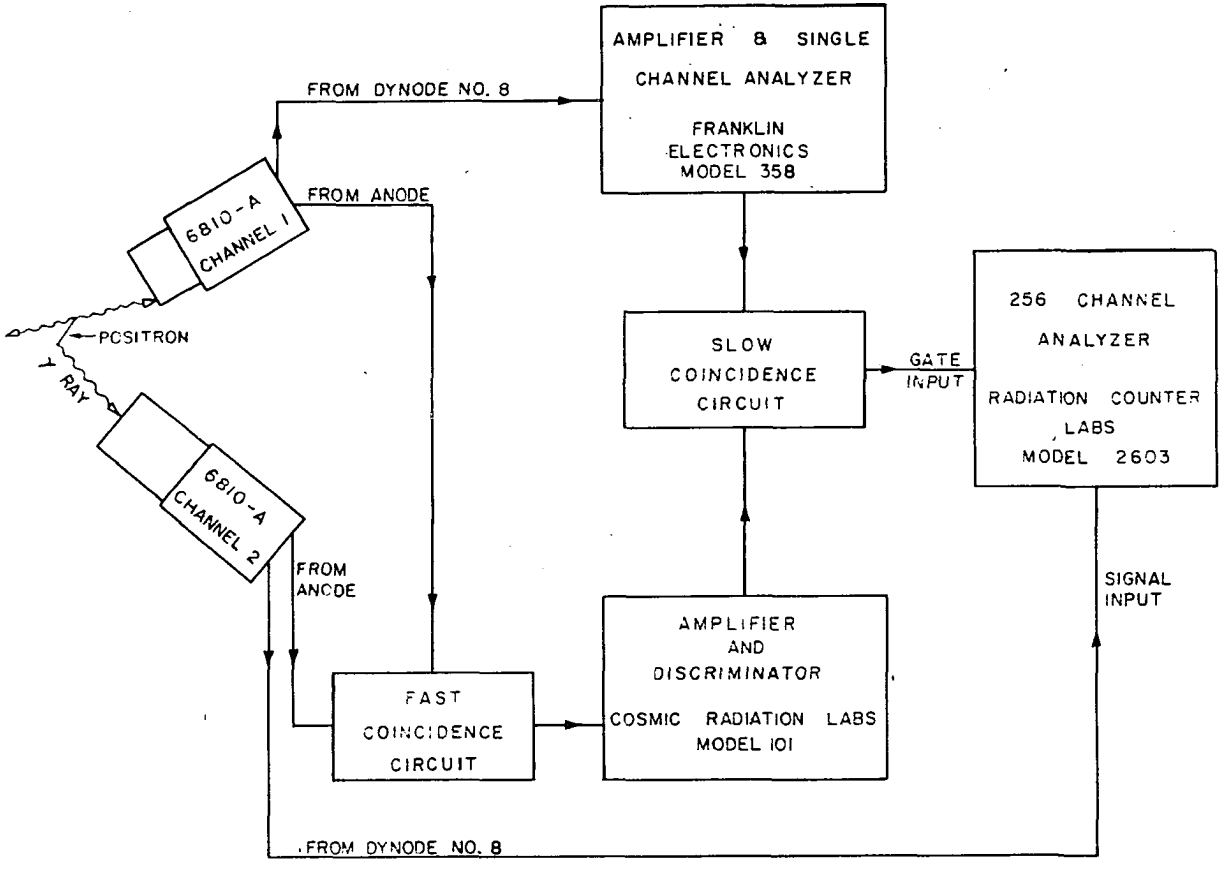

Figure 4. Block diagram of the electronic circuitry used for coincidence measurements

purpose was a Model 101 amplifier, obtained from Cosmic Radiation Laboratories, Blue Point, New York. This amplifier, which was a non-overloading amplifier, was of the Chase-Higinbotham design (48). The negative output from the discrimination section of the Model 101 amplifier was directed into one of the inputs of the slow coincidence circuit.

Each channel had two detector output signals, that from the anode, which had a fast rise time and large pulse height making it ideal for application to the fast coincidence circuit, and the eighth dynode signal, which was a small signal and could be amplified for pulse-height analysis. The eighth dynode signal from Channel 2 was directed to the A-61 amplifier of the 256-channel analyzer. The eighth dynode signal from Channel 1 was amplified and analyzed by a single-channel analyzer, both functions being performed by a Model 358 amplifier obtained from Franklin Electronics, Inc., Bridgeport, Pennsylvania. This amplifier was also non-overloading and was patterned after the Oak Ridge National Laboratories DD-2 Amplifier (49, 50). The single-channel analyzer was set to select pulses in the photopeak region of annihilation radiation. Its output was directed into the other input of the slow coincidence circuit. Hence, the slow coincidence circuit produced an output when annihilation radiation was detected in Channel 1 in fast coincidence with gamma radiation detected by Channel 2. The slow coincidence

circuit output was used to gate on the 256-channel analyzer to allow analysis of the Channel 2 signal.

The schematic diagram of the detector circuitry is shown in Figure 5. The voltage divider network for the 6810A photomultiplier tube is shown, along with the circuitry used for providing the signal from the eighth dynode. The anode output pulses were fed with direct coupling into the fast coincidence circuit. The eighth dynode was the last dynode not to be shunted to ground by a condenser, and was used to provide a second output signal for the functions not involving the fast coincidence circuit. This signal was tapped from the eighth dynode with a coupling network which gave a desirable shape to the signal. Since the small dynode fluctuation during the electron multiplication process provided a positive signal, this signal was inverted and amplified by the 6CB6 to provide a proper signal for amplification and pulse-height analysis. The 6AU8 was used as a White follower to drive the signal into the long coaxial cable leading from the accelerator room to the control room where the subsequent amplification and analysis was made.

Figure 6 is the schematic diagram of the fast coincidence circuit used in the investigation. The circuit was built according to the design of Bell, Graham, and Petch (51), and was in reality an adding circuit to the extent that two simultaneous inputs provided an output pulse twice as large

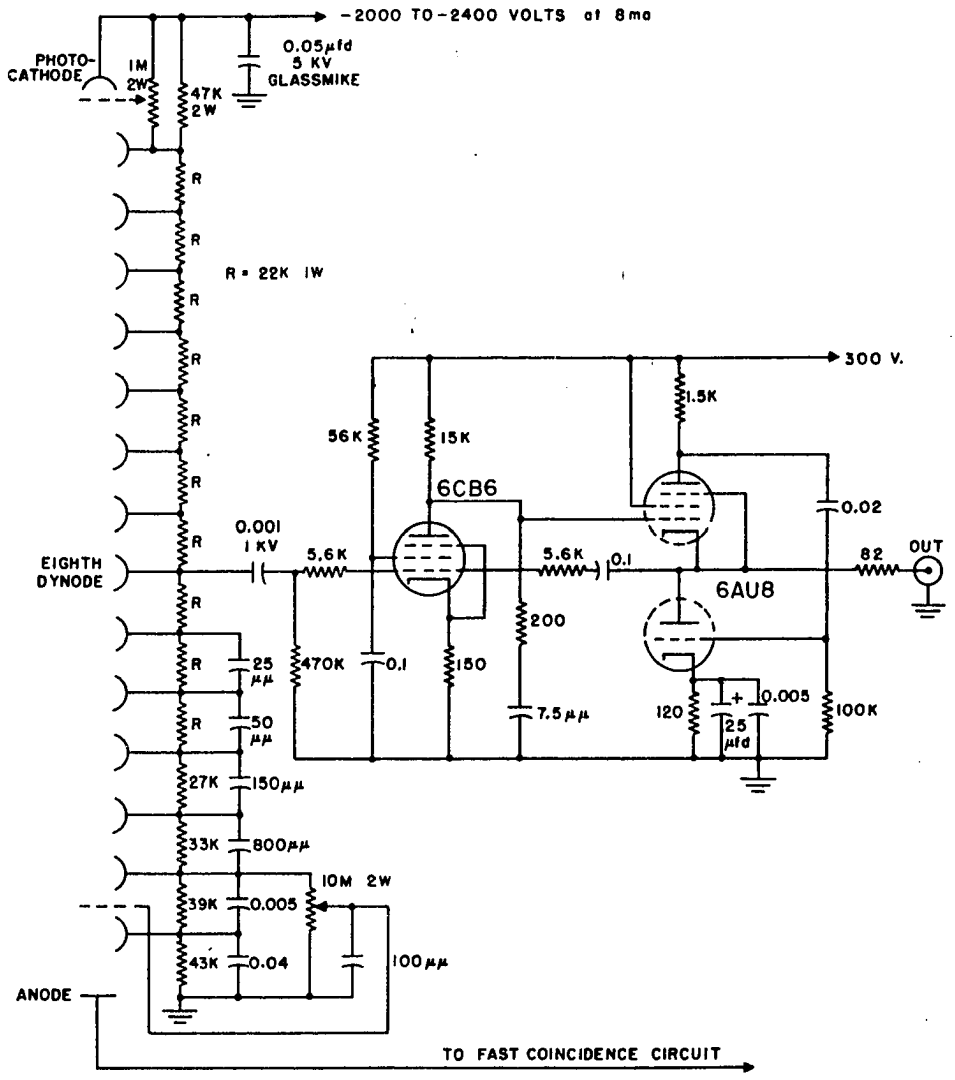

Figure 5. Schematic diagram of the photomultiplier tube voltage divider and the electronic circuitry for the eighth dynode output

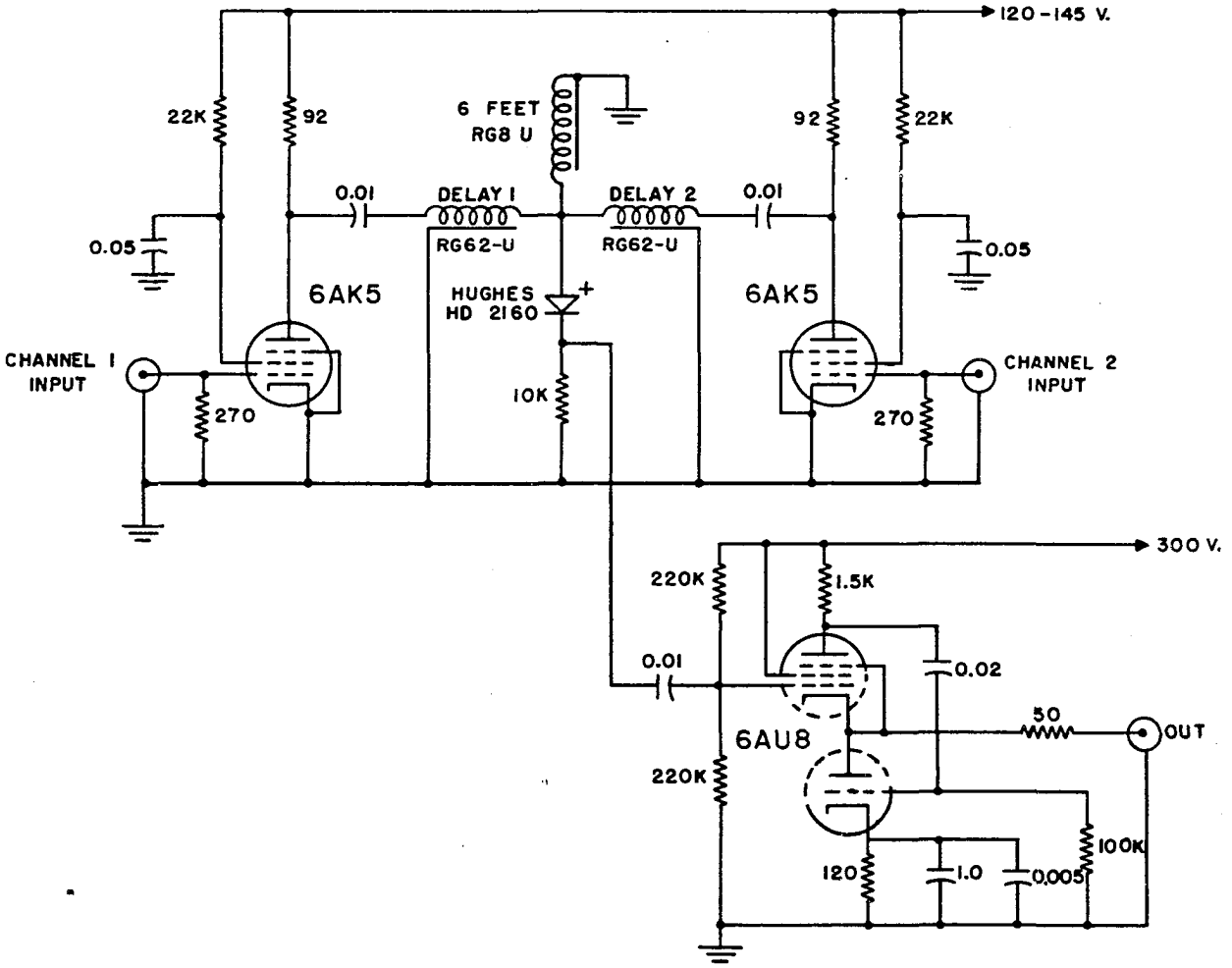

Figure 6. Schematic diagram of the fast coincidence circuit

as that for a single input. The 6AK5 tubes at each input acted as limiters, whose function was to invert and shape the input pulses, which were negative in polarity and of variable height, into flat-topped positive pulses which rose suddenly and had a long duration determined by the duration of the input pulses. The resulting pulses were further shaped by the 50 ohm RG8-U shorted delay line to shorten them to about 10^{-8} seconds duration. If two pulses appeared at the inputs within this time, an overlap of the individual pulses was present at the plate of the detection diode and an output signal with up to twice the single output pulse amplitude was seen, depending upon the degree of overlap present. The diode in the circuit was placed in a crystal oven (Model JK02, James Knights Co., Sandwich, Illinois) to achieve stability of its response and could have been biased to enhance the coincidence-to-singles ratio of output pulse heights to more than the factor of two. However, the bias was not necessary, and the amplitude discrimination to select coincidence outputs was performed after amplification by the Model 101 amplifier. The 6AU8 was again employed as a White follower to drive the long coaxial cable leading from the fast coincidence circuit in the accelerator room to the Model 101 amplifier located in the control room.

The resolving time of the fast coincidence circuit was

from 10 to 15 x 10^{-9} seconds for this investigation. This value was about the best possible for good coincidence efficiency in view of the reported decay time for a NaI(Tl) crystal of 25 x 10^{-8} seconds. A faster resolving time could be obtained, but then the long decay time of the crystal would play a part in causing some of the input pulses to be "jittered" out of coincidence.

One of the characteristics of this coincidence circuit which was evident upon inspection of the coincidence spectra obtained in the experiment was that of the low-energy cut-off. This effect arose in the first, or limiting, stage of the fast coincidence circuit as a result of insufficient input pulse height to cut off the 6AK5 tube, so that it then acted as an ordinary amplifier rather than a limiter, and had an output smaller than the limited output. Thus, a coincidence pulse in which one of the input pulses was too small for effective limiting action was not as large as that obtained by complete overlap of two limited pulses. It appeared instead to be identical to the output pulse resulting from incomplete overlap at the diode plate due to the inputs arriving just out of coincidence, and the spectral effect was thus one where the low energy pulses appeared to be out of coincidence.

The schematic diagram of the slow coincidence circuit is shown in Figure 7, and it was built according to a design

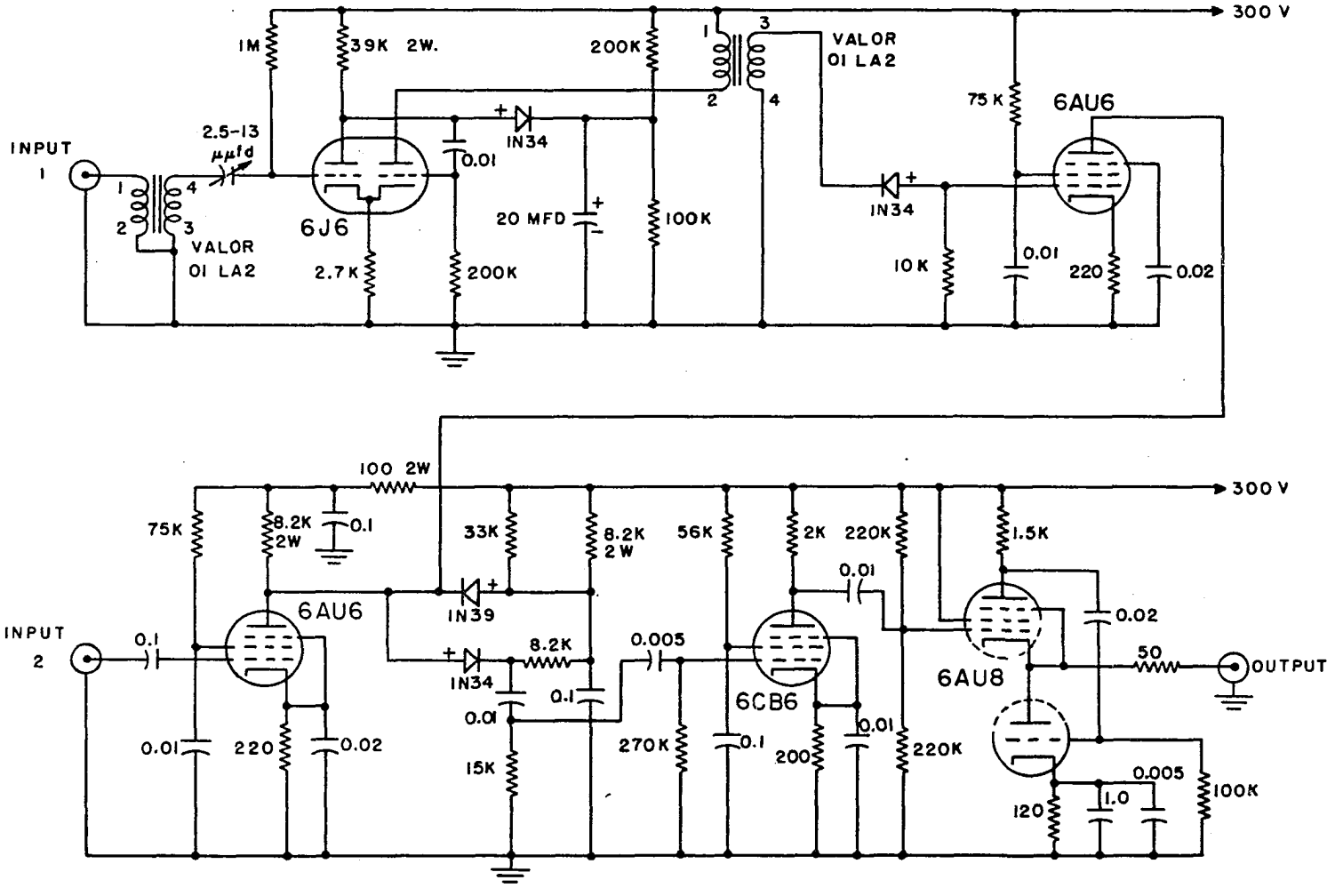

Figure 7. Schematic diagram of the slow coincidence circuit

by Garwin (52). In this circuit, the size of the coincidence output pulse was many times larger than the singles output pulse, so that discrimination between the two pulses was not difficult. The actual coincidence circuit consisted of the two 6AU6 tubes and the two diodes in their common plate circuit. The plate current of the two 6AU6 tubes was divided between the plate resistors on both sides of the 1N39 diode, with a slightly smaller resistor in series with the diode.

In quiescent operation, the 1N39 diode was conducting, and its forward resistance was the common AC load resistance of the tubes. For a single input, one of the 6AU6 tubes was cut off, reducing the plate current requirement to half the quiescent value. The output of such an event was seen across the low quiescent load resistance as the diode was cut off thus allowing the normal current to flow through the 8.2 kilo-ohm resistor not in series with the diode. For an additional coincidence input, however, the plate current in both tubes was cut off, resulting in a large output voltage. The 1N39 diode thus acted as a clamping diode for single inputs, allowing the common plate voltage to rise only enough to cut it off, and resulting in a small output. This made possible easy discrimination of the singles output.

The 1N34 diode acted as a discriminator against the output pulse resulting from a single input, with the result

that the size of the coincidence output pulse was about 100 times that of the singles output pulse. The 6J6 following Input 1 was used as a univibrator delay, in order to account for the different rise-times and times for pulse analysis in the two input channels. A delay of about one microsecond was used for the pulse from Input 1. The 6CB6 following the coincidence circuit was an amplifier, amplifying and inverting the positive coincidence pulse so that it was suitable for gating the 256-channel analyzer. The 6AU8 was a White follower, driving the cable leading to the analyzer gate. The slow coincidence circuit had a resolving time of about one microsecond, although it could be made faster. The time width of the input pulses was about 0.5 microseconds for each pulse, limiting the resolution capabilities of the circuit. With suitable input, the circuit could be made to have a resolving time of less than 10^{-8} seconds (52).

The 256-channel analyzer used in the investigation was a Model 2603 256-Channel Pulse-Height Analyzer obtained from Radiation Counter Laboratories, Inc., Skokie, Illinois. This analyzer employed analogue-to-digital conversion of the pulse-height-to-time type and contained a ferrite core memory capable of storing 65,535 counts per channel. The memory could be split into two 128-channel groups, and most of the spectra obtained during the investigation were analyzed over

128 channels only. The analyzer contained a non-overloading amplifier at its input and had coincidence provisions to enable gating the analysis of incoming pulses.

4. Cycling equipment

During an experimental run to obtain data, the accumulation of sufficient data required many cycles of bombardment and observation. The number of cycles in a day-long run ranged from 200 to 1200, depending upon the half-life of the nuclide under investigation. The cycle contained four timed intervals, the bombardment period with the sample in bombardment position, a short delay after bombardment to allow the sample holder to travel down the shuttle tube to the detection equipment, the analysis period, and a reset period in which the sample was drawn back into bombardment position, and the timers allowed to reset.

In detail, the bombardment period lasted about three half-lives for the nuclide under investigation and was timed by one or two adjustable timers which ran in tandem and were adjustable over the ranges 0-15 seconds and 0-120 seconds. During bombardment, a constant vacuum at the bombardment end of the shuttle tube kept the sample in bombardment position, and the photomultiplier tubes in the detection apparatus had their high voltage removed to avoid tube fatigue due to the high level of radiation in the accelerator room while the

beam was on. At the end of the bombardment period, the beam was shut off by biasing the injection pulse generator of the synchrotron, the vacuum valve was closed, and the air valve was opened to provide a blast of air to propel the sample to the other end of the shuttle tube and into position for analysis. A relay wired in parallel with the solenoidal air valve was activated along with the air valve and switched high voltage from a dummy load in the high voltage power supply to the photomultiplier tubes. A delay was then timed to allow transport of the sample and also to allow the photomultiplier tubes to come to equilibrium, and it usually lasted about one second. In some nuclides, this delay was increased in duration to allow very short-lived, unwanted activity to die out of the sample.

At the end of the delay period, the 256-channel analyzer was turned on to analyze the response from the detection apparatus, and the counting period timer started. During the counting period, as in the bombardment period, if a short-lived nuclide, such as S^{31}, was under observation, only the 0-15 second timer was used, while for the longer-lived nuclides, such as Na^{21}, the auxiliary 0-120 second timer was used in tandem with the 0-15 second unit. At the end of the counting period, the reset timer was started, the 256-channel analyzer was turned off, the air valve (and consequently the photomultiplier tube high voltage) was

turned off, and the vacuum valve was opened to allow transport of the sample back into bombardment position. At the end of this period, the bias on the synchrotron injection pulse generator was removed, allowing the beam to be switched on, all timers were reset, and the bombardment duration timer started. From this point, the cycle repeated.

The bombardment and counting period durations were set at about three times the half-life for the nuclide under investigation, the delay duration was about one second unless more time was necessary to allow unwanted short-lived decays to die out in the sample, and the reset duration was set for a period allowing ample time for the sample to be transported to the bombardment position from the counting position.

A schematic diagram of the cycle programming unit is shown in Figure 8. The auxiliary timers were the 0-120 second timers and the others had adjustable periods of 0-15 seconds. They were obtained from the R. W. Cramer Co., Inc., Centerbrook, Connecticut, as Type TE and Type TD1, respectively. The cycle programmer functions can be followed using the detailed description of the cycle above. The cycle programmer controlled the analyzer by acting as a switch which was closed during the counting period, and open the rest of the time. The analyzer was gated for the coincidence spectra by the coincidence circuitry through the delayed coincidence input to the analogue-to-digital converter and

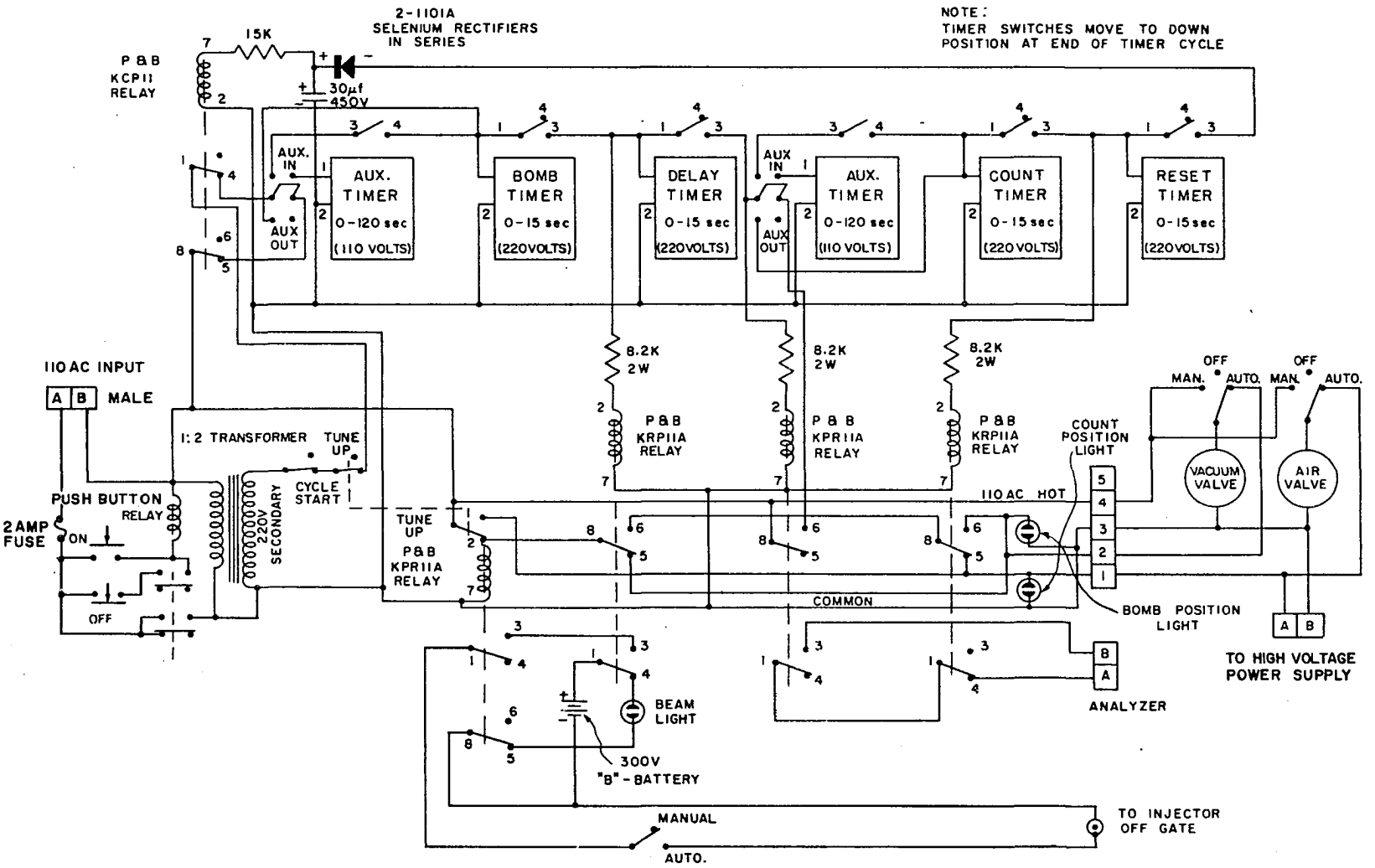

Figure 8. Schematic diagram of the cycle programming circuit

was turned off and on by the cycle programming unit through the prompt coincidence mode of the converter. The converter was switched to prompt coincidence (with no prompt coincidence input) and the short-circuit from the programmer during the counting period was shunted across the prompt coincidence switch, disabling this switch and allowing normal (or delayed coincidence, for the coincidence spectra) operation of the analyzer.

D. Tests and Calibration

Since the ability of the experimental arrangement to allow observation of gamma rays indicative of branching transitions in mirror nuclei depended highly upon the reliability of the fast coincidence circuit, tests were made on this circuit at the beginning of each experimental run to determine if adjustment was necessary so that it had a resolving time of about 15×10^{-9} seconds. This was done by putting coincident inputs into the circuit and running a coincidence curve for the circuit, which is a plot of coincidence counting rate versus time delay in either channel. By placing different lengths of RG62-U coaxial cable in one channel of the fast coincidence circuit, the pulse from that channel could be artificially delayed with respect to the other input pulse. When the delay was long enough to cause insufficient overlap of the added single pulses from each

channel to register a coincidence, the coincidence counting rate fell to zero. If the delay was well within the resolving time of the circuit, the counting rate was identical to that with no relative delay between the channels. The full time-width of the coincidence curve at half the maximum coincidence counting rate was equal to twice the resolving time of the circuit.

The most convenient way of obtaining a coincidence curve in this experiment was to remove the lead absorber between the detection crystals of the two channels and place an annihilation radiation source between the crystals. The source used here was Na^{22}. A coincidence curve resulting from the 0.511-0.511 Mev coincidences of annihilation radiation is shown in Figure 9(a).

The coincidences desired in the experiment were between gamma radiation in Channel 2 and annihilation radiation in Channel 1. The energies of the gamma rays which were of possible interest ranged from 0.35 Mev to 2.5 Mev. Since the rise times of the pulses coming from the limiters in the coincidence circuit were faster for high-energy radiation than for that at low energies, it was appropriate to test the coincidence circuit to see if this difference in rise times was great enough to cause high-energy events to be out of coincidence with the lower-energy annihilation radiation. In this test, the source of Na^{22} was used, but was

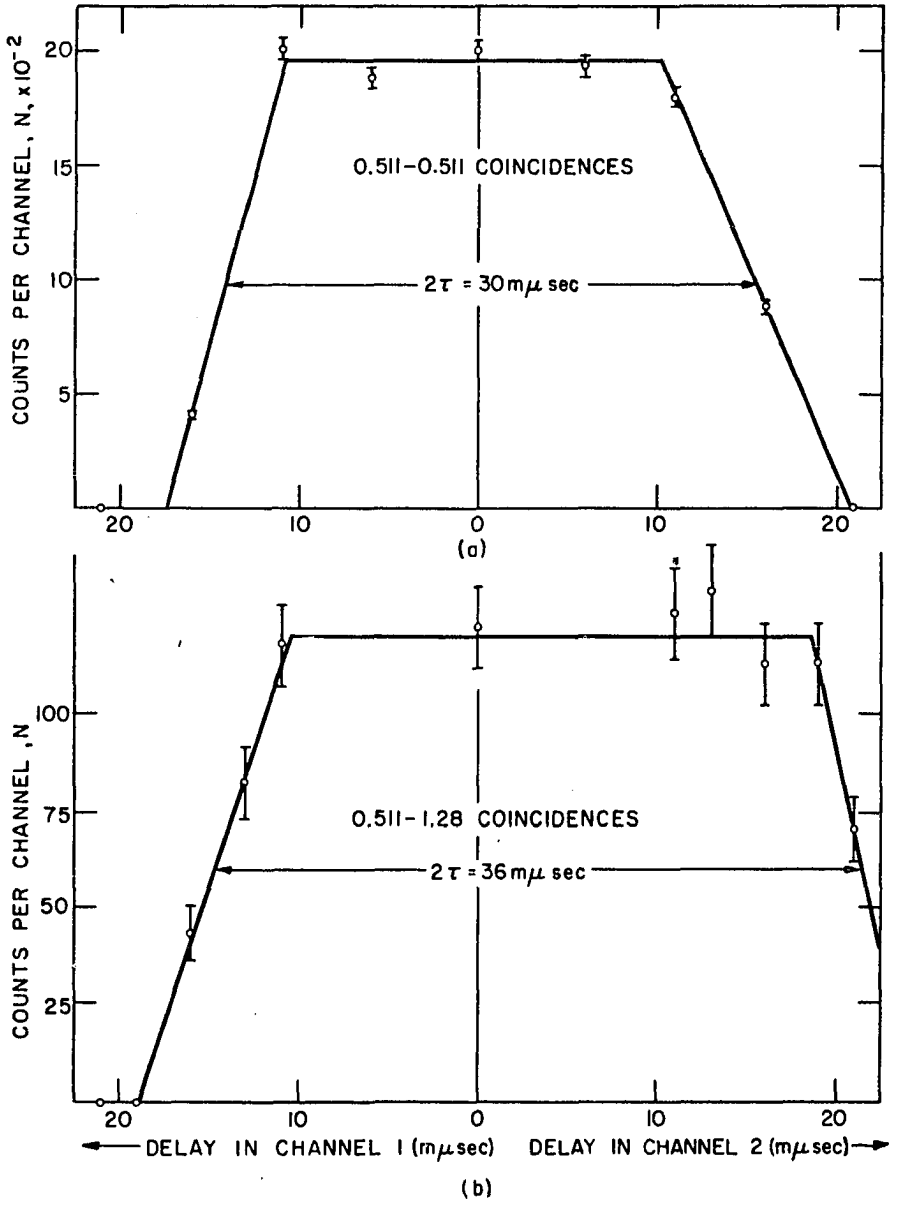

Figure 9. Coincidence counting rate as a function of delay
(a) Coincidence curve of 0.511 Mev - 0.511 Mev coincidences
(b) Coincidence curve of 0.511 Mev - 1.28 Mev coincidences

placed out of line with the crystals (see Figure 2(a)) and the lead absorber replaced between the crystals. The coincidence curve was determined for the coincidences between annihilation radiation in Channel 1 and the 1.28 Mev gamma ray in the decay of Na^{22} in Channel 2, and is shown in Figure 9(b). The conclusion reached as a result of this test was that there was a noticeable effect in the coincidence circuit arising from rise-time differences in the limiter pulses, which was seen as a shift of the centroid of the coincidence curve, making it asymmetric with respect to the delay origin, but that for zero relative delay between the coincidence circuit channels, the circuit would function satisfactorily over the energy range encountered in this investigation.

The stability of the electronic circuitry was held to a maximum by the location of as much of the circuitry as possible in the air-conditioned control room, the use of regulated line voltage for the high voltage power supply, and the provision for ventilation for the circuits and detectors which were located in the accelerator room. The coincidence circuit stability was assured by the use of the crystal oven to heat the diode to 75° Centigrade in order to keep its forward resistance constant and provide constant-height coincidence pulses. During a day-long run, the accelerator room became progressively warmer, which then correspondingly lowered the gains of the photomultiplier tubes,

but this effect was not serious and could be accounted for by frequent calibration of the response of the detectors.

Calibrations of the detectors were made over several energy ranges to be able to determine where gamma radiation might have been found. For the decays of Na^{21} and Mg^{23}, the calibration points were 0.356 Mev, 0.511 Mev, and 0.661 Mev, obtained from Ba^{133}, annihilation radiation, and Cs^{137}, respectively. For Al^{25}, Si^{27}, and S^{31}, the calibration energies were 0.511 Mev from annihilation radiation, 0.661 Mev from Cs^{137}, 1.28 Mev from Na^{22}, and 1.17 and 1.33 Mev from Co^{60}. For Ca^{39}, annihilation radiation was used for 0.511 Mev and Co^{60} used for 1.17, 1.33, and 2.50 Mev, the last energy being a result of a sum of the other two gamma rays incident upon the crystal. During an experimental run, the calibrations were taken at regular intervals to determine the effects of temperature-induced drifts in the detectors.

E. Experimental Procedure

The experimental procedure outlined here will be an account of a run for a mirror nuclide. The electronic equipment was turned on at least 12 hours prior to the start of the investigation to allow temperature equilibrium in the circuit components to take place. Appreciable drift during this warm-up was evident only in the first two or three hours. The last components to achieve stability were the

voltage dividers for the photomultiplier tubes, but these were heated and temperature equilibrium with the photomultiplier tubes was achieved in, at most, three hours.

After warm-up of the electronic circuitry was assured, the fast coincidence circuit was checked to give a resolving time of from 10 to 15 x 10^{-9} seconds. If the nuclide under investigation was of interest for energies lower than 0.511 Mev, the coincidence spectrum was checked using Na^{22} to make sure that spectral cut-off of the coincidence circuit was well below the energy region of interest. Since it was desired to have the resolving time of the coincidence circuit remain at about 15 x 10^{-9} seconds, the adjustment in the low-energy cut-off was made through the gains of the detectors.

The next step in the investigation was to determine the solid angle subtended by the detection crystal of Channel 2 at the sample position. This was done by using Na^{22} positioned as in Figure 2(a) near where the sample would be centered and consisted of analyzing the singles annihilation radiation spectra for both Channel 1 and Channel 2, and then analyzing the coincidence spectrum for the 1.28 Mev gamma ray in the decay of Na^{22}. The information from these spectra was used to calculate an empirical value for the solid angle of Channel 2, since the branching ratio of the decay of Na^{22} was known to be nearly 100 per cent. It can be noted here

that the same types of spectra were obtained for the nuclides under investigation, and the branching ratio was then determined using the solid angle found with Na^{22}.

The shuttle tube was positioned and the Channel 2 detector calibrated in the energy region of interest. Then, using the cycling system, a determination of singles spectra for both detector channels was made, after which a coincidence run was made. At the conclusion of each singles or coincidence run, the spectrum held by the 256-channel analyzer was read out and the beam dosage for the sample during the run was recorded. The coincidence run generally lasted ten times the number of cycles as did the singles runs, and was followed by two more singles determinations. At this time another calibration was made to determine if any drift had been experienced by the photomultiplier tubes. Also, since the singles spectra displayed the annihilation radiation peak, they were used for drift check and calibration. The second calibration was followed by a third singles determination, then an accidental coincidence run, differing from the first coincidence run only by the inclusion of 30×10^{-9} seconds delay in one channel of the fast coincidence circuit, so that true coincidences (those within the resolving time of the circuit) were no longer possible, but accidental coincidences were still possible at the same counting rate. Another singles determination was made at the conclusion of

the accidental coincidence run, and the above schedule was repeated, time allowing. At least two such day-long runs were made for all the nuclides under investigation, except for Ca^{39}. If it was thought desirable, another determination of the Channel 2 solid angle was made at the end of the day. In the case of Mg^{23} only, the accidental coincidence run was replaced by a run using C^{11}, to determine the rate of accidental coincidences and also to account for the shape and extent of the scattering peak displayed at low energies in the coincidence spectra.

Before, after, and sometimes during each coincidence run, a check was made on the inputs to the slow coincidence circuit. The height of the fast coincidence circuit singles pulses was monitored to give indications of malfunction of that circuit. The Franklin Amplifier was checked to see if its single-channel analyzer was set to straddle the annihilation radiation photopeak from the detector of Channel 1. Most of the spectra were taken on only 128 channels of the analyzer, which made possible a check on the Franklin Amplifier window settings by momentarily interrupting a coincidence run and using the other 128 channels for the check. In the case of Mg^{23}, where the gamma radiation was very close in energy to that of annihilation radiation, the importance of making a spot check on the single-channel analyzer settings was evident since to avoid destroying in

part the asymmetry of the experimental set-up, the window could not completely straddle the annihilation radiation photopeak without admitting some of the Mg^{23} gamma radiation, and instead was set to straddle only the upper two-thirds of the photopeak. This setting left the lower discrimination level on a steeply sloping portion of the spectrum where a small gain change would have a large effect in the counting rate from the window. Consequently, frequent checks were made for Mg^{23} to assure that the single-channel analyzer was adjusted properly.

The frequency with which singles spectra were analyzed was largely due to concern about the time-dependent background radiation visible only in the singles spectra. This background radiation was due partly to the build-up of I^{128} activity in the NaI(Tl) detection crystals by neutron activation, and partly to the long-lived activity built up in the sample holder. A blank sample holder was always given a singles run identical to that for the sample, and with a sufficiently long preliminary period of cycling so that the activity due to the holder could be accounted for, and also the intensity of the I^{128} activity estimated.

III. ANALYSIS OF DATA

A. Calculation of the Branching Ratio

The branching ratio of a transition is defined as the percentage of total decays that is contained in the transition. Thus, a determination of the branching ratio for a transition can be made by measuring the intensity of the transition and comparing this intensity with the measured intensity of the total decay. Since the nuclides under investigation here decayed by positron emission, the total decay intensity was measured by the amount of annihilation radiation detected, while the branching transition intensity was measured by the amount of gamma radiation detected for the gamma rays which followed branch decays.

The branching ratio can be found by examination of the singles spectra for the decay. This method is useful only where the gamma ray indicating the present of a branching transition is sufficiently different in energy from that of annihilation radiation and sufficiently intense, so that it is identifiable in the singles spectrum and its intensity can be measured. To calculate the branching ratio for the decay with this method, the following approach is used: the number of events found in the photopeak of annihilation radiation is equal to

$$N_{0.511} = 2N_0 \Omega (\epsilon P/T)_{0.511} ,$$

where N_0 is the intensity of the source, Ω is the solid angle subtended by the detector at the source, ϵ is the probability of detection of the incident radiation by the detection crystal, P/T is the peak-to-total ratio for the crystal, giving the probability that the radiation, if detected by the crystal, will lose all of its energy in the crystal and thus produce a count in the photopeak of the spectrum, and the 2 arises from the fact that there are two annihilation radiation quanta emitted per decay. The detection efficiency and peak-to-total ratio are functions of the same parameters (energy, crystal size, source distance), and so their product can be considered a function of energy for a given detection geometry.

The number of photopeak events found for the gamma ray is then

$$N_\gamma = \beta N_0 \Omega (\epsilon \, P/T)_\gamma \quad ,$$

where β is the branching ratio and $(\epsilon \, P/T)_\gamma$ is the detection efficiency times the peak-to-total ratio for the gamma ray. Solving these two equations for β gives

$$\beta = \frac{2N_\gamma \, (\epsilon \, P/T)_{0.511}}{N_{0.511}(\epsilon \, P/T)_\gamma} \qquad (1)$$

Hence, to find the branching ratio by analyzing the singles spectra, it is sufficient to determine the number of counts from the detector in the photopeaks of a spectrum from an-

nihilation radiation and the gamma ray, and to know the detection efficiencies for detection in the photopeaks of the spectrum.

This method was used only in the case of S^{31} in this investigation, since the branches found in the decays of Na^{21} and Mg^{23} did not result in gamma radiation which could be identified sufficiently well in the singles spectra.

The calculation of the branching ratio from the coincidence method is approached in a similar manner. The amount of annihilation radiation seen in the photopeak of the singles spectrum from the detector of Channel 1 is

$$N_{0.511}^{(1)} = 2\, N_o\, \Omega^{(1)}\, (\epsilon\, P/T)_{0.511}^{(1)} ,$$

while the number of events in the photopeak of a gamma ray in a coincidence spectrum from the detector of Channel 2 is

$$N_\gamma^c = 2\beta\, N_o\, \Omega^{(1)}\, \Omega^{(2)}\, (\epsilon\, P/T)_{0.511}^{(1)}\, (\epsilon\, P/T)_\gamma^{(2)} ,$$

where the superscripts (1) and (2) refer to the detection channel. Solving these equations for β gives

$$\beta = \frac{N_\gamma^c}{N_{0.511}^{(1)}\, \Omega^{(2)}\, (\epsilon\, P/T)_\gamma^{(2)}} . \qquad (2)$$

Hence, to find the branching ratio using the coincidence method, it is necessary to know the number of counts in the photopeaks of the gamma ray in the coincidence spectrum from Channel 2 and the annihilation radiation in the singles

spectrum from Channel 1, the solid angle subtended by the Channel 2 detection crystal at the source, and the detection efficiency of detecting the gamma ray in the photopeak region of the spectrum for Channel 2.

The determination of the number of counts in the photopeak region of a singles spectrum was done by adding the number of total counts per channel for the region and subtracting from this sum the estimated contribution resulting from room background, I^{128} activity, annihilation in flight, and bremsstrahlung. The estimate of this continuous background was made by extrapolating back into the annihilation radiation photopeak region the shape of the continuous gamma-ray spectrum found in the energies beyond the photopeak interval. The number of counts in the photopeak region of a gamma ray from a coincidence spectrum was determined in an analogous manner, when a gamma ray was easily observed. When it appeared as though no gamma ray was present, a smooth curve was drawn through the data connecting the energy regions surrounding the possible photopeak region, and the data of the photopeak region were compared to the values from the smooth curve to estimate an upper limit to the intensity of the branch under question.

The number of counts found under the photopeaks of the spectra were then normalized to give an equivalent counting rate before use in Equations 1 or 2. Since the coincidence

spectra were taken over longer periods of counting time than were the singles spectra, the amount of activity studied, or N_o, was not the same in each case. Each spectrum was taken using the same observation cycle, however, and it was necessary then only to normalize the counting rates observed to the amount of activity which was viewed by the apparatus during the register of each spectrum. This was done by normalization to unit beam dosage as determined by the dosemeter which was located behind the sample during bombardment. The reading on the dosemeter indicated the amount of beam which had passed through the sample, or the amount of activity built up in the sample. Thus, normalization to the dosemeter reading for each run gave the counting rate per unit activity produced, and made possible the comparison of counting rates for coincidence and singles runs.

The values for (ϵ P/T) were determined from the values available in the literature (45, 47). In the investigation for Mg^{23} only, Channel 2 had a 1-1/2 inches by 1 inch detection crystal, and the values used for (ϵ P/T) for Channel 2 were determined using different tabulations (45) than for the investigations of the other nuclides (47), for which the Channel 2 detection crystal had dimensions of 1-3/4 inches by 2 inches. For these other investigations, with the possible exception of Na^{21}, the greater (ϵ P/T) figure obtainable with the larger crystal made it more desirable to

use in the experiment. The values for $(\epsilon P/T)$ used in the investigation were obtained considering the sample or source to be a point source of gamma radiation located at the center of the sample, 4.2 cm. from the crystal. It was assumed that the values so obtained represented acceptable estimates for the extended-source samples which were actually used, since the dependence of $(\epsilon P/T)$ with source distance at this distance from the detection crystal is nearly linear over the sample extensions present in this investigation.

The solid angle for Channel 2 was determined experimentally using a source of Na^{22}, which has a known branching ratio. Equation 2 can be rearranged to solve for $\Omega^{(2)}$ in terms of the Na^{22} branching ratio so that it becomes

$$\Omega^{(2)} = \frac{N^{c}_{1.28}}{N^{(1)}_{0.511} (\epsilon P/T)^{(2)}_{1.28} \beta} .$$

where the branching ratio β is very close to 100 per cent. Hence, the solid angle determination required the knowledge of the number of events in the photopeaks of singles annihilation radiation and coincidence gamma radiation from Channels 1 and 2, respectively, and the detector photopeak efficiency of Channel 2 for the 1.28 Mev gamma ray. Figure 10 shows the singles spectra for Na^{22}, obtained in a typical solid angle determination, where Figure 10(a) is the Channel 1 spectrum and Figure 10(b) is the spectrum from Channel 2, both spectra obtained in 10 minutes of counting time. Figure

Figure 10. Singles gamma-ray spectra of Na^{22}

(a) Na^{22} singles spectrum from Channel 1 detector

(b) Na^{22} singles spectrum from Channel 2 detector

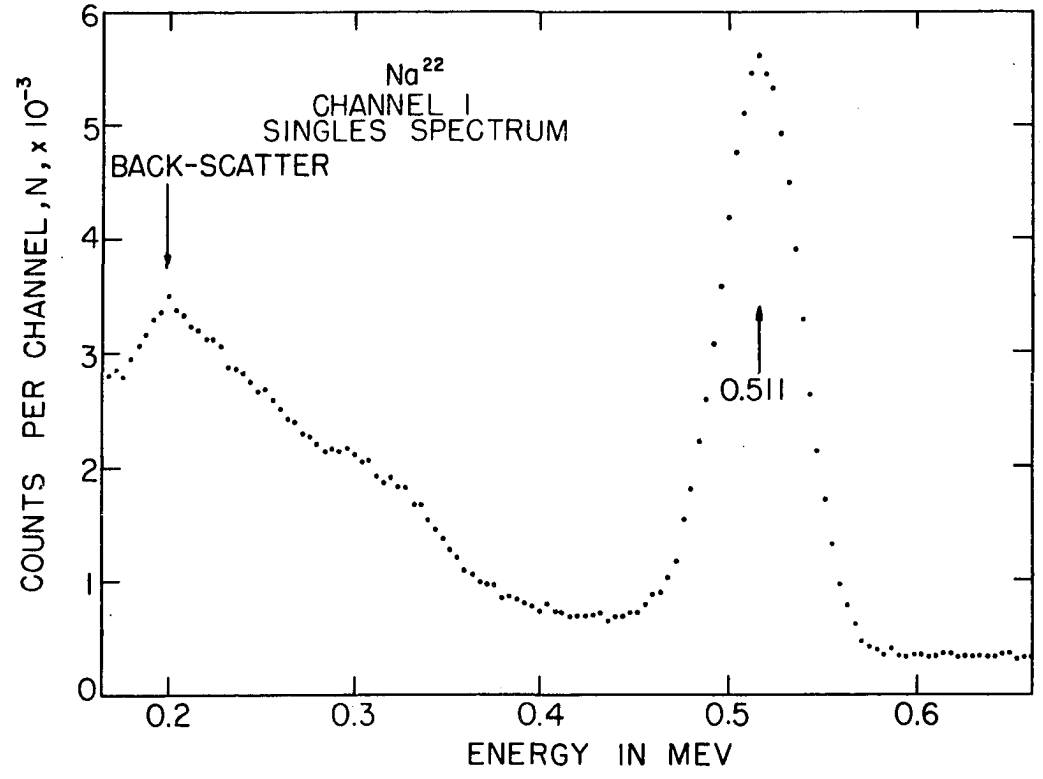
Na22
CHANNEL 1
SINGLES SPECTRUM
BACK-SCATTER
0.511
COUNTS PER CHANNEL, N, x 10-3
ENERGY IN MEV
0
1
2
3
4
5
6
0.2
0.3
0.4
0.5
0.6

(a)

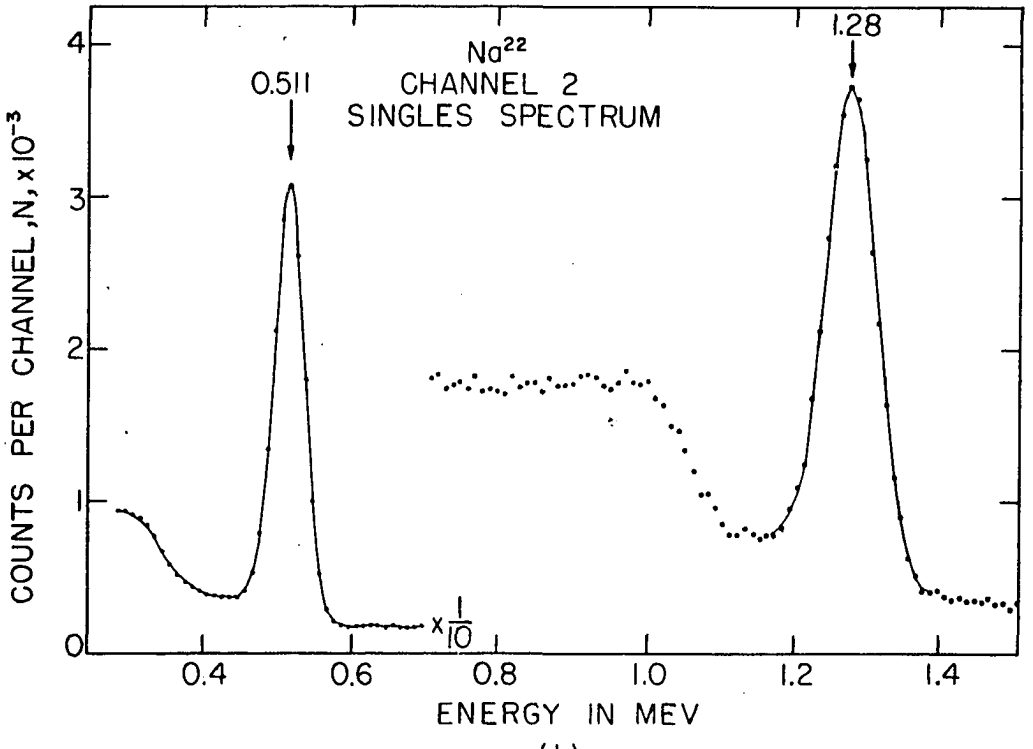
Na22
CHANNEL 2
SINGLES SPECTRUM
0.511
1.28
x 1/10
COUNTS PER CHANNEL, N, x 10-3
ENERGY IN MEV
0
1
2
3
4
0.4
0.6
0.8
1.0
1.2
1.4

(b)

11 shows the coincidence spectrum obtained in the same determination, and is the result of 50 minutes of counting time. The prominent photopeak of the 1.28 Mev gamma ray can be seen in both the singles and coincidence spectra for Channel 2, and it is seen that the intensity of the annihilation radiation was clearly depressed using the coincidence technique. The annihilation radiation seen in Figure 11 was mostly due to the Compton effect detection of the gamma ray which lost only 0.511 Mev in the Channel 1 detection crystal, with the coincident annihilation radiation detected by Channel 2.

The solid angles which were determined throughout the investigation were about 4-1/2 per cent for the experiments on all the nuclides except Mg^{23}. The solid angle used in the Mg^{23} experiment was about three per cent. This smaller value resulted from the fact that the crystal of Channel 2 was smaller in this case, and the single-channel analyzer of Channel 1 was set to straddle only a portion of the annihilation radiation photopeak, thus reducing the acceptance of coincidences and having the same effect as the reduction of the solid angle.

B. Corrections and Errors

There were several corrections applied in the analysis of the data. One of the corrections applied during the in-

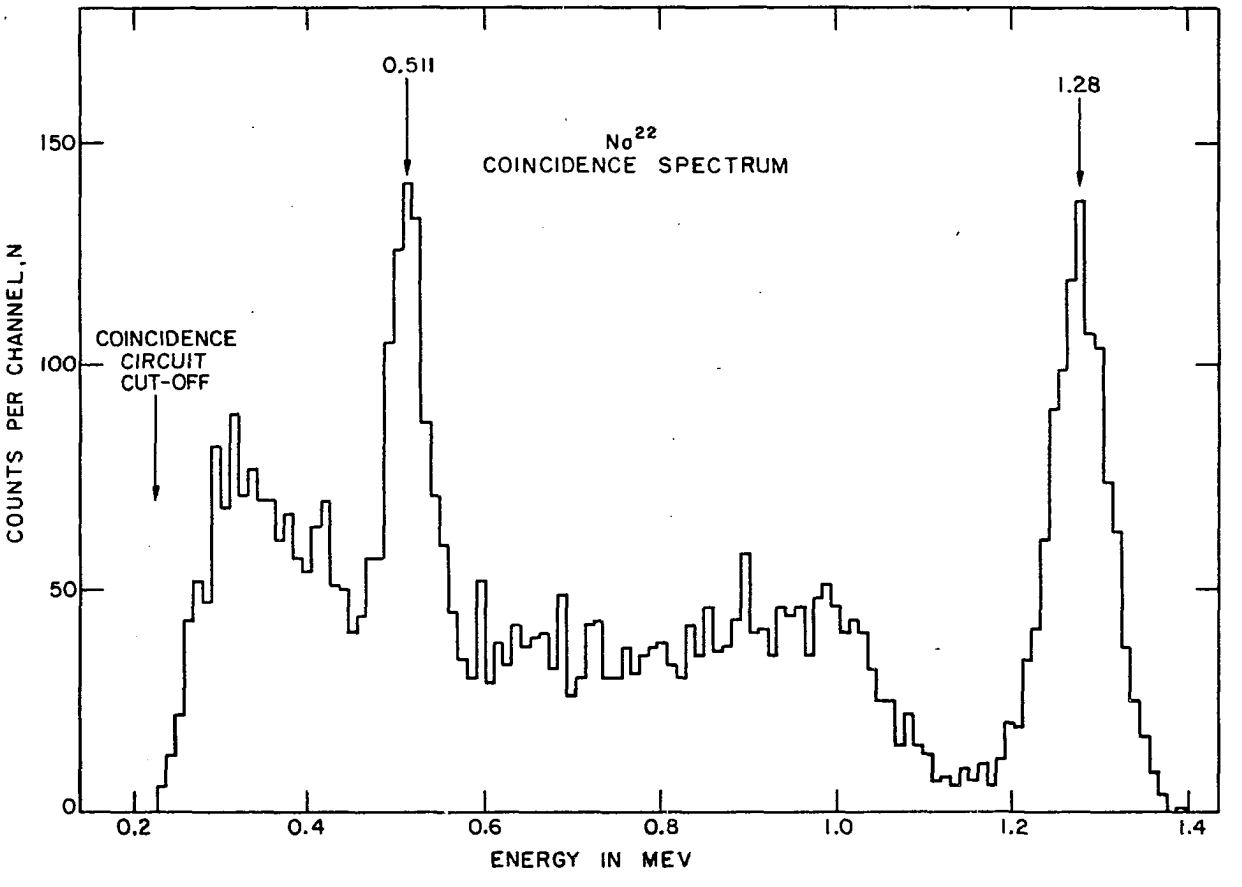

Figure 11. Coincidence gamma-ray spectrum of Na^{22}

vestigation of a mirror nuclide was a correction to the solid angle for Channel 2, determined by the analysis of the Na^{22} singles and coincidence spectra. The statistical error of the solid angle determined in this way was less than three per cent, so the value of the solid angle was certainly precise enough for use. However, the serious question as to whether this solid angle also represented the experimental situation when a mirror nuclide sample was undergoing analysis could be resolved only approximately. Since the activity of interest from Channel 2 during a coincidence run was the possible gamma radiation coming from the entire sample, the investigation of a mirror nuclide involved dealing with an extended source of gamma radiation whereas the solid angle determination was made using nearly a point source.

To estimate the effect from the two geometries, a comparison was made between the average solid angle of the Channel 2 detection crystal as viewed by the whole sample and the solid angle as viewed by the Na^{22} source. The average solid angle was determined by finding the solid angle from each intersection point of a grid superposed on the cross-sectional area of the sample and averaging the solid angles so evaluated over the entire grid. This average was five per cent lower than the solid angle subtended at the Na^{22} source location. The average value for the solid

angle was only slightly larger than the value at the center of the sample, so a weighted average, considering a plausible activity distribution within the sample, was not considered to be necessary in determining the correction. Hence, the solid angle obtained by the method using Na^{22} was lowered by five per cent for use in the analysis of mirror nuclei data. It should be noted that a twenty per cent error in the estimation of the solid angle correction would impose only a one per cent error on the value of the solid angle actually used, which would be less than the effects of statistics on this value.

Another correction which was applied to the data in the analysis was that accounting for the effects of absorption of the gamma ray in the sample and brass annihilator. Calculations were made for the three mirror nuclei in whose decays gamma rays were seen, and the calculations were checked experimentally in the case of Mg^{23} to see if they yielded an accurate correction. The calculations for absorption were made assuming that the gamma ray originated in the center of the sample and thus had to travel obliquely through a half-thickness of the sample and the 1/16 inch thick brass annihilator without being scattered out of the direction incident to the crystal. A scattering of 25 degrees or more was considered sufficient to eliminate detection in the photopeak of the spectrum of the detector as well as to

remove a photon from a direction incident to the crystal. Thus, the Compton effect cross-section was modified accordingly and the total absorption cross-section determined for the sample material and brass at the energies involved. The absorption of the gamma ray was then calculated.

The experimental value for the absorption of 0.440 Mev gamma radiation in the case of Mg^{23} was obtained by interpolating between the values of absorption of 0.356 Mev gamma rays from Ba^{133}, 0.511 Mev annihilation radiation from Na^{22}, and 0.661 Mev gamma radiation from Cs^{137}. The absorber consisted of pieces of aluminum and brass whose thicknesses closely duplicated the assumed path length of the gamma ray through the sample and annihilator. The value of absorption experimentally found was in good agreement with the calculated amount, and substantiated the method of calculation.

It was thought that the geometrical approximation was reasonable, since the absorption, although exponentially dependent upon path length through the absorber, was different by less than ten per cent if considered as due to travel from the center of the sample or considered the average of the absorptions arising from travel from both sides of the sample. It was not known which approximation would best represent the true effect, and since the approximations were self-consistent to within ten per cent, the one where the gamma ray was considered to travel from

the center of the sample was used, since it was easy to calculate. The absorption correction affected the number of counts seen in the gamma-ray photopeak by 25 per cent at most, and so a ten per cent deviation in the absorption correction would add little effect to the other errors present.

The singles counts found in the photopeak of annihilation radiation were subject to correction from the effects of origin from other than the mirror nuclide activity investigated. The additional activity produced in the sample holder was corrected for in each case, the correction being estimated from the amount of annihilation radiation seen in the blank sample holder runs. Since the blank sample holder was cycled in the same way as was the sample for the singles runs, there was no reason to suspect that the correction for this effect was inaccurate. Another correction was made in the case of S^{31} for the contribution to the annihilation radiation peak from P^{30}, which was also produced in the sulfur sample by the synchrotron beam. The correction was made by estimating the relative yields of S^{31} and P^{30} from photonuclear reactions on S^{32}. An estimate of from five to ten per cent for the yield of P^{30} as compared to the yield of S^{31} was thought to be reasonable, and the correction was made for eight per cent. No values were available for the integrated photo-neutron cross-section of S^{32} for brems-

strahlung of up to 45 Mev although the integrated cross-section was available for the $S^{32}(\gamma,pn)P^{30}$ reaction, so it was impossible to appeal to experimental determinations for the relative yields.

The above corrections were not applied to the analyses of Si^{27} and Ca^{39}, where the statistical deviations were very high and would render these corrections as insignificant.

The experimental errors quoted for the values of the branching ratios were determined as composites of the effects of statistical deviations and errors in the solid angles, absorption corrections, and values used for the photopeak efficiency of the detectors. The errors in the solid angles and absorption corrections were considered to give a deviation of five per cent to the branching ratio, so that this figure then contained a reasonable allowance for the indeterminancy of these corrections. The values for $(\epsilon P/T)$ were considered to be determined at least to an accuracy of five per cent. Finally, the normal standard deviation for the statistics arising from the number of counts was included. The effects of these independent per cent deviations were added by taking the square root of the sums of squares to give the final deviation, or experimental error, to the values for the branching ratios determined in this investigation. In this way, a liberal but realistic allowance was made for the deviations arising from the ex-

perimental method.

For the branching ratios of Na^{21}, Mg^{23}, and S^{31}, then, the errors in the reported branching ratios were determined in the above manner. For the decays of Al^{25}, Si^{27}, and Ca^{39}, however, the statistical deviation completely dominated the picture, so the upper limits to any possible branches in these decays were considered to be the maximum allowed probable value under standard deviation.

C. Analysis for the Nuclides Investigated

1. Na^{21}

The experimental spectra obtained in the study of Na^{21} are shown in Figure 12. Figure 12(a) is a spectrum of a typical singles analysis, and shows no indication of a branching transition gamma ray at the expected energy of 0.347 Mev. A weak gamma ray at this energy would be overshadowed in a singles spectrum by the Compton edge resulting from the presence of the intense annihilation radiation. Figure 12(b) is the coincidence spectrum obtained by adding the results of the two experimental runs made on Na^{21}. The gamma ray indicative of branching in the decay of Na^{21} is clearly evident in the coincidence spectrum, and appears at the energy expected for the presence of branching of the decay to the first excited state of Ne^{21}. No attempt was made to look for gamma rays of 1.73 and 1.38 Mev, correspond-

Figure 12. Gamma-ray spectra obtained from Na^{21}
(a) Singles spectrum
(b) Coincidence spectrum

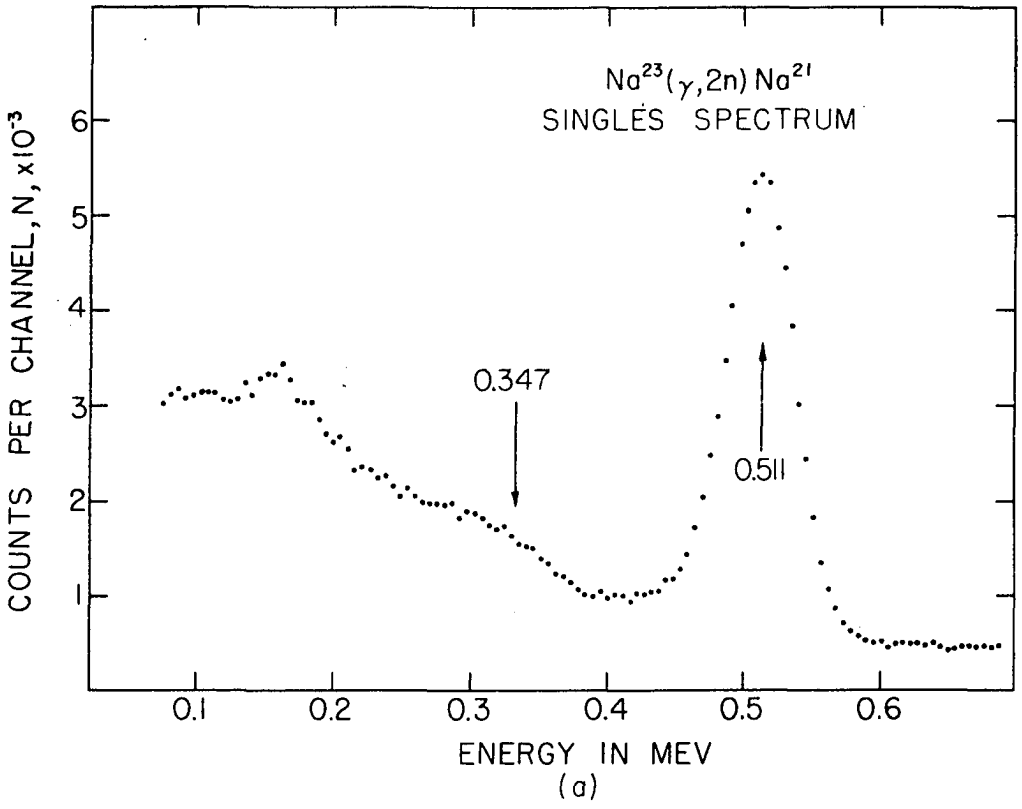
$Na^{23}(\gamma,2n)Na^{21}$
SINGLES SPECTRUM
COUNTS PER CHANNEL, N, x10⁻³
0.347
0.511
ENERGY IN MEV
(a)

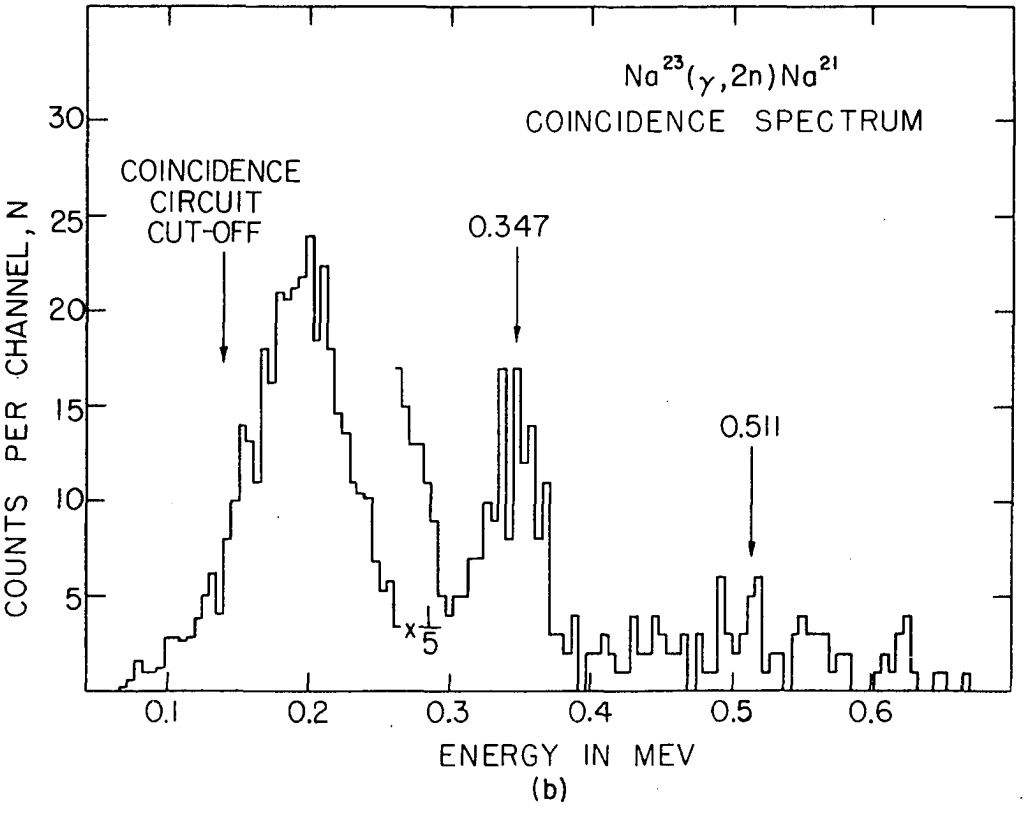
$Na^{23}(\gamma,2n)Na^{21}$
COINCIDENCE SPECTRUM
COINCIDENCE CIRCUIT CUT-OFF
0.347
0.511
x 1/5
COUNTS PER CHANNEL, N
ENERGY IN MEV
(b)

ing to a branch to the second excited state of Ne^{21}, for the energetics involved in such a branch discourage a transition to this level of detectable intensity, using the coincidence method for detection.

The activity of the Na^{21} sample was not as intense as was the case for the other nuclides, because of the relative difficulty of production by the (γ,2n) photonuclear process as compared to the (γ,n) process production of most of the other nuclides investigated. Despite this limitation, however, enough statistics were accumulated in the coincidence runs so that a reasonably precise determination of the branching ratio was possible. The two coincidence runs were analyzed separately, one yielding a branching ratio of 2.3 ± 0.4 per cent and the other 2.1 ± 0.3 per cent. These values, when averaged together, yield a reported value of 2.2 ± 0.3 per cent for the experimentally determined branching ratio for the ground-state to excited state branch of the decay of Na^{21}.

The calculations for the branching ratios of Na^{21} involved an 18 per cent absorption correction, and employed photopeak efficiencies of 0.086 and 0.405 for the 1.28 gamma ray in Na^{22} and the 0.347 Mev gamma ray of Na^{21}, respectively. The errors reported for the individual determinations of the branching ratio were dominated by the standard deviation of the number of counts observed in the gamma-ray photo-

peak of the coincidence spectra.

2. $\underline{Mg^{23}}$

Figures 13 and 14 show typical experimental spectra obtained in the investigation of Mg^{23}. Figure 13(a) is the singles spectrum, and shows a slight indication of a branching transition in the decay of Mg^{23} to the first excited state of Na^{23}. Figure 13(b) is the spectrum of a coincidence run and is featured by the prominent 0.440 Mev gamma ray confirming the existence of the branching transition. No effort was made to search for gamma rays of higher energies using the coincidence technique, for such gamma rays would be of very low intensity if present at all, just by consideration of the energy available for branches to higher excited states of Na^{23}. Figure 14(a) is the same spectrum illustrated in Figure 13(b), and is repeated for convenience of comparison with Figure 14(b), which is the coincidence spectrum for Mg^{23}, including corrections for scattering and accidental ccincidences as determined by the coincidence spectrum of C^{11}, which has no branching transitions. This type of correction was used only for the case of Mg^{23}, because the investigation of Mg^{23} was the initial effort in the experiment, and it was desired to know just how much of the coincidence spectrum was due to the various effects of annihilation radiation alone.

Figure 13. Gamma-ray spectra obtained from Mg^{23}
(a) Singles spectrum
(b) Coincidence spectrum

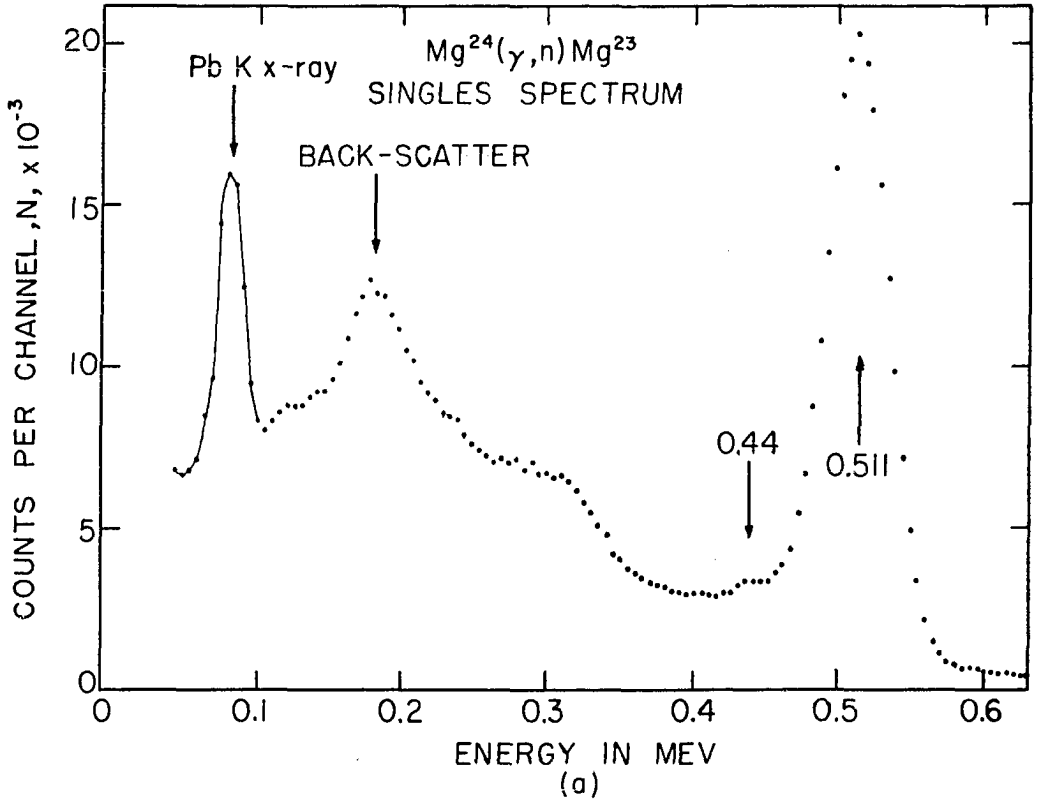
Pb K x-ray
$Mg^{24}(\gamma,n)Mg^{23}$
SINGLES SPECTRUM
BACK-SCATTER
0.44
0.511
COUNTS PER CHANNEL, N, x 10^{-3}
ENERGY IN MEV
(a)

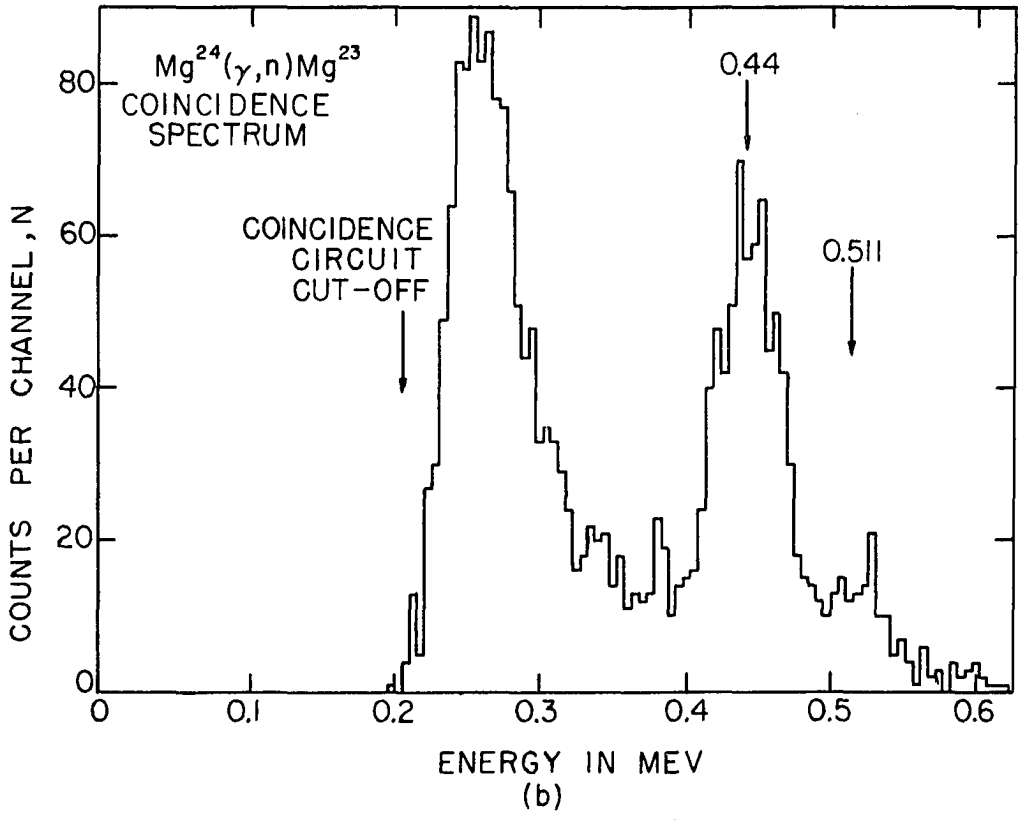
$Mg^{24}(\gamma,n)Mg^{23}$
COINCIDENCE
SPECTRUM
COINCIDENCE
CIRCUIT
CUT-OFF
0.44
0.511
COUNTS PER CHANNEL, N
ENERGY IN MEV
(b)

Figure 14. Coincidence gamma-ray spectra from Mg^{23} showing the effects of backscattering of annihilation radiation

(a) Uncorrected Mg^{23} coincidence spectrum

(b) Mg^{23} coincidence spectrum after subtraction of coincidence spectrum of C^{11}

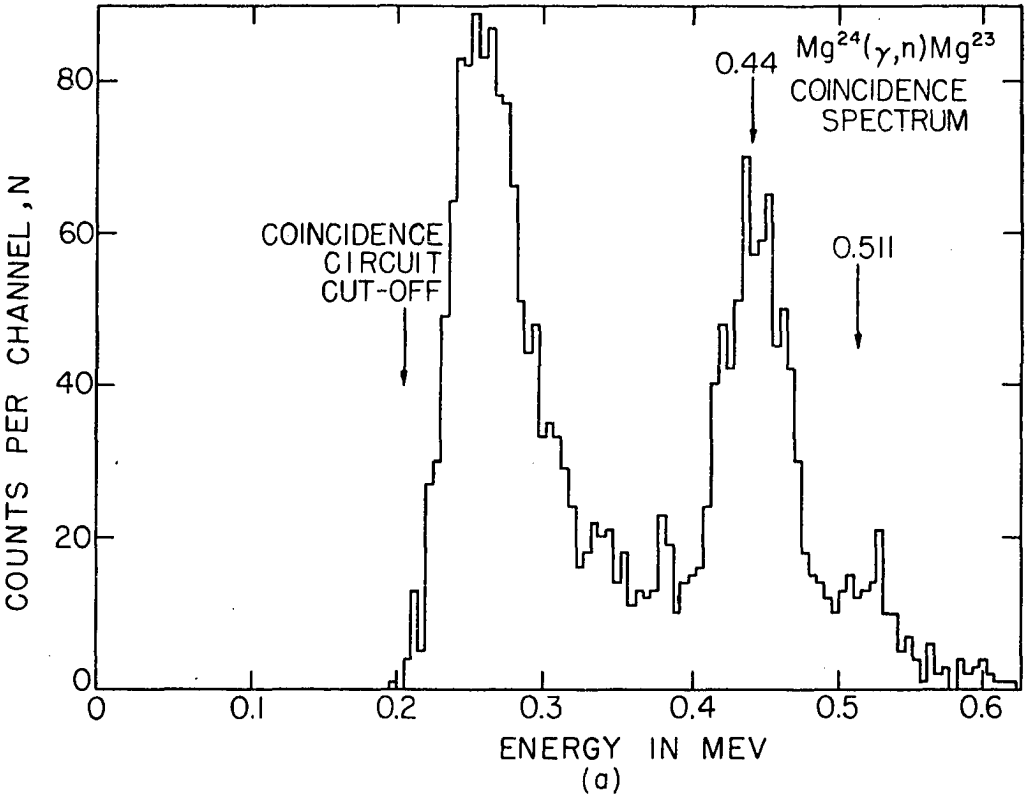
COUNTS PER CHANNEL, N
80
60
40
20
0
0
0.1
0.2
0.3
0.4
0.5
0.6
ENERGY IN MEV
(a)
$Mg^{24}(\gamma,n)Mg^{23}$
COINCIDENCE
SPECTRUM
0.44
0.511
COINCIDENCE
CIRCUIT
CUT-OFF

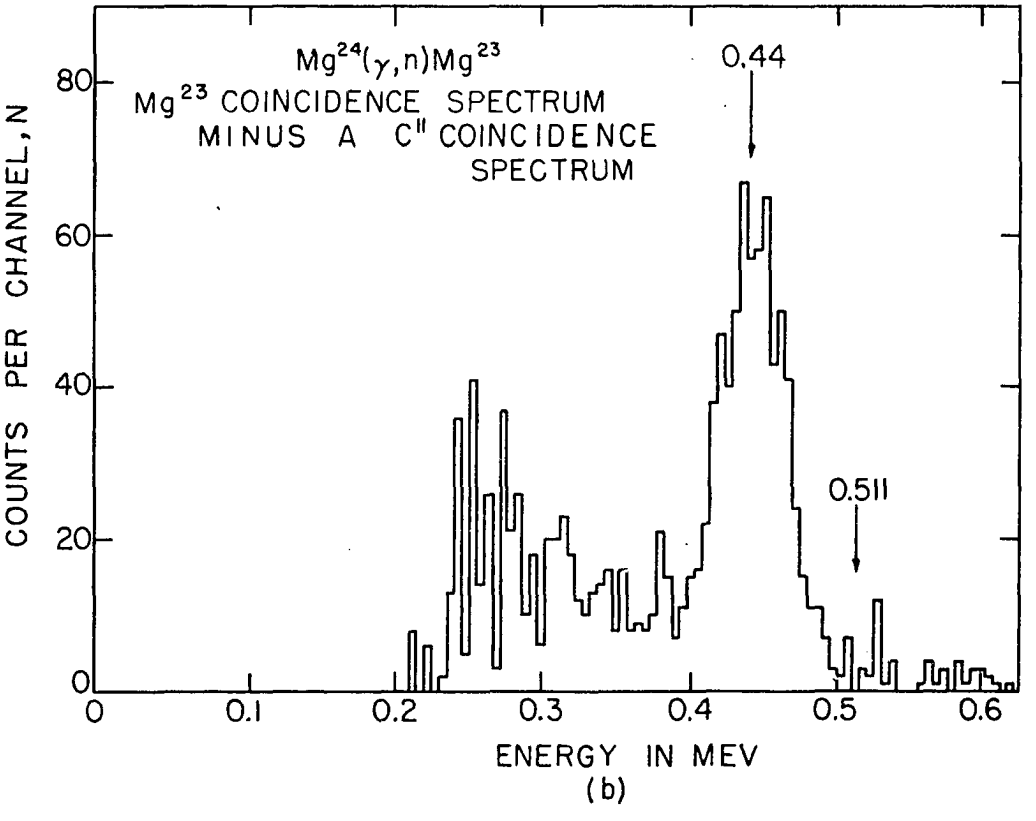
COUNTS PER CHANNEL, N
80
60
40
20
0
0
0.1
0.2
0.3
0.4
0.5
0.6
ENERGY IN MEV
(b)
$Mg^{24}(\gamma,n)Mg^{23}$
Mg^{23} COINCIDENCE SPECTRUM
MINUS A C^{11} COINCIDENCE
SPECTRUM
0.44
0.511

The experiments on the decay of Mg^{23} differed from those for the other mirror nuclei in the investigation in that the detection crystal used in Channel 2 was 1-1/2 inches in diameter by 1 inch thick. For the other experiments, a 1-3/4 inches by 2 inches crystal was obtained since a high detection efficiency was desirable for the gamma rays in question from the other decays, especially for those at high energies. For this determination, then, the values of the photopeak efficiency of the Channel 2 detector were 0.049 for the 1.28 Mev gamma ray of Na^{22} and 0.211 for the 0.440 Mev gamma ray in Mg^{23}. The solid angle of Channel 2 was smaller for the Mg^{23} experiments than for the other nuclides, partly because of the smaller physical size of the crystal and partly since the whole energy region of the annihilation radiation photopeak was not included in the window of the single-channel analyzer. For the two determinations of the branching ratio of Mg^{23}, the solid angle was about three per cent.

The counting rate for the coincidence spectra was quite good for Mg^{23}, around 700 counts being accumulated in the photopeak of the gamma ray in each of the two runs. The absorption correction for the gamma ray intensity was 27 per cent, which was more than that for the Na^{21} investigation, mostly because the sample material density of magnesium was much larger than that of sodium, making absorp-

tion of the gamma ray by the sample itself a larger effect. As was mentioned in Section B of this chapter, the absorption for the case of the Mg^{23} gamma ray was both calculated and experimentally determined, the difference in the amount of absorption estimated by the two approaches being less than five per cent of the mean value, and the experimental value was used in this analysis.

The branching ratio was calculated from the two experimental determinations to be 8.9 ± 0.7 and 9.3 ± 0.8 per cent, which gave a combined value of 9.1 ± 0.5 per cent.

3. Al^{25}

Some of the gamma-ray spectra obtained in the study of the decay of Al^{25} are shown in Figure 15, where a singles spectrum is shown in Figure 15(a) and Figure 15(b) is a coincidence spectrum. No gamma ray was expected as a result of a branching transition to the 0.58 Mev first excited state of Mg^{25} due to consideration of decay selection rules, so the investigation was concentrated at 0.98 Mev on the possibility of gamma radiation resulting from a transition to the second excited state of Mg^{25}. Transitions to higher excited states of Mg^{25} were not expected, the energetics involved preventing intensities for such transitions which could be detected using the coincidence technique.

There was no indication of a gamma ray at 0.98 Mev in

Figure 15. Gamma-ray spectra obtained from Al^{25} and Al^{26m}
(a) Singles spectrum
(b) Coincidence spectrum

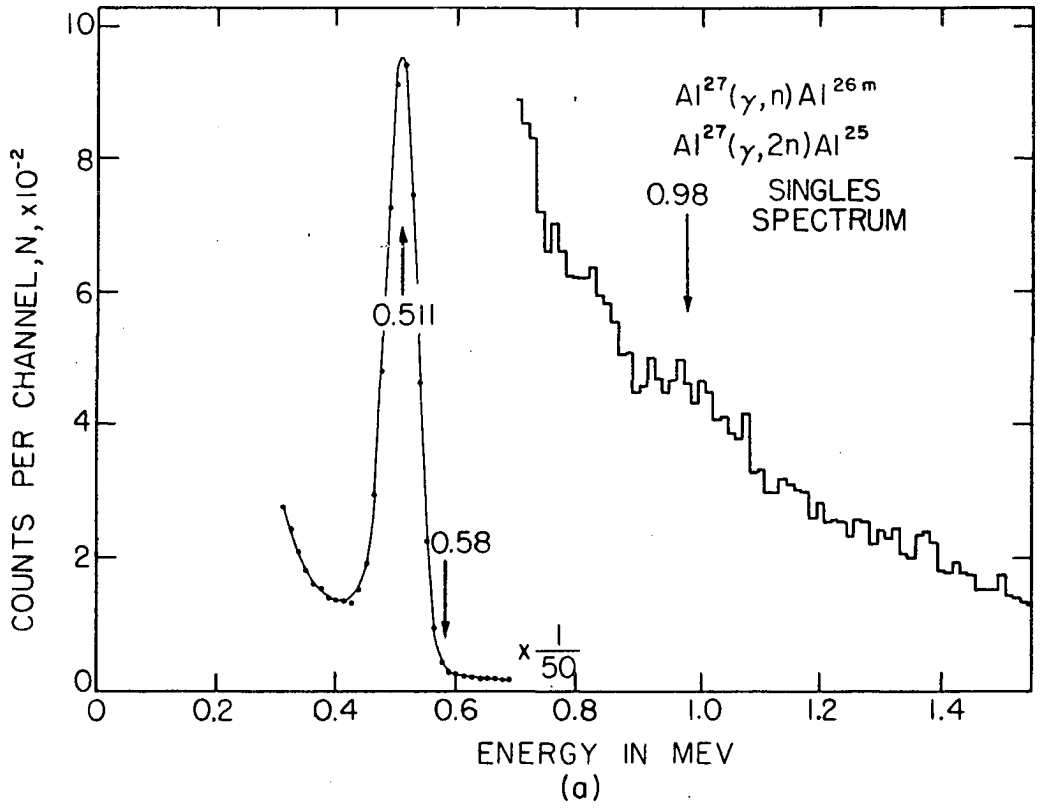
COUNTS PER CHANNEL, N, x10⁻²
ENERGY IN MEV
Al²⁷(γ,n)Al^26m
Al²⁷(γ,2n)Al²⁵
SINGLES SPECTRUM
0.98
0.511
0.58
x 1/50
(a)

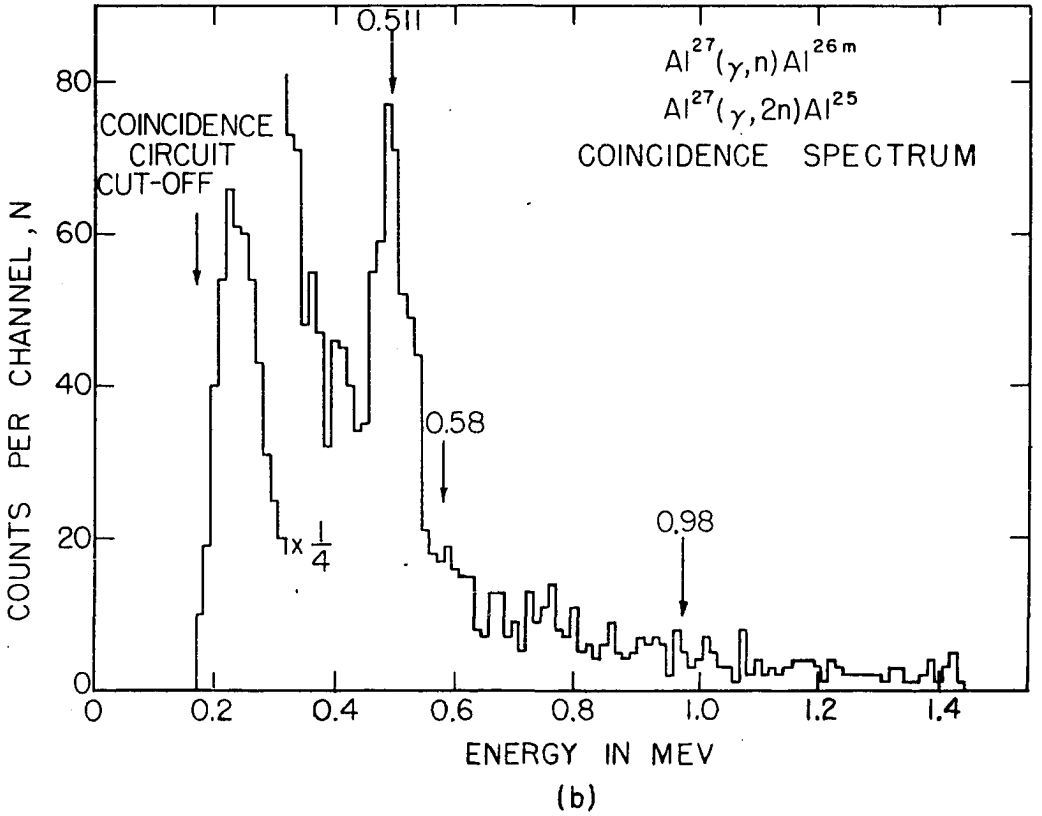
COUNTS PER CHANNEL, N
ENERGY IN MEV
Al²⁷(γ,n)Al^26m
Al²⁷(γ,2n)Al²⁵
COINCIDENCE SPECTRUM
COINCIDENCE CIRCUIT CUT-OFF
0.511
0.58
0.98
1x 1/4
(b)

the coincidence spectrum, and an estimate of the upper limit of possible branching was made. An estimate of the maximum number of counts in the photopeak of a possible gamma ray at 0.98 Mev was made by using points on each side of the possible photopeak at 0.98 Mev to draw a smooth curve through the photopeak region, and determining the excess of the number of counts in the photopeak region of the spectrum to the number of counts corresponding to the smooth curve. Only 4 ± 8 net counts for a possible gamma ray were determined for the investigation in this manner for two combined coincidence spectra. Although no absorption correction was made for the calculation of branching ratio of Al^{25}, a correction was applied to account for the amount of annihilation radiation in the singles spectra which was due to Al^{25}. The number of singles events due to Al^{25} was considered to be nine per cent of the total annihilation radiation response, this number being the result of the estimated relative yields of ten to one for Al^{26m} to Al^{25}, produced from the bombardment of Al^{27} by 45 Mev X-rays. Certainly the upper limit for the branching ratio given in this investigation was subject to the accuracy of this estimate for the yields of Al^{26m} and Al^{25}. This estimate for the relative yields was quite liberal, for it was based upon the probable relative yields of the (γ,n) and (γ,2n) reactions. The estimate did not take into consideration the fact that both

Al^{26} and Al^{26m} are products of the (γ,n) reaction, but only the decay of Al^{26m} is observable with the times of analysis used. Thus, the activity of Al^{25} estimated in this manner was probably underestimated, and the resulting upper limit for the branching ratio was quite liberal. Calculation of the branching ratio, where a photopeak efficiency for Channel 2 of 0.113 at 0.98 Mev was used, resulted in the value of 0.3 ± 0.6 per cent, for an upper limit of 0.9 per cent for the transition.

The singles spectrum shows a bump at about 1.0 Mev, indicating the possible presence of the 0.98 Mev gamma ray. This bump was considered to be due to accidental summing of the annihilation radiation within the duration of the scintillation detector pulse, the consideration accounting for the observed intensity within a factor of two, and the energy of 1.022 Mev for such accidental summing being right for possible confusion with a gamma ray at 0.98 Mev. Using Equation 1 to determine the intensity of this effect, an answer of 0.4 per cent was obtained, which was within the upper limit for the branching transition intensity.

The coincidence spectrum shows a prominent annihilation radiation peak, which was accounted for by considering coincidences between annihilation radiation in Channel 2 and pre-annihilation bremsstrahlung incident upon Channel 1 which lost 0.511 Mev in the detection crystal. An estimate

of the predicted intensity for this peak by the mechanism thought to be responsible was in excellent agreement with the observed intensity (53). The continuous distribution shown on the coincidence spectrum was considered to arise from the detection of bremsstrahlung in Channel 2 coincident with annihilation radiation in Channel 1, and from annihilation-in-flight radiation for which one photon was detected by Channel 2 and the other lost about 0.511 Mev in Channel 1. These features of the coincidence spectrum of Al^{25} and Al^{26m} were also repeated for the decays analyzed below.

4. Si^{27}

The singles and coincidence spectra obtained in the study of Si^{27} are shown in Figure 16(a) and 16(b), respectively. A branching transition to the 0.842 Mev first excited state of Al^{27} was not expected from consideration of selection rules for the decay, so the study was turned to the possibility of branching to the second excited state of Al^{27}, which would yield a 1.013 Mev gamma ray. At this energy in the spectra, the singles spectrum could not be used to observe a weak branch because of the presence of the higher energy gamma rays, and there was no indication of a gamma ray for the coincidence spectrum.

The estimate of the maximum number of counts under the

Figure 16. Gamma-ray spectra obtained from Si^{27}
(a) Singles spectrum
(b) Coincidence spectrum

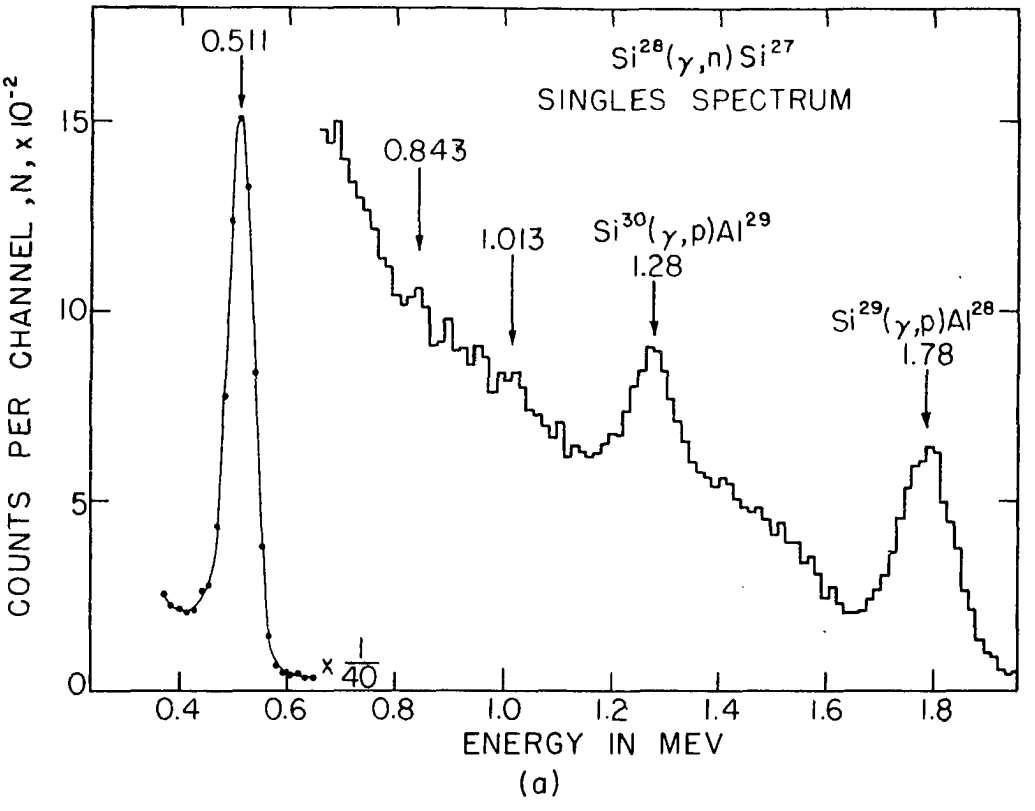
0.511
$Si^{28}(\gamma,n)Si^{27}$
SINGLES SPECTRUM
0.843
1.013
$Si^{30}(\gamma,p)Al^{29}$
1.28
$Si^{29}(\gamma,p)Al^{28}$
1.78
COUNTS PER CHANNEL, N, x 10^{-2}
15
10
5
0
x 1/40
0.4
0.6
0.8
1.0
1.2
1.4
1.6
1.8
ENERGY IN MEV

(a)

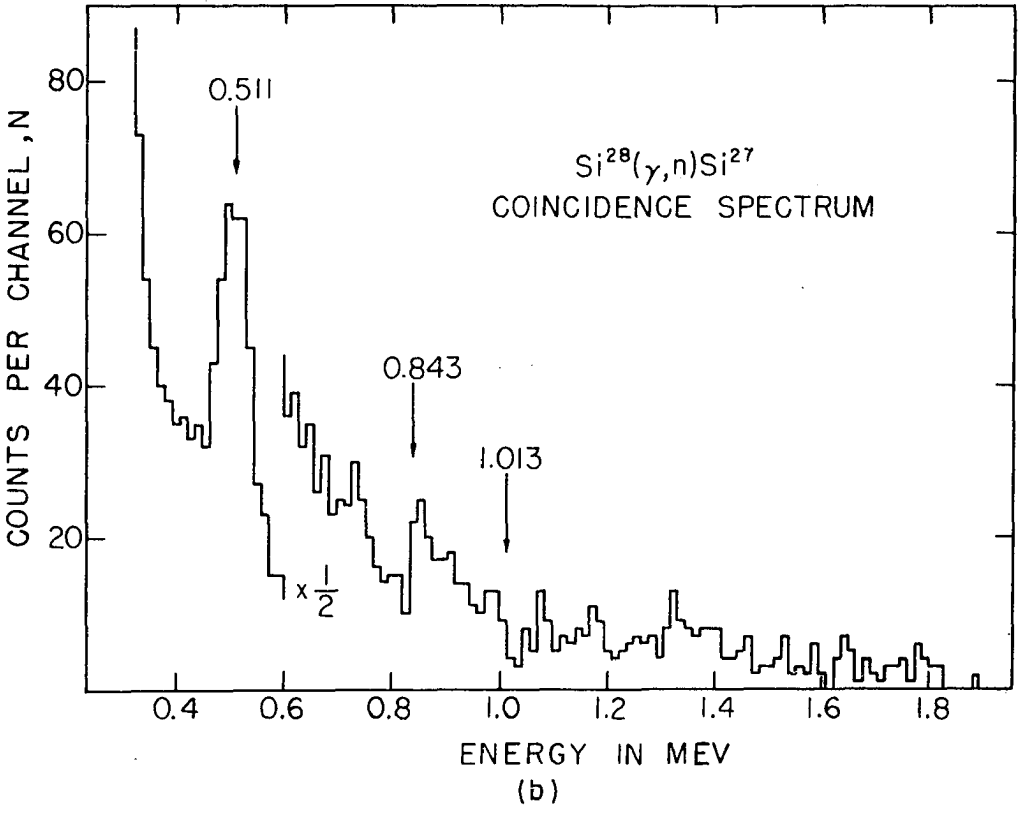
0.511
$Si^{28}(\gamma,n)Si^{27}$
COINCIDENCE SPECTRUM
0.843
1.013
COUNTS PER CHANNEL, N
80
60
40
20
x 1/2
0.4
0.6
0.8
1.0
1.2
1.4
1.6
1.8
ENERGY IN MEV

(b)

photopeak of the possible gamma ray was made in the same way as for the Al^{25} decay, with a result of 17 ± 16 counts being registered for three combined coincidence spectra. The resulting branching ratio, using a photopeak efficiency for Channel 2 of 0.108 for 1.013 Mev, was 0.1 ± 0.1 per cent, giving an upper limit to the transition of 0.2 per cent.

The singles spectrum of Figure 16(a) shows that there was detectable contamination arising from the production of Al^{28} and Al^{29} by means of (γ,p) reactions on Si^{29} and Si^{30}, respectively. Although these decays gave rise to the gamma radiation indicated in Figure 16(a), they were not visible in the coincidence spectra since they were negative electron decays and were not accompanied by annihilation radiation.

5. S^{31}

Figures 17 and 18 show the spectra obtained in the investigation of S^{31}. Figure 17(a) is a typical singles spectrum and Figure 17(b) is the sum of two coincidence spectra. Branching of the decay of S^{31} was not expected to be present to the 1.27 Mev first excited state of P^{31} because of the selection rules covering the decay, but both the singles and coincidence spectra indicated a weak gamma ray corresponding to such a transition. Figure 18(a) is the same coincidence spectrum shown in Figure 17(b), repeated for convenient comparison to the accidental coincidence

Figure 17. Gamma-ray spectra obtained from S^{31}
(a) Singles spectrum
(b) Coincidence spectrum

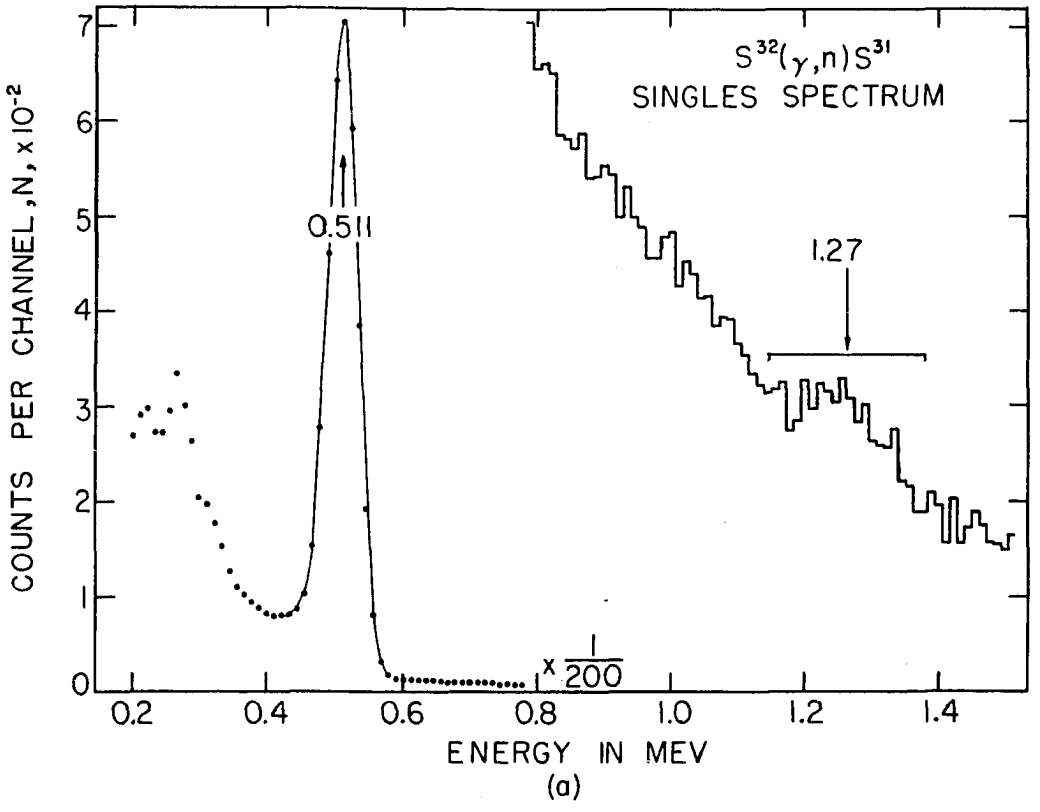
$S^{32}(\gamma,n)S^{31}$
SINGLES SPECTRUM
0.511
1.27
x 1/200
COUNTS PER CHANNEL, N, x 10⁻²
ENERGY IN MEV

(a)

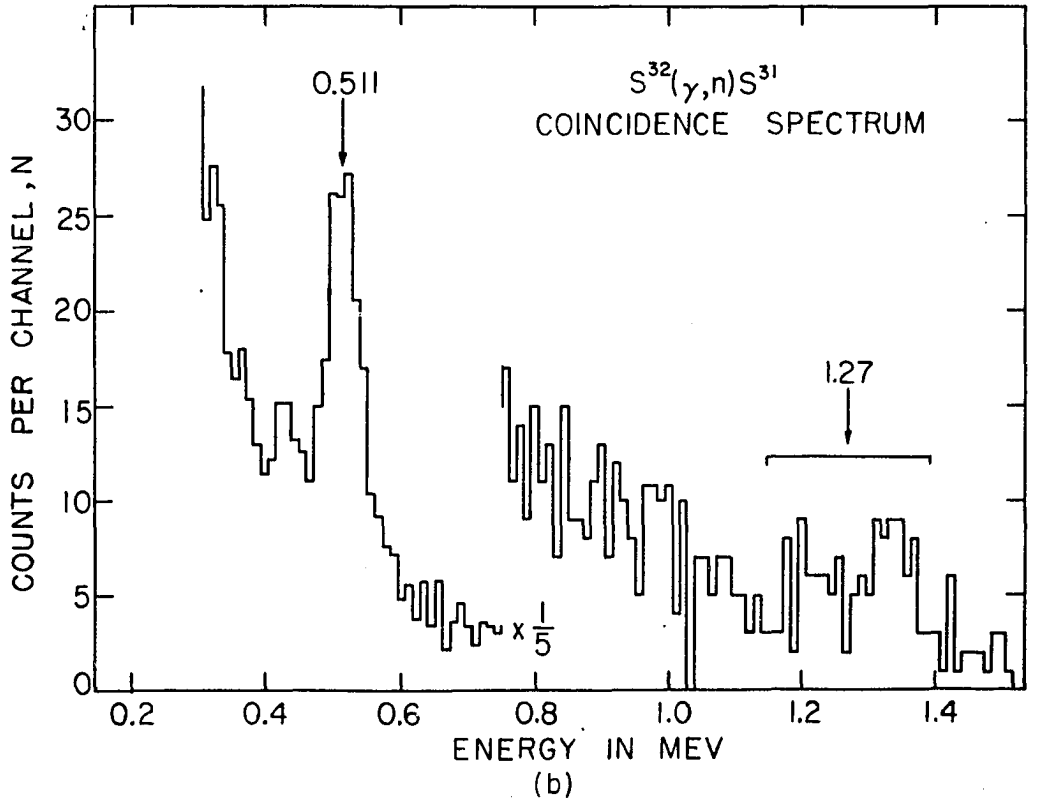
$S^{32}(\gamma,n)S^{31}$
COINCIDENCE SPECTRUM
0.511
1.27
x 1/5
COUNTS PER CHANNEL, N
ENERGY IN MEV

(b)

Figure 18. Coincidence gamma-ray spectra from S^{31} showing relative intensity of real and accidental coincidences
(a) Coincidence spectrum
(b) Accidental coincidence spectrum

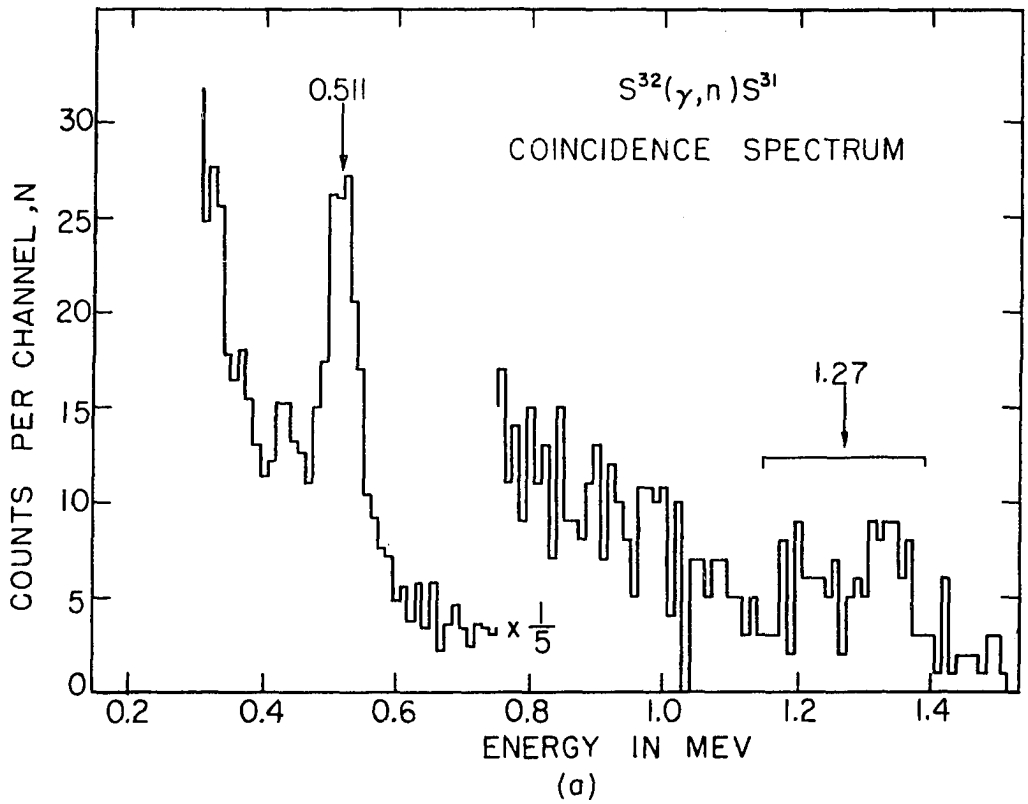
0.511
$S^{32}(\gamma,n)S^{31}$
COINCIDENCE SPECTRUM
1.27
$\times \frac{1}{5}$
COUNTS PER CHANNEL, N
ENERGY IN MEV
(a)

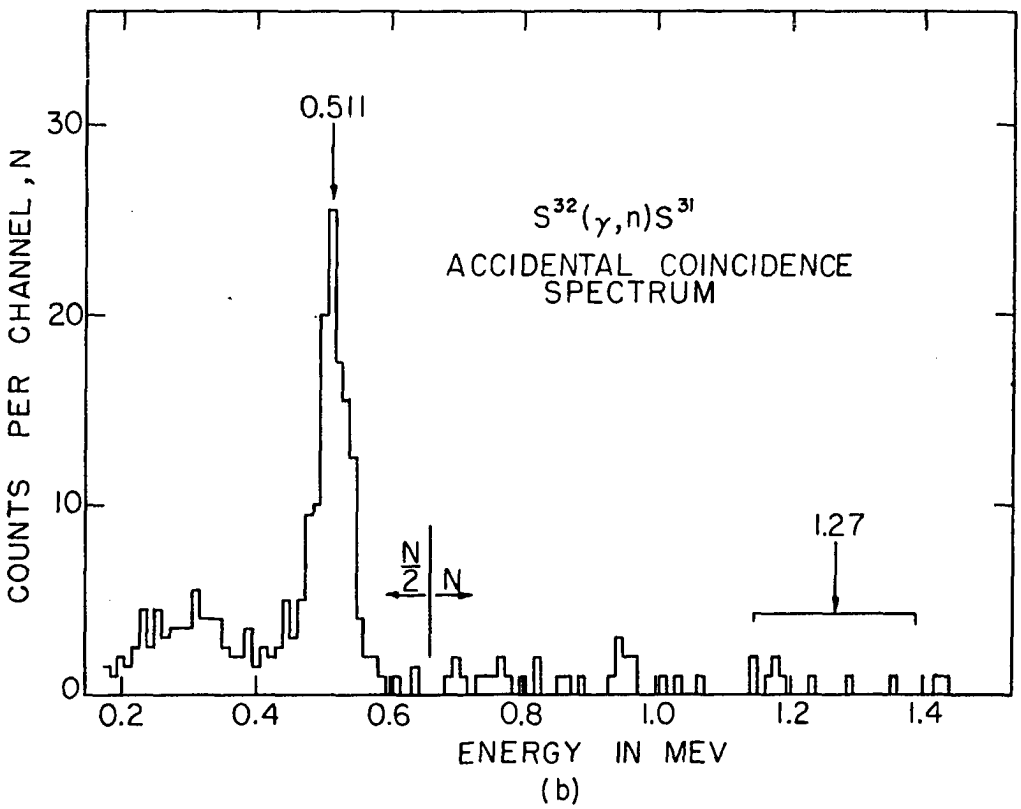
0.511
$S^{32}(\gamma,n)S^{31}$
ACCIDENTAL COINCIDENCE SPECTRUM
1.27
$\frac{N}{2}$ N
COUNTS PER CHANNEL, N
ENERGY IN MEV
(b)

spectrum in Figure 18(b). The accidental coincidence rate for S^{31} was the highest experienced in the entire investigation, since the singles counting rate of annihilation radiation was greatest for S^{31}. The accidental coincidence spectrum is shown here to indicate that no serious effects resulted from accidental coincidences.

With a photopeak efficiency of 0.086 for the 1.27 Mev gamma ray of S^{31}, and using an absorption correction of 9 per cent, the branching ratio for the transition to the first excited state of P^{31} in the decay of S^{31} was calculated to be 1.08 $\pm$ 0.09 per cent for the combined coincidence runs.

The singles spectrum of Figure 17(a) also indicated the presence of a 1.27 Mev gamma ray. The intensity of the gamma ray was determined independently by analysis of the singles spectra and the branching ratio was calculated using Equation 1. Corrections of the intensities of the annihilation radiation and gamma ray were made for absorption in the source and brass annihilator, and allowance made for the fact that part of the annihilator was shielded from the detection crystal, which would decrease the source strength of annihilation radiation as viewed by the detector. The calculation led to a branching ratio of 1.12 $\pm$ 0.09 per cent.

The value for the branching ratio for this transition in S^{31} was combined from the independent determinations using

the two methods, and was then 1.1 ± 0.1 per cent. It might be noted here that the sensitivity of the coincidence technique was getting close to its limit in the study of S^{31}. It was estimated that this method could not convincingly detect gamma rays which were less intense than about 0.2 per cent, unless sufficient time were taken to improve the statistics in the coincidence runs. For this reason, possible transitions in a mirror nuclide decay, which were expected to be much less than one per cent purely from consideration of the energetics for the decay, were not studied, and the limitations of the method were then kept in sight in the investigation.

6. Ca^{39}

The singles and coincidence spectra for the study of Ca^{39} are shown in Figure 19. The branch decay to the first excited state of K^{39} was possibly not expected to occur by consideration of selection rules, although the spin assignment of the first excited state of K^{39} was not certain in this consideration, and the gamma ray of 2.53 Mev indicating the presence of such a branch did not show up in either the singles or coincidence spectra. However, the production of K^{38} by the competing photonuclear reaction (γ,pn) on Ca^{40} was evident in both the singles and coincidence spectra, for the decay of K^{38} is also by positron emission and proceeds

Figure 19. Gamma-ray spectra obtained from Ca^{39}
(a) Singles spectrum
(b) Coincidence spectrum

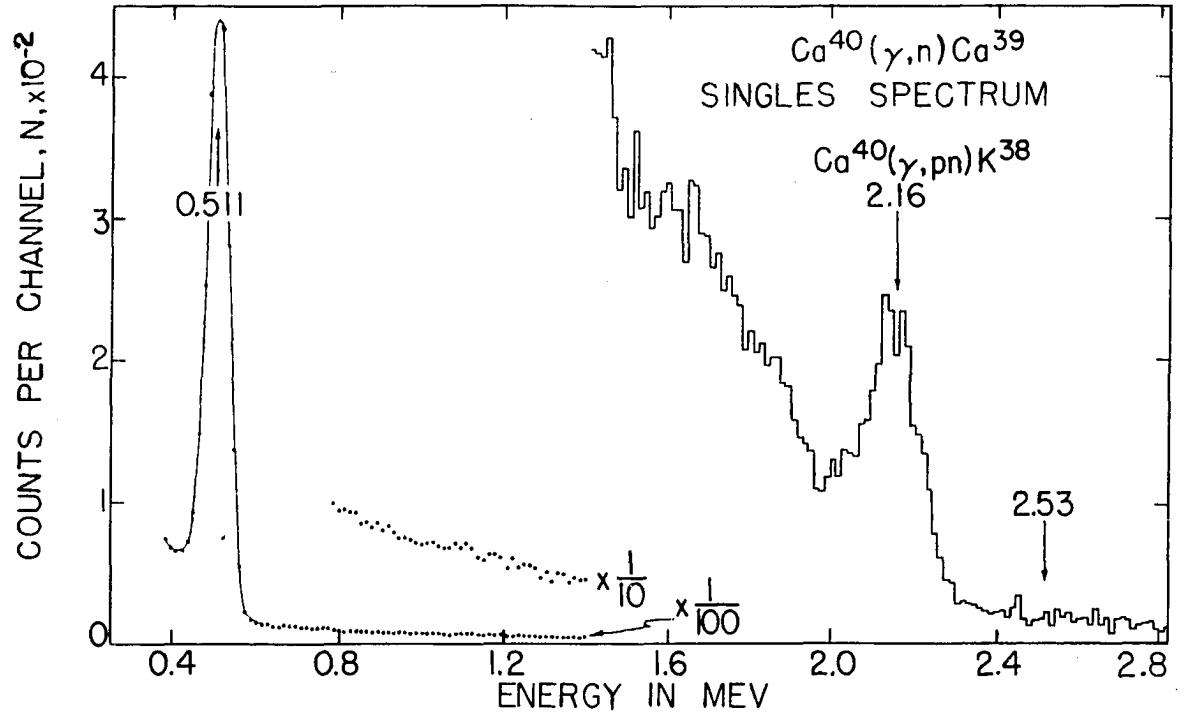
COUNTS PER CHANNEL, N, x10⁻²
Ca⁴⁰(γ,n)Ca³⁹
SINGLES SPECTRUM
Ca⁴⁰(γ,pn)K³⁸
2.16
0.511
2.53
x 1/10
x 1/100
ENERGY IN MEV

(a)

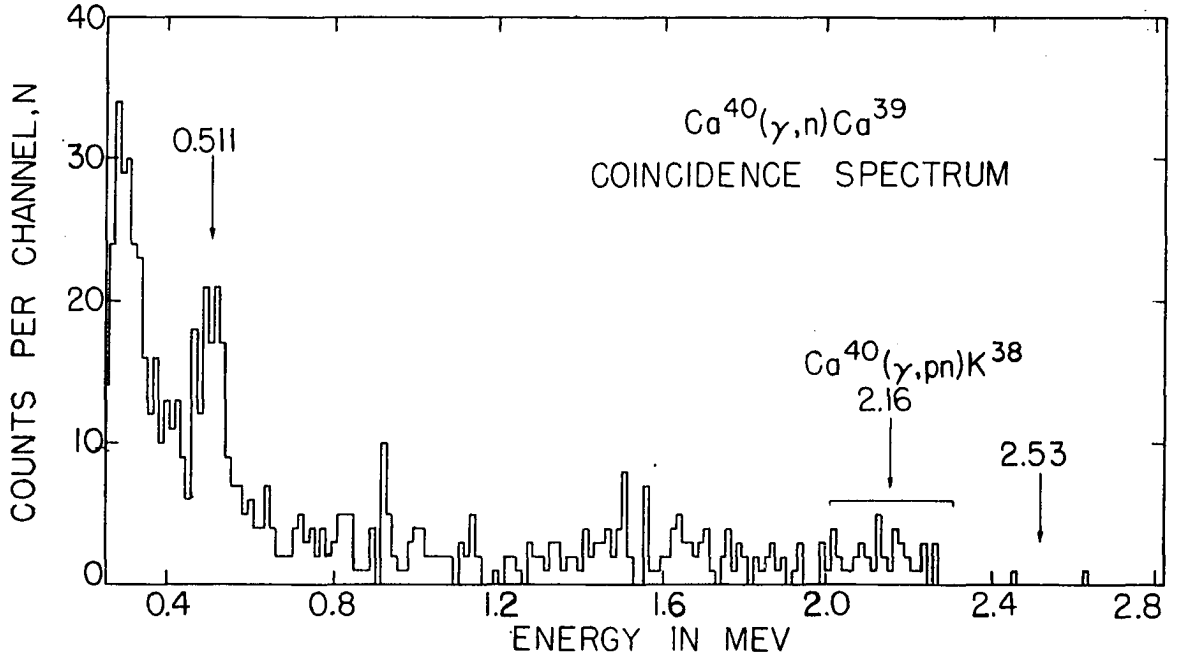
COUNTS PER CHANNEL, N
Ca⁴⁰(γ,n)Ca³⁹
COINCIDENCE SPECTRUM
0.511
Ca⁴⁰(γ,pn)K³⁸
2.16
2.53
ENERGY IN MEV

(b)

entirely to the first excited state of A^{38}.

The estimate of the branching ratio for Ca^{39} was made using a photopeak efficiency of 0.039 for the 2.53 Mev gamma ray and utilizing the total number of counts in the photopeak region of a 2.53 Mev gamma ray. The branching ratio was found to be 0.3 ± 0.3 per cent which resulted in an upper limit of 0.6 per cent for the transition probability.

Only one run was made in the study of Ca^{39}, partly because of the previous work done on its branching ratio (14), and partly because no indication of a branch decay was present from the beginning, even though the sample activity was rather intense. The absence of room background at 2.53 Mev made conditions ideal for the appearance of a very weak gamma ray at this energy, but no indication was seen, so the run was not repeated.

IV. DISCUSSION

A. Decay Schemes

1. Level diagrams

The success of any model of the nucleus is based partially upon its ability to account for the experimental features exhibited in the study of radioactive decay. For the particular case of mirror nuclei, the structure of the excited states of the daughter nuclei, together with the selection rules for the positron decays, should be predicted accurately by a valid nuclear model. The unified model of the nucleus gives an excellent semi-quantitative explanation for the experimental situation as seen in mirror nuclei, although the spherical shell model can also be applied to the situation, and its interpretation is perhaps just as acceptable as that given by the unified model.

To be able to describe the decay of a mirror nuclide, the model employed must be able to predict the spins, parities, relative order, and approximate energies of the ground and excited states of the daughter nucleus. By charge symmetry of nuclear forces, then, the parent nucleus should have approximately the same level scheme. Using the selection rules appropriate for the model, the presence of branches in the decay should be predicted. Comparison of these features of the nuclear decay and structure with the

experimental results can, if carried out in enough detail, indicate the validity of the model used.

It is appropriate at this time to discuss the shell model in preparation to introducing the features of the unified model. The shell model is a very simple scheme based upon the assumptions that each nucleon in the nucleus moves according to an average spherical potential, and that this motion is independent of the instantaneous positions of the rest of the nucleons. There exist two limits for such a potential, which fulfill the further requirements of consistency with the experimentally indicated nucleon density in the nucleus and the short finite extent of nuclear forces. For the purpose of calculation of the nuclear energy levels, these limiting potentials are the infinite harmonic oscillator and the infinite square well. The actual nuclear levels are believed to occur somewhere in between the levels predicted by these potentials.

With the addition of spin-orbit coupling to the shell model potential interaction, the nuclear level system for light nuclei becomes that pictured in Figure 20 (33, p. 58). The spin-orbit coupling is added in accordance with experimental evidence that it has a sizeable effect on the nuclear interaction, and its addition provides the level scheme with large energy separations between certain levels. The system of levels obtained is analogous to the Bohr atomic model,

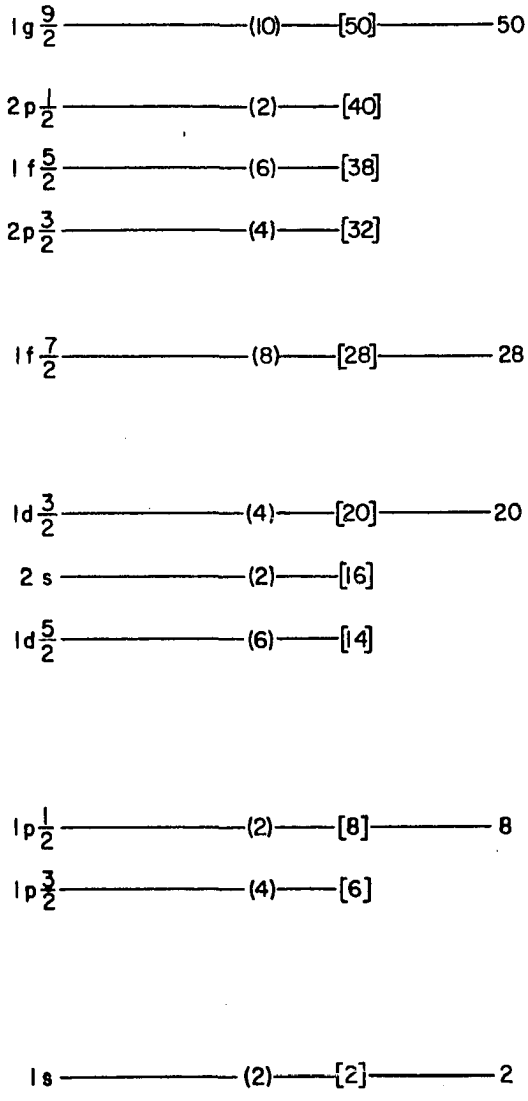

Figure 20. Level diagram of nuclear levels for spin-orbit coupling in a spherical potential

and the levels are filled according to the Pauli exclusion principle. When two levels are encountered which are widely separated in energy, the filling of the lower level is analogous to the shell closure of atomic electron levels. The closure of a nuclear shell comes at one of several so-called "magic numbers", and the shell model prediction of the magic numbers agrees completely with the experimental evidence indicating the presence of the magic numbers. In Figure 20, the levels are identified, from left to right, by the (n, j, l) quantum numbers describing the nucleon orbits for the levels, the number of nucleons which can be placed in each level (= 2j + 1), the number of nucleons contained through each level, and the magic numbers.

For nuclei which appear to be approximately spherical in shape, the shell model can be used to give quite accurate assignments of spin and parity to the first few levels of a nucleus, as well as to predict with limited success other nuclear properties such as magnetic moment. Semi-empirical coupling rules have been developed for the consideration of the spins and parities of the ground states of nuclei using the shell model. For an odd-A nucleus such as a mirror nucleus, these coupling rules state that the ground-state properties of the nucleus are found from consideration of only the nucleons which are odd in number. The coupling rules further regulate the contribution of the odd-numbered

nucleons by ruling that the total angular momentum is that resulting from the coupling of the nucleons in the last partially filled level.

For the particular nuclei studied in this experiment, the ground-state spins and parities can be explained correctly by the shell model. Consideration of the excited states is not so unambiguous, however, for single-particle excitations are often possible in many ways and there is some difficulty in determining the excitations preferred for a particular level and in accounting for the effects of multiple-particle excitations. The daughter nuclei which occurred in this experiment can be described, at least in the lower excited states, quite well by the shell model. More details of the basic shell model can be found in the excellent monograph on the subject by Mayer and Jensen (33).

The shell model is formulated using an isotropic average nuclear potential and considering nucleon motion in this potential as being independent of the motions of the other nucleons in the nucleus. This formulation yields a nuclear level structure analogous to atomic shell structure. However, the fact that the nuclear potential arises from the nucleons themselves provides a basis for departure from the comparison of nuclear and atomic models, for the atomic model arises from consideration of the motions of electrons in an external central potential, provided by the heavy

nucleus and indeed, relatively independent of electronic motion. Consideration of deformities of the nuclear shape which are indicated experimentally in the nuclei whose neutron and proton numbers are not close to the magic numbers, has led to the formulation of the unified model. This model is essentially one in which the individual-particle motion of the shell model is coupled with collective motion of the nucleus, which is assumed to be much slower. The interplay of these motions results in the predictions for nuclear properties which are dependent upon the amount of nuclear deformation present.

The unified model has been quite successful in the explanation of nuclear levels and properties for heavy nuclei which are highly deformed. The mirror nuclei investigated, with the exception of Ca^{39}, have neutron and proton numbers which are intermediate between the magic numbers 8 and 20. There are indications that these nuclei have rather large deformations, although many of the properties which lead to these indications are satisfactorily explained by the shell model. It will be assumed here that the shell model does not describe these nuclei so well as does the unified model, although this assumption is questionable, but might be justified simply because the assignments of nuclear levels seem to be less complicated using the unified model than for the shell model.

Figure 21 (54, p. 391) shows the levels obtained for the unified model as a function of spheroidal deformation for light nuclei. This type of nuclear level diagram can be continued to the heavier nuclei (55). δ is a nuclear deformation parameter, and η is the ratio of the deformation parameter to the strength of spin-orbit coupling. Positive or negative values for the deformation parameters indicate that the nuclear deformation is prolate or oblate, respectively. The shell model levels are shown at zero deformation, and their degeneracy of $(2j + 1)$ is split into $(2j + 1)/2$ sub-levels as the deformation is turned on. These levels can be considered as single-particle levels with double degeneracy.

For highly deformed nuclei, the nuclear rotational motions which are possible give rise to bands of rotational states with level spacing comparable to the single-particle level spacing which are superimposed upon the single-particle states, making the picture even more complex. These bands are characterized by K-values, or the values of the projection on the nuclear symmetry axis of the total angular momentum for the single-particle state. The spins of the rotational states increase by unity with each state in a band for odd-A nuclei. The energies of the rotational states increase as $I(I + 1)$, where I is the spin of the state, for all the rotational bands except the $K = 1/2$ band. Rotational

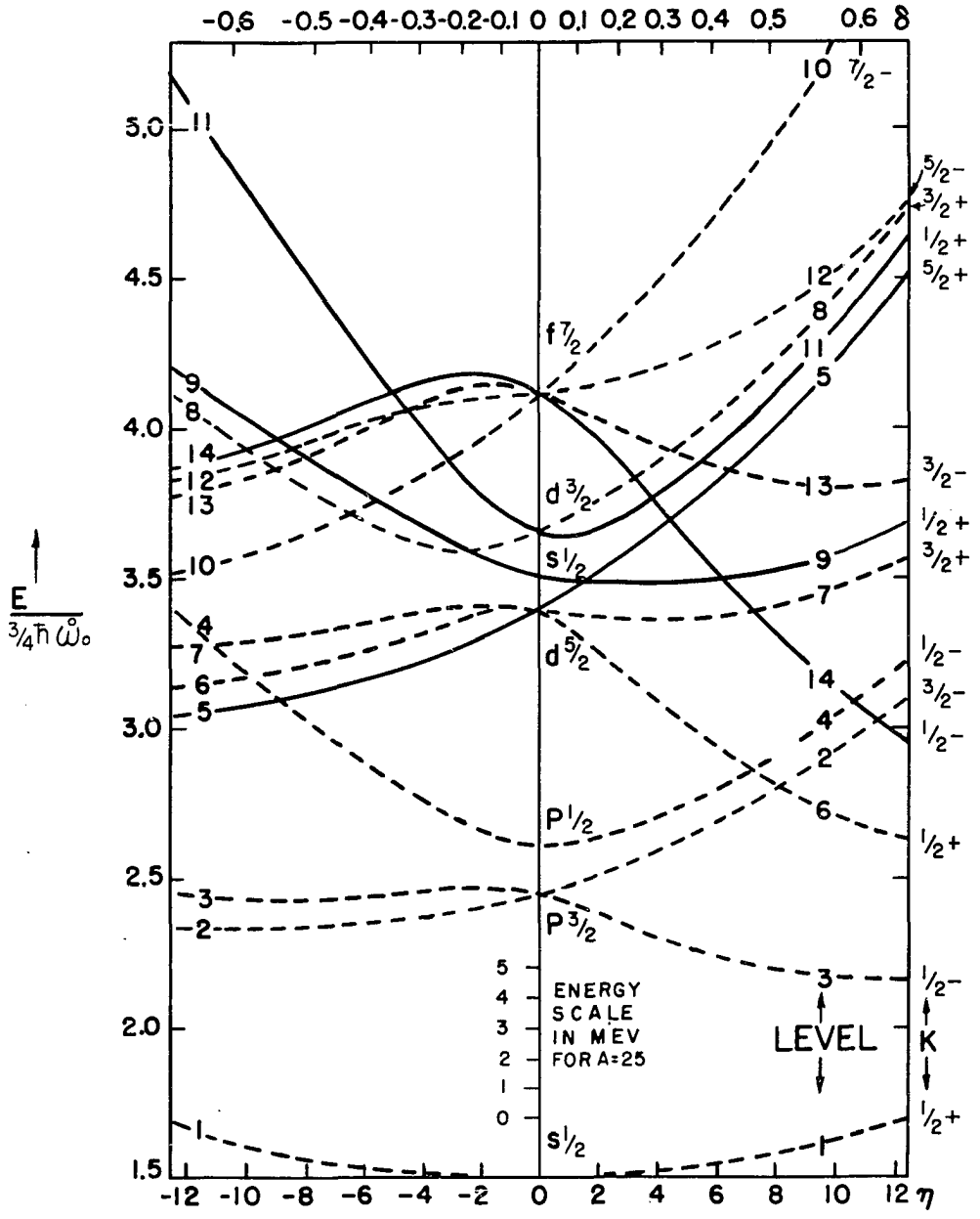

Figure 21. Level diagram of nuclear levels for a spheroidal potential with spin-orbit coupling

bands in odd-A nuclei for which K = 1/2 are characterized by a partial decoupling of the nucleon spin and rotational motion interaction, resulting in an anomalous spacing and ordering of levels. There is further interaction possible between states which have the same spin but are in different rotational bands called rotation-particle coupling which can make the spin and/or energy order of a rotational band anomalous.

The unified model with high deformations is generally successful in accounting for the energy level schemes of Ne^{21}, Na^{23}, Mg^{25}, and P^{31}. Ne^{21}, Na^{23}, and Mg^{25} all appear to have large prolate deformations, if the unified model is to be applied to the description of these nuclei. The equilibrium deformation of the light nuclei appears to change to oblate in the region of Si^{28} (56), so Al^{27} is very nearly spherical, and P^{31} is oblate. K^{39}, being nearly doubly magic, is not known to be deformed, but may have a small prolate deformation. Assignments of the nuclear levels to the unified-rotational model levels are found in the literature for Na^{23} (57, 58), Mg^{25} (54), and P^{31} (56). Those made below for Ne^{21}, Al^{27}, and K^{39} were made using analogy to the assignments for the other nuclei, where applicable.

To use the Nilsson scheme (55) for assignment of nuclear levels to single-particle or rotational states, an estimate of deformation of the nucleus in question must be made, and

rotational splittings estimated. For odd-A nuclei, then, the single-particle levels are filled in sequence with the nucleons of odd number, placing two nucleons in each state shown in Figure 21, until the final nucleon is alone in one of the single-particle levels. This level is then considered to describe the ground state of the nucleus, for the nucleons of even number and the odd number minus one nucleons of odd number filling single-particle levels are considered to pair off in the levels they occupy so as not to contribute to the nucleus description. Excited states are then accounted for using rotational and/or single-particle excitations on the last odd nucleon. This procedure fairly accurately describes assignments for the daughter nuclei levels for this investigation.

The decay schemes of the radioactive nuclei enccuntered in this investigation are shown in Figures 22-27. Figure 22(a) shows the decay scheme of Na^{22} (59) and the lower energy levels of Ne^{22} (60). The positron decay of Na^{22} is almost entirely a transition to the first excited state of Ne^{22}, and the resultant 1.276 Mev gamma ray was used in this experiment for purposes of solid angle determination and detector energy calibration. The notation of the decay schemes includes spin and parity assignments (when known) to the left of a nuclear level, the energy of the level in Mev to its right, the end-point energy of the highest energy

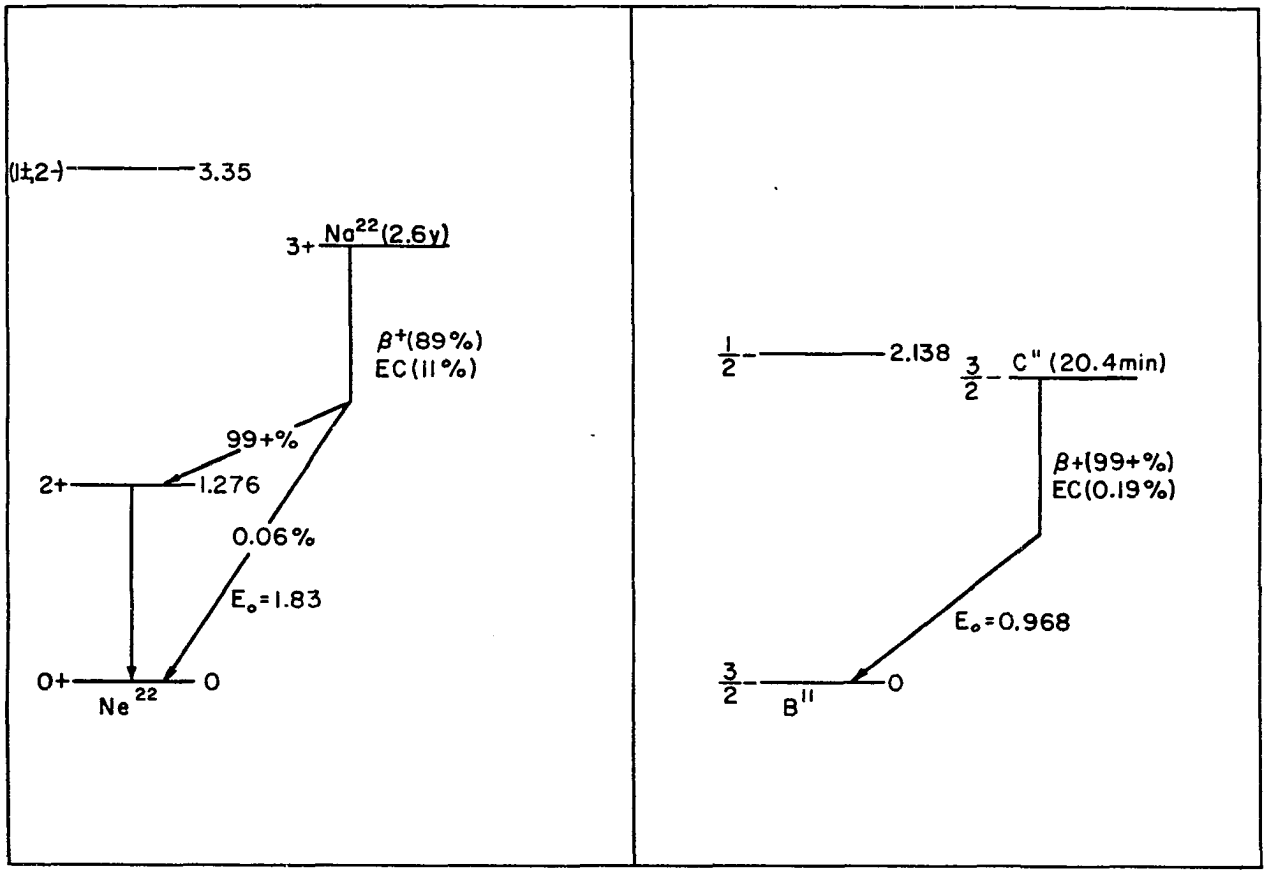

Figure 22. Decay schemes of Na^{22} and C^{11}
(a) Na^{22}
(b) C^{11}

beta group, and the half-life of the total decay. Figure 22(b) shows the decay scheme of C^{11} (59) and the level diagram for B^{11} (60). The C^{11} decay was used as a pure annihilation radiation source for the Mg^{23} study, since no branching is energetically possible in this decay.

Figure 23(a) is the decay scheme of Na^{21}. The maximum end-point energy of Na^{21} (10, 11), the half life (17), and the energy levels of Ne^{21} (61, 62) are shown. The branching which is shown is a result of this investigation. The energy levels of Ne^{21} are accounted for using the unified model with rotational states and large prolate deformation. The ten protons of Ne^{21} do not contribute to the properties of its low-lying states, by consideration of the single-particle coupling rules and orbital symmetry. The eleven neutrons of Ne^{21} fill levels 1-4, and 6 in Figure 21 and one neutron is left in level 7, using a deformation of between $\eta = 0$ and $\eta = 6$, this level giving the 1d5/2, k = 3/2 configuration to the ground state.

By analogy with the coupling found for the eleven protons of Na^{23}, the first excited state for Ne^{21} is the first excited rotational level based on the K = 3/2 ground state single-particle level. The second and third excited states are not so clear-cut in origin, partly because the parity of the second excited state is not known, although it is reasonable to assume it is positive. If the third

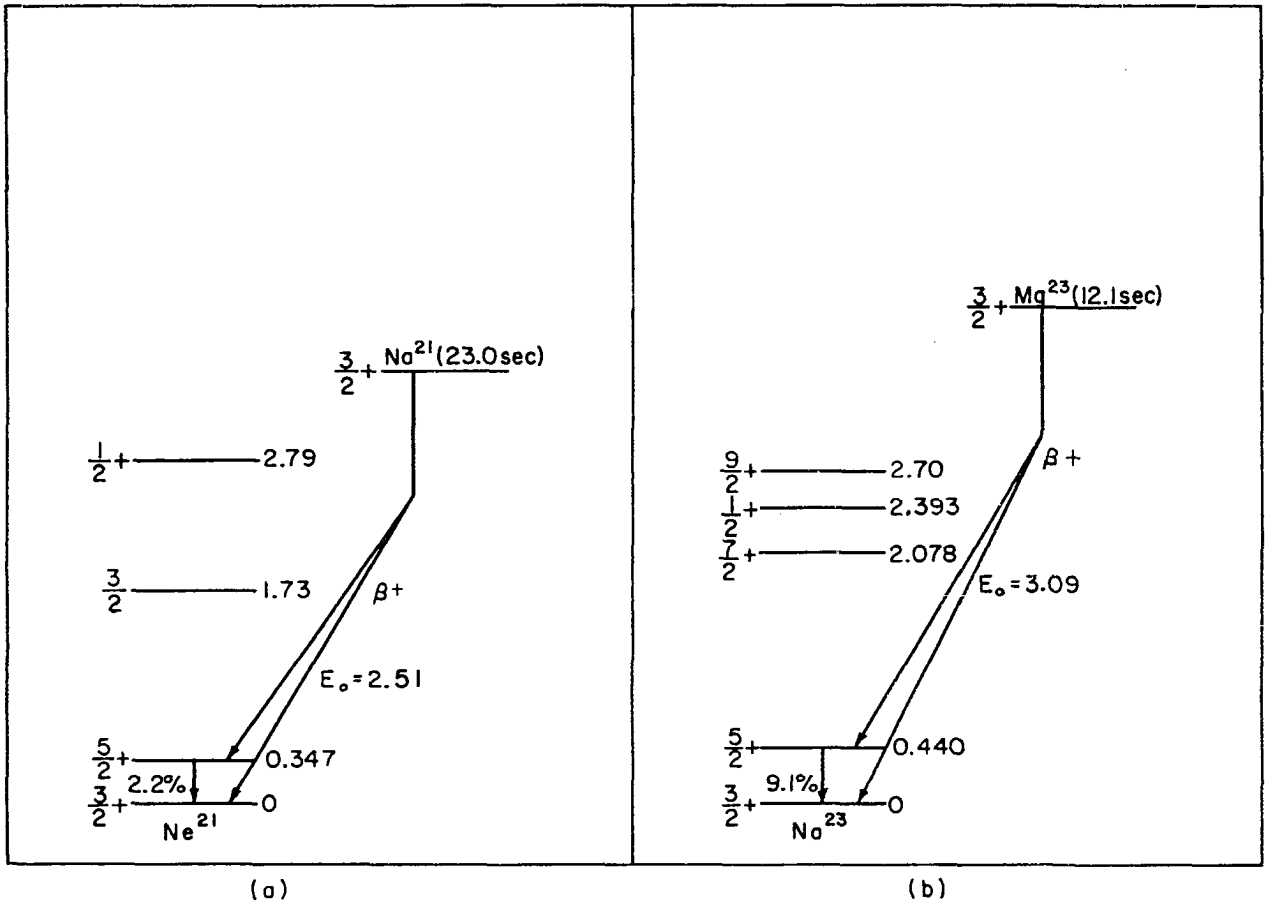

Figure 23. Decay schemes of Na^{21} and Mg^{23}
(a) Na^{21}
(b) Mg^{23}

excited state is a 2s1/2, K = 1/2 level, then with rotational spacing for the K = 1/2 band unusually anomalous, the second excited state may be the rotational ground state of the K = 1/2 band. This explanation is not unambiguous, however, for the large energy separation between the second and third excited states make it hard to believe that the I = 3/2, K = 1/2 state could be so far below the I = 1/2, K = 1/2 state from the decoupling effects of the K = 1/2 band and the rotation-particle coupling from higher rotational bands. Since the second excited state is energetically unfavored for a positron transition, it is sufficient to know only the character of the first excited state for Ne^{21}, which is more confidently assigned as 1d5/2, K = 3/2, I = 5/2.

Figure 23(b) is the decay scheme of Mg^{23}. The maximum end-point energy (10, 11), the half-life (16), and the energy levels of Na^{23} (57, 63) are shown, and the indicated branching is a result of this investigation. The energy levels of Na^{23} have been described in terms of the unified-rotational model by Paul and Montague (58). The ground state is of the configuration 1d5/2, K = 3/2, with a deformation of about $\eta = 6$, while the first, second, and fourth excited states are rotational states based on the ground state, and the third excited state is the 2s1/2, K = 1/2 single-particle level. Paul and Montague have calculated

the effects of configuration mixing through rotation-particle coupling, and their predictions of the level order would be accurate through the fourth excited state if a little more mixing were allowed, depressing the I = 9/2, K = 3/2 rotational state a little more. Again, for Na^{23}, only the first excited state is of interest when considering branching, since energetic considerations greatly hinder transitions to higher excited states of Na^{23}.

The decay scheme of Al^{25} is shown in Figure 24(a). The half-life (17), maximum end-point energy (10, 11), the level scheme of Mg^{25} (54, 64, 65), as well as a weak branch in the decay (25) are shown. No additional branches to the lower excited states were found in this investigation. The energy levels of Mg^{25} are well accounted for by the unified model (54). The ground state is the 1d5/2, K = 5/2 single-particle level for a fairly small positive deformation, and the third excited state is the first rotational excitation of the rotational band based on the ground state. The first, second, and fourth excited states all belong to the rotational band of the 2s1/2, K = 1/2 single-particle level. The deformations which had to be used for this explanation were not constant for the different rotational bands, presumably because effects of rotation-particle coupling were not included in this description.

Figure 24(b) shows the decay scheme of Al^{26} (59), which

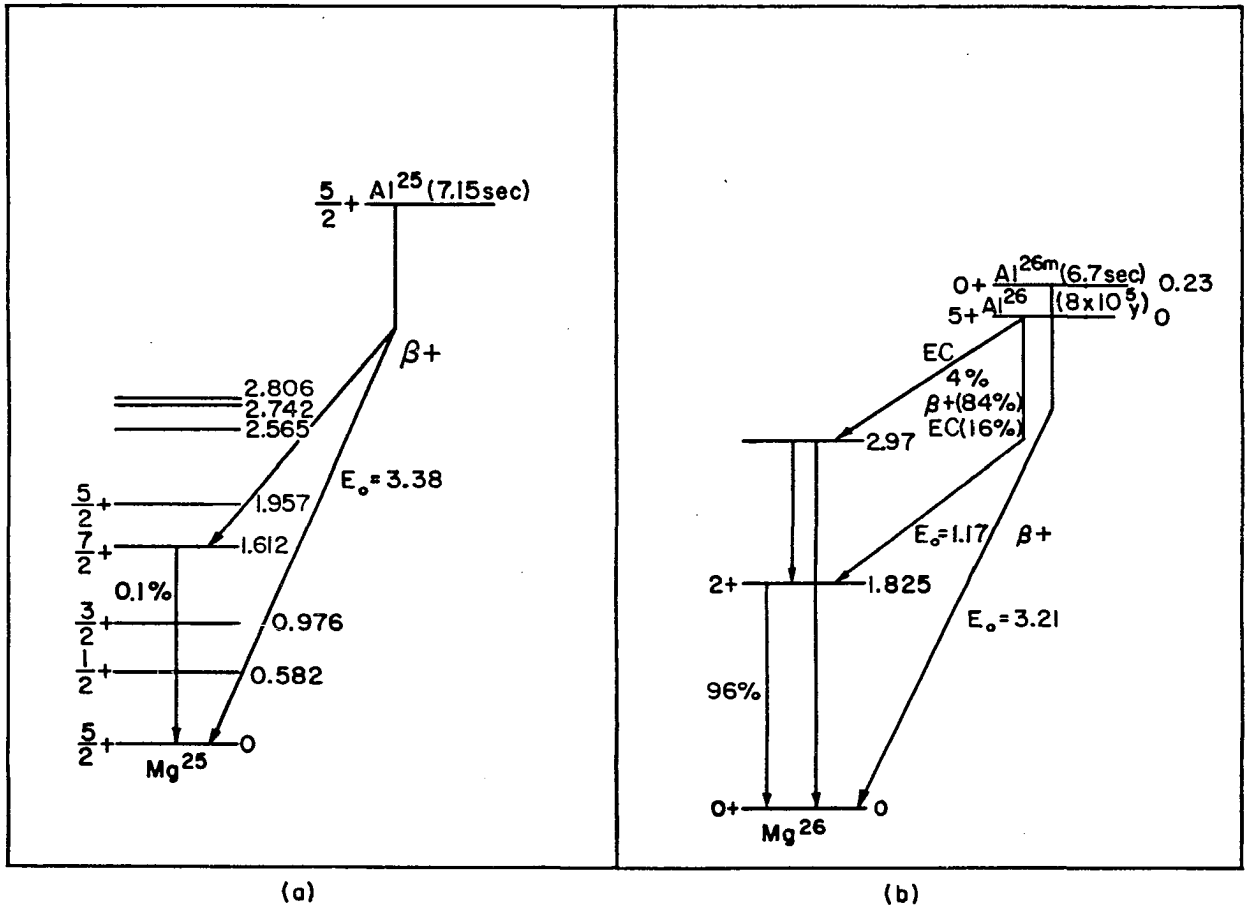

Figure 24. Decay schemes of Al^{25} and Al^{26}
(a) Al^{25}
(b) Al^{26}

indicates the absence of branching in the decay of Al^{26m}. It might be noted that had branching to the first excited state of Mg^{26} been present, the resultant gamma ray would not have been in the energy range of interest for the Al^{25} study, so would not have seriously interfered in this study.

Figures 25(a) and 25(b) show the decays of Al^{28} and Al^{29} (59, 66). These decays are pictured here to account for the gamma rays observed in the singles spectra of the study of Si^{27}.

The decay scheme of Si^{27} is shown in Figure 26(a). The half-life (16), end-point energy (10, 11), and levels for Al^{27} (66) are indicated, but no indication of branching was found in the study of Si^{27}. Since the deformation of the nucleus changes sign around Si^{28} (56), a small positive deformation for Al^{27} offers a possible explanation of the energy levels. The ground state is a 1d5/2, K = 5/2 level, while the first, second, and fourth excited states of Al^{27} appear to be reasonably explained as rotational states based upon the 2s1/2, K = 1/2 single-particle level. The third excited state arises possibly from the 1d3/2, K = 1/2 level with anomalous rotational spacing or perhaps from the 1d3/2, K = 3/2 level due to small negative deformation. However, the exact assignment of this level is not important for this discussion, since a branch to this level is energetically hindered to the extent that it might be un-

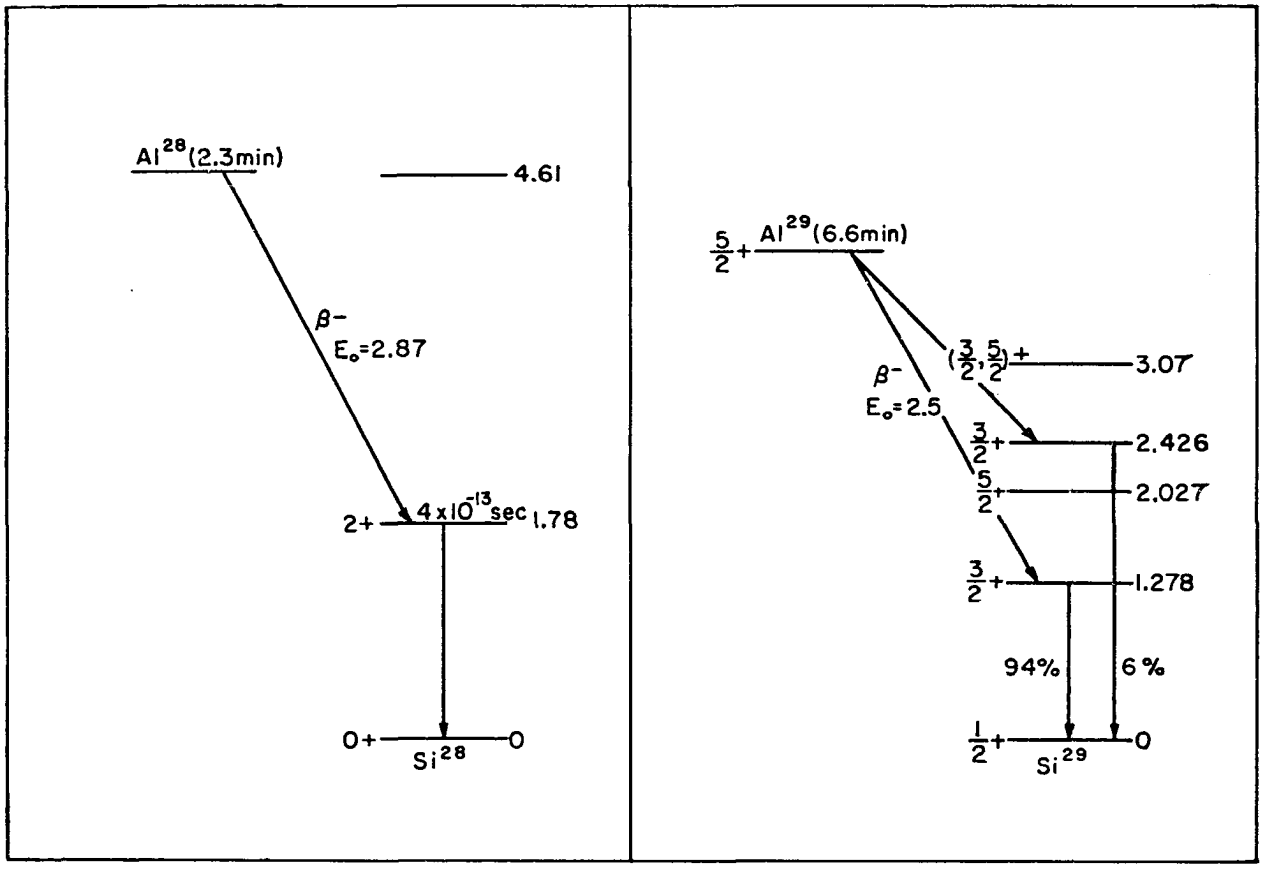

Figure 25. Decay schemes of Al^{28} and Al^{29}

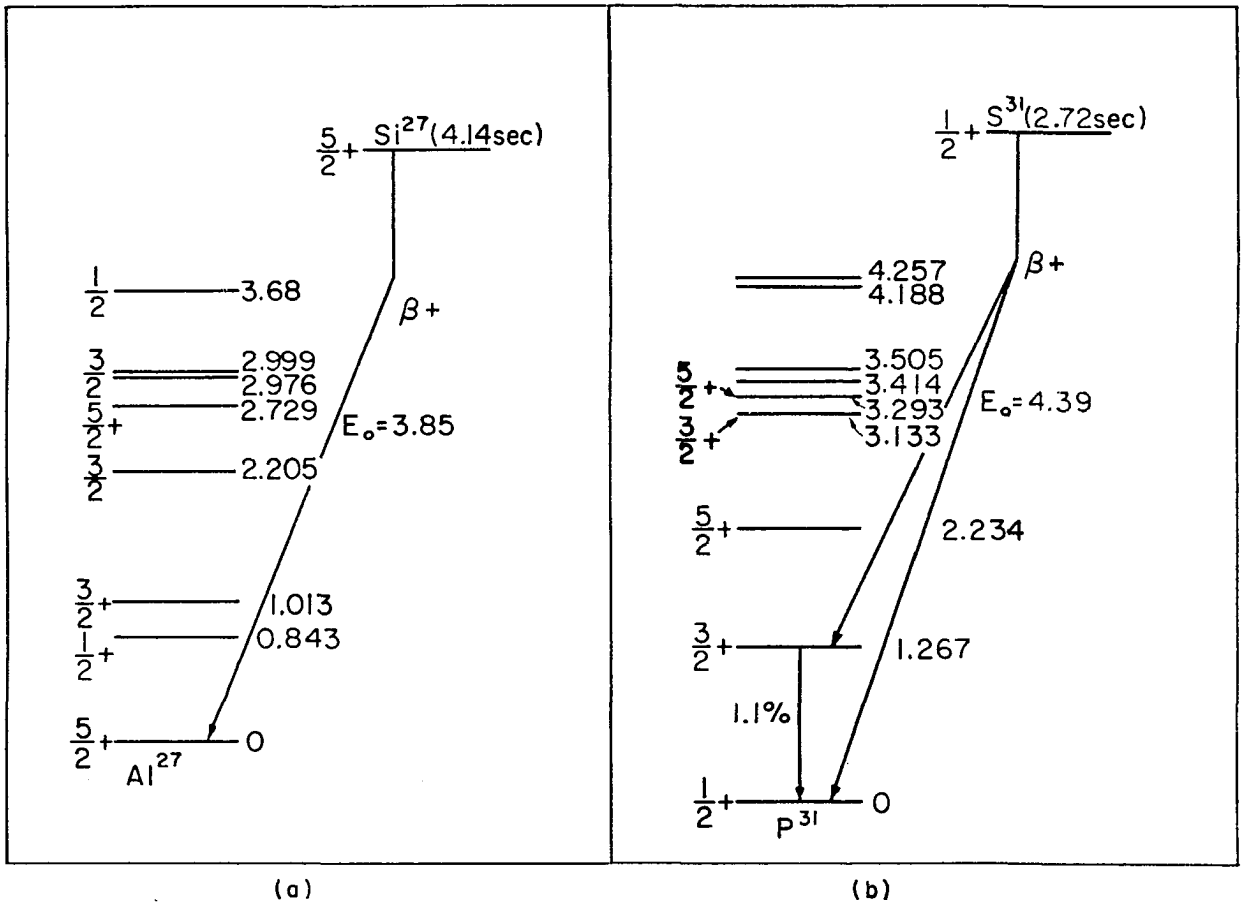

Figure 26. Decay schemes of Si^{27} and S^{31}
(a) Si^{27}
(b) S^{31}

detectable with the method utilized in this investigation.

Figure 26(b) is the decay scheme of S^{31}. The half-life (16), maximum end-point energy (10, 11), and the energy level system for P^{31} (67) are indicated along with the branching transition found in the study of S^{31} in this investigation. The energy levels of P^{31} are fairly well described by the unified model (56), using a negative deformation of about = -3. The ground state is a 2s1/2, K = 1/2 single-particle level, and the second excited state is the first rotational level in the band based on the ground state. This K = 1/2 rotational band has anomalous order in that the I = 5/2 state has a lower energy than the I = 3/2 state (which forms the third excited state of P^{31}). The second excited state belongs to the 1d3/2, K = 3/2 single-particle level.

Figure 27(a) is the decay scheme for K^{38} (59), for which the 2.16 Mev gamma ray was seen on both the singles and coincidence spectra in the study of Ca^{39}. The decay scheme of Ca^{39} is shown in Figure 27(b). The half-life (14), end-point energy (14), and energy levels of K^{39} (68) are indicated. No branching was found as a result of the study of Ca^{39}. The ground state of K^{39} is 1d3/2, K = 3/2, indicating the possible presence of a small positive deformation. The first four excited states could then be assigned to the 1f7/2, K = 1/2, 3/2, 5/2, 7/2 single-particle levels, but

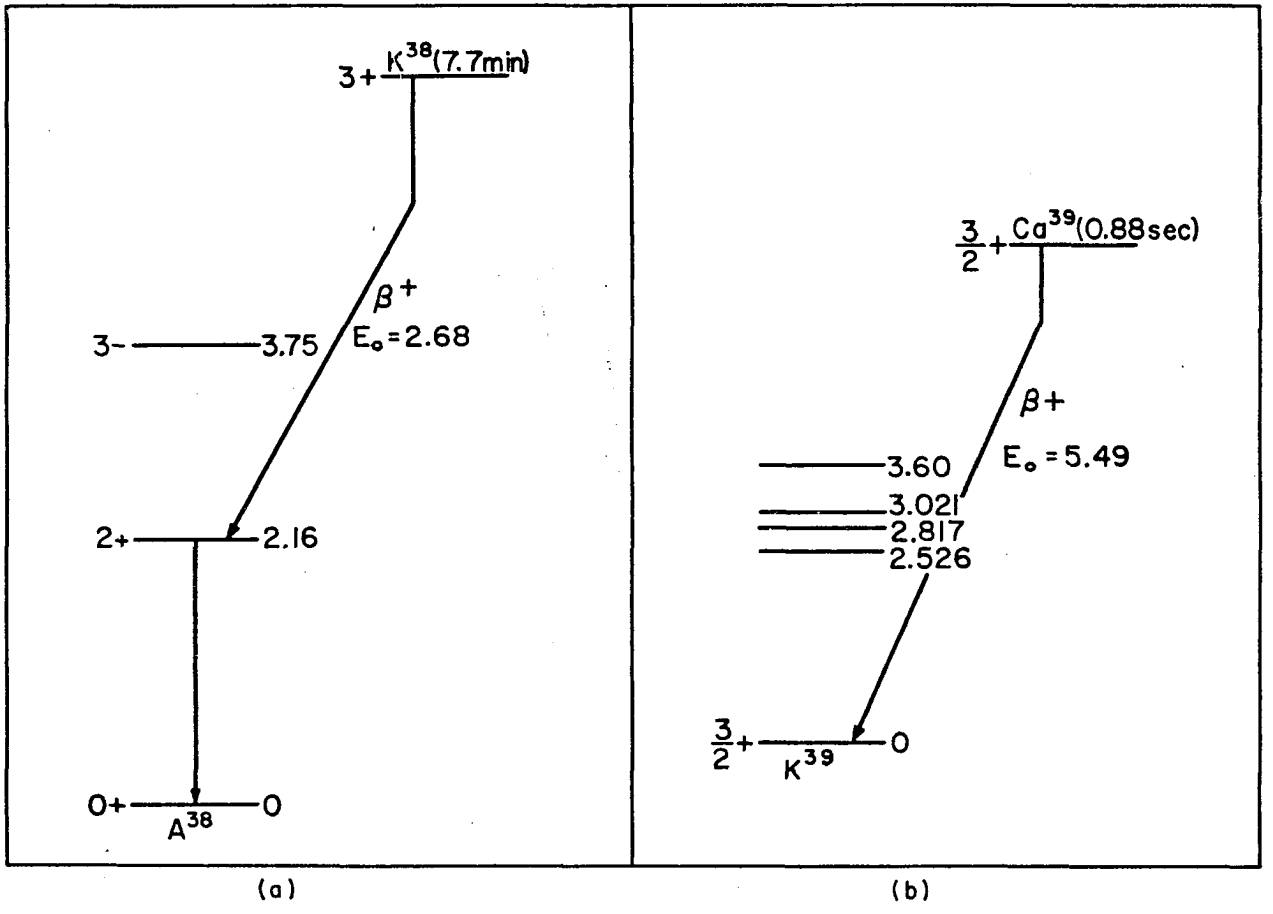

Figure 27. Decay schemes of K^{38} and Ca^{39}
(a) K^{38}
(b) Ca^{39}

the absence of experimental values for the spins and parities of these levels makes it impossible to have confidence in such an assignment. However, due to the large energy gap between the ground and excited states, it is reasonable to assume that at least some of these excited states are contained in the 1f7/2 single-particle levels.

The above decay schemes for the mirror nuclei investigated were composed of what is considered to be the most reliable data to date, and thus represent the present experimental decay picture. The assignments of nuclear configurations to the daughter nuclei levels were either taken from the literature, assuming the unified model representation, or assigned by reasonable comparisons with others or reasonable assumptions of the nuclear deformation. It is to be noted that the shell model representation can not be ruled out as being valid in this discussion, since it, too, can give reasonable assignments to the level configurations although more complicated excitation processes would be necessary for some of the higher excited levels. In view of this ambiguity, it stands to reason that a careful theoretical analysis of the level systems of these mirror nuclei comparing the unified and shell model representations is much needed, and may help remove the ambiguity, when more detail is included in the analysis, such as gamma and beta transition probabilities, nuclear moments, etc.

2. Selection rules and expected branching

The selection rules for allowed beta-decay transitions are stated in the introduction as ($\Delta I = 0$, no) for the Fermi interaction and ($\Delta I = 0, \pm 1$ (no $0 \rightarrow 0$), no) for the Gamow-Teller interaction. The ΔI refers to the allowed nuclear spin change between initial and final states for the interaction, and the "no" refers to no change in parity between initial and final states for the interaction.

Transitions which are not allowed by these selection rules are known as forbidden transitions, and are much less intense than allowed transitions from consideration of the resultant nuclear matrix elements. Forbidden transitions are classed in two ways, by order and as ℓ-forbidden. A first forbidden transition, for instance, involves a change in parity and the spin may change by $0, \pm 1, \pm 2$. For $n \neq 1$, an n^{th}-forbidden transition follows the selection rules ($\Delta I = \pm n, \pm (n+1)$), with parity change for n odd. An ℓ-forbidden transition, which may also be order-forbidden, involves initial and final states for which the parities are alike, but the orbital angular momenta are different. Since ℓ is not a good quantum number for the unified model, transitions can be ℓ-forbidden only between states described by the shell model. For the unified model representation, the selection rules for a transition from a state (K_i, $I_i \pi_i$) to a state (K_f, $I_f \pi_f$) are (69), $|I_i - I_f| \leq L \leq I_i + I_f$,

$\pi = \pi_i \pi_f$, $|K_i - K_f| \leq L$, where L is the transition multipolarity and π the parity. Allowed transitions have $L = 0, 1$ and $\pi = +$. A retardation effect is present for K-forbidden transitions, for which $\nu = \Delta K - L$, if positive, is the degree of this forbiddenness.

For the mirror nuclei in question, if a ground-state to excited-state transition is predicted to be forbidden by consideration of the selection rules, it would probably amount to less than one per cent of the total decay. Also, since the excited-state transitions have significantly less energy available for decay, the consideration of energetics would further decrease the intensities of branching transitions. The possibility of the presence of branching transitions can be determined on the basis of the selection rules, using the configuration assignments from the unified model, and the consideration of energetics involved in the transitions.

One more consideration is necessary in the determination of predictions for branching. Since the beta-decay interaction is considered to be a single-particle interaction, branching transitions which would involve the interaction of two nucleons are not possible under the present construction of beta-decay theory. Thus, a transition is not possible when it requires a change in status of more than one nucleon during the interaction.

The success of the predictions of branching as determined by the above selection rules depends upon the purity of the configurations describing the nuclear levels involved. Configuration mixing in these levels could alter the situation greatly, but was not considered in the predictions. From the fact that rotation-particle coupling seems to be important in the assignment of unified model levels to most of the excited states of the daughter nuclei, it is not unexpected that the branching transitions observed may also depend upon the configuration mixing that is present.

A very rough estimate of the branching ratio for transitions to different states of the same rotational band is possible by simply taking the ratio of the vector addition coefficients which are appropriate for the addition of the initial spin and multipolarity to form the final spin in each transition (69, p. 11). Such an estimate is rigorous, if pure rotational states are involved. However, in the nuclei to which branches were observed to rotational states based on the ground state, the rotational states could not be considered to be pure due to the rotation-particle coupling necessary to account for the level energies.

For the decay of Na^{21}, the selection rules above result in allowed transitions to the ground and first excited states of Ne^{21}. A transition to the second excited state of Ne^{21}

is possibly K-forbidden for the Fermi part of the interaction, and in addition is energetically unfavored. In the experiments on Na^{21}, the first excited state branch was observed, so that the decay of Na^{21} is qualitatively understood on the basis of the unified model. It should be pointed out that the shell model can also be used to interpret the decay of Na^{21} with the same result, so further study of the interpretation such as using the value of the observed branching ratio to compare with calculated values would be needed to see which model more accurately describes the situation. A crude estimate of the branching ratio considering energetic (59, p. 598) and rotational wave function (69, p. 11) effects gives a value of 13 per cent (compared to the experimental value of 2.2 per cent), indicating that the unified model in this crude interpretation (using pure configurations) is descriptive of the branching only in a qualitative sense.

Mg^{23} was observed to decay to the ground and first excited states of Na^{23}. No other branches appeared by inspection of the singles spectra. A branch to the second excited state of Na^{23} is energetically unfavored and second-order forbidden. A branch to the third excited state is energetically unfavored and forbidden since it would necessitate a two-particle interaction in the transition. This transition would require one $1d5/2$, $K = 3/2$

proton to decay into a 1d5/2, K = 3/2 neutron and further require the other 1d5/2, K = 3/2 proton to be elevated into a 2s1/2, K = 1/2 state. The configuration for the second excited state of Na^{23} is not as easy to assign using the shell model as it is using the unified model, so it appears that the unified model satisfactorily describes, at least qualitatively, the situation. An estimate of the branching intensity from energetic and rotational wave function effects, such as was done for Na^{21}, yields a value of 11 per cent, which is surprisingly close to the observed value of 9.1 per cent.

No branching to the first two excited states of Mg^{25} was observed in this investigation for the decay of Al^{25}. The unified model interpretation of the levels involved allows transitions to the ground and third excited states of Mg^{25}. Branching to the first and fourth excited states is second-order forbidden, while branching to the second excited state is K-forbidden. Transitions to higher energy levels of Mg^{25} are energetically unfavored. The absence of branching as determined by this study to the second excited state of Mg^{25} indicates that K must be at least approximately a good quantum number. The unified model appears again to describe the situation satisfactorily, since the consideration of branching using the shell model would allow a transition to the second excited state, using the simplest con-

figuration assignment of the last odd neutron in the 1d3/2 level. From energetic considerations alone, which can be considered an upper limit for the shell model representation, the branching to this level is estimated at about 25 per cent. The transition allowed to the third excited state using the unified model has been observed by Maeder and Stahelin (25) to be of very low intensity. A crude estimate of this intensity using energetic and pure rotational wave function effects as was done for Na^{21} and Mg^{23} gives about 2 per cent for this intensity (compared to the experimental value of 0.1 per cent), so some further effect due to configuration mixing may be necessary to place the unified model in more quantitative agreement for this value. Further calculations of the predicted branching intensity need to be made for comparison with the data using both the unified and shell models to be able to determine the accuracy of the description of each model.

The decay of Si^{27} was observed in this experiment to contain no branching. The use of the selection rules allows only the ground state transition. Branching to the first and second excited states of Al^{27} is second-order forbidden and K-forbidden, respectively, besides being forbidden because it involves a two-particle transition in each case, as does branching to the third excited state. Branches to higher excited states in Al^{27} are energetically unfavored.

The shell model representation of the levels of Al^{27} would also have forbidden excited-state branches for the reason that two-particle transitions would be needed, so no preference can be given to the unified or shell model descriptions using just this evidence.

A branch was found in this investigation to the first excited state of P^{31} in the study of the decay of S^{31}. The selection rules allow only the transition to the ground state of P^{31}. A branch to the first excited state is forbidden since it would involve a two-particle transition, while the second excited-state branch is second-order forbidden. Branches to the higher excited states of P^{31} are energetically unfavored. Since the shell model and unified model, with pure configurations, predict the same degrees of forbiddenness for branches in the decay of S^{31}, no preference can be given to either representation on the basis of the experimentally observed branch.

The presence of the branching transition in the decay of S^{31} can be explained on the basis of the configuration mixing in the spherical shell model description of the ground state of P^{31}, as found by Parkinson (70). Using the shell model representation, Parkinson found the ground state of P^{31} to be principally an admixture of three configurations, the principal configuration of $n(2s1/2)^2p(2s1/2)^1$, with admixtures of the $n(2s1/2)^2p[(2s1/2)^1(1d5/2)^{-1}(1d3/2)^1]$

and $n[(2s1/2)^1(1d3/2)^1]p(2s1/2)^1$ configurations. It is reasonable to assume that the S^{31} ground state is also an admixture mostly of these three states. The first excited state of P^{31} can be assumed to be made up of single-particle excitations of the ground-state configurations. There is no zero-order transition possible between the principal configurations of the S^{31} ground state and P^{31} first excited state. One of the excited state configurations is that of $n[(2s1/2)^1(1d3/2)^1]p[(2s1/2)^2(1d5/2)^{-1}]$, and this configuration can participate in an allowed first-order intensity beta transition from the principal configuration of the S^{31} ground state. There exist possibilities for other allowed transitions between the admixture configurations of the S^{31} ground state and P^{31} first excited state which are then of second-order intensity, and so give a small contribution. The excited state of P^{31} can then de-excite, causing the emission of the 1.27 Mev gamma ray observed in the experiment.

This same argument for the branching of the S^{31} decay via non-pure configurations can also be carried out using the unified model, for which the configurations $(2s1/2, K = 1/2)$, $(1d3/2, K = 3/2)$, and $(1d5/2, K = 3/2)$ are substituted for the 2s1/2, 1d3/2, and 1d5/2 shell-model configurations, respectively. The configurations of the unified model are not expected to be pure configurations

since admixtures had to be assumed to explain the energy level order of P^{31} (56).

The decay of Ca^{39} was not observed to have any branching in this investigation. Assuming that the first three excited states of K^{39} are not rotational levels based on the ground state but are instead single-particle levels of the 1f7/2 type which are slightly separated from the effects of small nuclear deformation, any transition to these states would be a two-particle transition besides being first-order forbidden. Branches to higher states are energetically unfavored. When the spins and parities for the levels of K^{39} are known, the preference between shell model and unified model descriptions for the decay of Ca^{39} should be seen more easily, since both models predict the absence of branching with reasonably assumed configurations.

It is to be noted that the unified model, while satisfactory to explain the findings of this experiment, is not unambiguously a better description than is the spherical shell model for the nuclei included in this investigation. The assignment of configurations to the daughter nuclear levels is not so easy using the shell model when the third or fourth levels come into consideration, but it is no less easy to assign the mixture of configurations necessary to account for the spacing of these levels using the unified model. It is hoped that the future may reveal more detailed

analyses of these decays using both models and perhaps these analyses can remove the ambiguity in the present interpretations.

B. Comparative Lifetimes

The comparative lifetimes previously reported (11, 14) for the mirror nuclei investigated in this experiment were calculated with the assumption that no branching existed in the decays of these nuclei. The fact that branching does exist in the decays of Na^{21}, Mg^{23}, and S^{31} alters the comparative lifetimes for the ground-state to ground-state transitions since the decay probabilities for these transitions are no longer as large as had been thought.

The change in the comparative lifetimes which results from branching is made through the half-lives, then, as follows: the total decay probability of a radioactive decay is the sum of the decay probabilities for each transition by which the decay can occur. For the purpose of this investigation, in which an indication was found for no more than two transitions in any decay, the total decay probability can be written

$$N_{total} = \frac{\ln 2}{t_{\frac{1}{2}}} = N^{(1)} + N^{(2)} = \ln 2 \, (1/t^{(1)}_{\frac{1}{2}} + 1/t^{(2)}_{\frac{1}{2}}) \ ,$$

where (1) and (2) refer to the ground-state to ground-state and ground-state to excited-state transitions, respectively.

In terms of the branching ratio as defined in this experiment, the values for $t^{(1)}_{\frac{1}{2}}$ and $t^{(2)}_{\frac{1}{2}}$ can be found easily, for then $N^{(2)} = \beta N$, so that

$$t^{(2)}_{\frac{1}{2}} = t_{\frac{1}{2}}/\beta ,$$

and

$$t^{(1)}_{\frac{1}{2}} = t_{\frac{1}{2}}/(1 - \beta) .$$

An appreciable correction to the comparative lifetime is the result only for the case of Mg^{23}, due to the intrinsic uncertainty in the presently available values for ground-state to ground-state comparative lifetimes. Table 1 lists the comparative lifetimes for the nuclides covered in this investigation. The values of f were calculated with the f-function tables of Moszkowski and Jantzen (71), using the end-point energies given and the half-lives as modified by branching. The references are given for end-point energies and uncorrected half-lives.

Table 1. Comparative lifetimes for the nuclides studied in this experiment

Parent isotope	Daughter level (Mev)	End-point energy (Mev)	Total $t_{1/2}$ (sec)	Transition $t_{1/2}$ (sec)	ft (sec)	References
Na^{21}	0	2.51 ± 0.02	23.0 ± 0.2	23.5 ± 0.2	3910 ± 150	(11, 17)
	0.347	2.16 ± 0.02		1045 ± 140	90400 ± 11900	
Mg^{23}	0	3.09 ± 0.01	12.1 ± 0.1	13.3 ± 0.1	5490 ± 100	(11, 16)
	0.440	2.65 ± 0.01		133 ± 7	27700 ± 1600	
Al^{25}	0	3.38 ± 0.03	7.15 ± 0.12	7.16 ± 0.12	4300 ± 190	(11, 17)
	1.612	1.77 ± 0.03		7150 ± ?	247000 ± ?	
Si^{27}	0	3.85 ± 0.02	4.14 ± 0.03		4410 ± 130	(11, 16)
S^{31}	0	4.39 ± 0.03	2.72 ± 0.02	2.75 ± 0.02	5160 ± 170	(11, 16)
	1.267	3.12 ± 0.03		247 ± 22	98900 ± 10200	
Ca^{39}	0	5.490 ± 0.025	0.88 ± 0.01		4330 ± 100	(14, 14)

V. SUMMARY

The experimental knowledge of the decays of mirror nuclei was found to contain little information about possible branching in these decays. In this investigation, branching was studied in the positron decays of Na^{21}, Mg^{23}, Al^{25}, Si^{27}, S^{31}, and Ca^{39}. These activities were produced by bombardment of their respective natural elements in the X-ray beam of the Iowa State University Synchrotron.

The branching of transitions was determined by looking for nuclear gamma rays in fast coincidence with the positron annihilation radiation. The search was restricted to gamma rays which had energies expected from a consideration of the nuclear levels for the daughter nuclei. Interference in the gamma-ray spectra which was due to the intense annihilation radiation was minimized by geometrical arrangement of the coincidence detectors.

The decays of Al^{25}, Si^{27}, and Ca^{39} had no branching intense enough to be observed using this method. Upper limits for branching in these decays were estimated, and were less than one per cent. Branching which had not been reported previously was found in the decays of Na^{21} (2.2 per cent), Mg^{23} (9.1 per cent), and S^{31} (1.1 per cent), each branch proceeding to the first excited state of the daughter nucleus.

Except possibly for K^{39} and Al^{27}, the daughter nuclei

can be interpreted as having rather large nuclear deformation, so an attempt to describe the daughter states and the presence of branching was made using the concepts of the unified model. This description was generally successful in accounting for the qualitative aspects of the observed branching, and no attempt was made to extract accurate expected intensities of branching from the unified model for comparison to the experimentally determined intensities. The comparative lifetimes for the main and branch transitions were calculated.

It is conceivable that further refinements of the measurements of this investigation could be developed, particularly with regard to increasing the sensitivity of the method. Much experimental work is also needed to obtain more accurate values of the end-point energies of the decays and the total decay half-lives.

Much theoretical work in the interpretation of the data is necessary, using the viewpoints of both the unified and spherical shell models. The unified model interpretation of the results of the experiment is certainly not unambiguously preferable to possible interpretations based on the spherical shell model, except in the case of Al^{25}. For this transition, the unified model predicts no branching to the second excited state of Mg^{25}, in agreement with the results of this investigation, while such a branch is ex-

pected under the shell model interpretation. Only detailed theoretical consideration of the present experimental data can hope to resolve the general ambiguity which shows up in the description of mirror nuclei.

VI. BIBLIOGRAPHY

1. R. D. Evans. The atomic nucleus. McGraw-Hill Book Company, Inc., New York. 1955.

2. L. N. Cooper and E. M. Henley, Phys. Rev. 92, 801 (1953).

3. B. G. Jancovici, Phys. Rev. 95, 389 (1954).

4. B. C. Carlson and I. Talmi, Phys. Rev. 96, 436 (1954).

5. J. M. Blatt and V. F. Weisskopf. Theoretical nuclear physics. John Wiley and Sons, Inc., New York. 1952.

6. F. I. Boley and D. J. Zaffarano, Phys. Rev. 84, 1059 (1951).

7. R. M. Kline and D. J. Zaffarano, Phys. Rev. 96, 1620 (1954).

8. W. A. Hunt and D. J. Zaffarano. Radioactive disintegration spectra of some short-lived nuclides. U. S. Atomic Energy Commission Report ISC-469 [Ames Lab., Ames, Iowa]. March 1954.

9. L. S. Ring, Jr. and D. J. Zaffarano. Beta spectra of some short-lived nuclides. U. S. Atomic Energy Commission Report ISC-648 [Ames Lab., Ames, Iowa]. June 1955.

10. J. A. Welch, Jr. and R. Wallace, Bull. Am. Phys. Soc. Ser. 2, 3, 206 (1958).

11. J. A. Welch, Jr. Beta spectra of the mirror nuclei with A = 19 to 39. U. S. Atomic Energy Commission Report UCRL-3888 [California, Univ., Berkeley. Radiation Lab.]. August 2, 1957.

12. O. C. Kistner, A. Schwarzschild, and B. M. Rustad, Phys. Rev. 104, 154 (1956).

13. O. C. Kistner, A. Schwarzschild, B. M. Rustad, and D. E. Alburger, Phys. Rev. 105, 1339 (1957).

14. O. C. Kistner and B. M. Rustad, Phys. Rev. 112, 1972 (1958).

15. O. C. Kistner and B. M. Rustad, Phys. Rev. 114, 1329 (1959).

16. M. V. Mihailović and B. Povh, Nuclear Phys. 7, 296 (1958).

17. S. E. Arnell, J. Dubois, and O. Almén, Nuclear Phys. 6, 196 (1958).

18. J. E. Cline and P. R. Chagnon, Bull. Am. Phys. Soc. Ser. 2, 3, 206 (1958).

19. K. Siegbahn and S. E. Petersson, Arkiv Mat., Astron. Fysik 32, Sect. B, No. 5 (1946).

20. L. M. Langer, C. S. Cook, and M. B. Sampson, Phys. Rev. 71, 906 (1947).

21. V. Perez-Mendez and P. Lindenfeld, Phys. Rev. 83, 864 (1951).

22. J. B. Warren, K. A. Laurie, D. B. James, and K. L. Erdman, Can. J. Phys. 32, 563 (1954).

23. M. G. White, L. A. Delsasso, J. G. Fox, and E. C. Creutz, Phys. Rev. 56, 512 (1939).

24. G. Schrank and J. R. Richardson, Phys. Rev. 86, 248 (1952).

25. D. Maeder and P. Stahelin, Helv. Phys. Acta 28, 193 (1955).

26. J. Varma, Proc. Phys. Soc. (London) 69, Sect. A, 641 (1956).

27. H. Roderick, O. Lonsjo, and W. E. Meyerhof, Phys. Rev. 97, 97 (1955).

28. W. E. Meyerhof and G. Lindstrom, Phys. Rev. 93, 949 (1954).

29. J. Scobie and G. M. Lewis, Phil. Mag. 2, 1089 (1957).

30. E. Fermi, Z. Physik 88, 161 (1934).

31. H. J. Lipkin. Post-conference summary of recent developments in beta-decay. In H. J. Lipkin, ed. Proceedings of the Rehovoth Conference on Nuclear Structure,

Rehovoth, September, 1957. pp. 461-463. Interscience Publishers, Inc., New York. 1958.

32. J. S. Allen, Rev. Mod. Phys. 31, 791 (1959).

33. M. G. Mayer and J. H. D. Jensen. Elementary theory of nuclear shell structure. John Wiley and Sons, Inc., New York. 1955.

34. A. Winther and O. Kofoed-Hansen, Kgl. Danske Videnskab. Selskab, Mat.-fys. Medd. 27, No. 14 (1953).

35. O. Kofoed-Hansen and A. Winther, Kgl. Danske Videnskab. Selskab, Mat.-fys. Medd. 30, No. 20 (1956).

36. J. S. Bell and R. J. Blin-Stoyle, Nuclear Phys. 6, 87 (1958).

37. G. L. Trigg, Phys. Rev. 86, 506 (1952).

38. J. P. Elliott and B. H. Flowers, Proc. Roy. Soc. (London), Series A, 229, 536 (1955).

39. A. M. Lane, Proc. Phys. Soc. (London) 68, Sect. A, 189 (1955).

40. A. M. Lane, Proc. Phys. Soc. (London) 68, Sect. A, 197 (1955).

41. H. Morinaga and E. Bleuler, Phys. Rev. 103, 1423 (1956).

42. H. Tyren and P. A. Tove, Phys. Rev. 96, 773 (1954).

43. J. E. Cline and P. R. Chagnon, Phys. Rev. 108, 1495 (1957).

44. C. M. Davisson. Interaction of gamma-radiation with matter. In K. Siegbahn, ed. Beta- and gamma-ray spectroscopy. pp. 24-51. Interscience Publishers, Inc., New York. 1955.

45. P. R. Bell. The scintillation method. In K. Siegbahn, ed. Beta- and gamma-ray spectroscopy. pp. 133-164. Interscience Publishers, Inc., New York. 1955.

46. W. E. Mott and R. B. Sutton. Scintillation and Cerenkov counters. In S. Flugge and E. Creutz, eds. Encyclopedia of physics (Handbuch der Physik), Vol. 45, Nuclear instrumentation II, pp. 86-173. Springer-Verlag, Berlin. 1958.

47. S. H. Vegors, Jr., L. L. Marsden, and R. L. Heath. Calculated efficiencies of cylindrical radiation detectors. U. S. Atomic Energy Commission Report IDO-16370 [Idaho Operations Office, AEC]. September 1, 1958.

48. R. L. Chase and W. A. Higinbotham, Rev. Sci. Instr. 23, 34 (1952).

49. E. Fairstein, Rev. Sci. Instr. 27, 475 (1956).

50. E. Fairstein, Rev. Sci. Instr. 27, 549 (1956).

51. R. E. Bell, R. L. Graham, and H. E. Petch, Can. J. Phys. 30, 35 (1952).

52. R. L. Garwin, Rev. Sci. Instr. 24, 618 (1953).

53. J. B. Gerhart, B. C. Carlson, and R. Sherr, Phys. Rev. 94, 917 (1954).

54. A. E. Litherland, H. McManus, E. B. Paul, D. A. Bromley, and H. E. Gove, Can. J. Phys. 36, 378 (1958).

55. S. G. Nilsson, Kgl. Danske Videnskab. Selskab, Mat.-fys. Medd. 29, No. 16 (1955).

56. C. Broude, L. L. Green, and J. C. Willmott, Proc. Phys. Soc. (London) 72, 1122 (1958).

57. Progress report for January, February, March 1958 to the U. S. Atomic Energy Commission, U. S. Atomic Energy Commission Report CU-174 [Columbia Univ., New York], 1958.

58. E. B. Paul and J. H. Montague, Nuclear Phys. 8, 61 (1958).

59. D. Strominger, J. H. Hollander, and G. T. Seaborg, Rev. Mod. Phys. 30, 585 (1958).

60. F. Ajzenberg-Selove and T. Lauritsen, Nuclear Phys. 11, 1 (1959).

61. T. Muller, Ann. phys. 3, 739 (1958).

62. H. B. Burrows, T. S. Green, S. Hinds, and R. Middleton, Proc. Phys. Soc. (London) 69, Sect. A, 310 (1956).

63. W. W. Buechner and A. Sperduto, Phys. Rev. 106, 1008 (1957).

64. P. J. Campion and G. A. Bartholomew, Can. J. Phys. 35, 1361 (1957).

65. H. E. Gove and A. E. Litherland, Phys. Rev. 107, 1458 (1957).

66. P. M. Endt and C. M. Braams, Rev. Mod. Phys. 29, 683 (1957).

67. P. M. Endt and C. H. Paris, Phys. Rev. 106, 764 (1957).

68. A. Sperduto and W. W. Buechner, Phys. Rev. 109, 462 (1958).

69. G. Alaga, K. Alder, A. Bohr, and B. R. Mottelson, Kgl. Danske Videnskab. Selskab, Mat.-fys. Medd. 29, No. 9 (1955).

70. W. C. Parkinson, Phys. Rev. 110, 485 (1958).

71. S. A. Moszkowski and K. M. Jantzen. Accurate calculations of f functions for superallowed beta transitions. University of California at Los Angeles, Department of Physics, Technical Report No. 10 - 26 - 55 (Mimeo.), 1955.

VII. ACKNOWLEDGMENTS

The writer wishes to express his gratitude to the following people who have helped make this investigation successful:

Dr. M. G. Stewart, who patiently and skillfully guided the investigation and offered many valuable suggestions in the development of the experimental method and in the analysis and interpretation of the data.

Dr. D. J. Zaffarano, who made the initial suggestion for the investigation and contributed much help in the development of the method.

Dr. B. C. Carlson, for the enlightening discussions concerning the theoretical interpretation of the results.

Dr. D. C. Lu and Mr. J. E. Griffin, for their help in the design of some of the electronic circuitry which was used in the experiment.

Mr. D. N. Yarger, who contributed many long hours and hard work in helping accumulate and analyze the data, and prepared the Na samples used in the investigation.

Mr. K. G. Tirsell, who prepared the Si, S, and Ca samples.

Dr. A. J. Bureau and the staff of the synchrotron, whose efforts to keep the synchrotron in excellent operating condition helped immensely in facilitating the investigation.

The writer also wishes to express his gratitude to the

National Science Foundation, for the fellowships which sustained him during his later years of graduate training and during the initial stages of this investigation.

This work was done using the facilities of the Ames Laboratory, under the auspices of the U. S. Atomic Energy Commission.